DEVELOPMENT OF LIQUID BODY ARMOR SYSTEMS

A Thesis Submitted to
the Graduate School of Engineering and Sciences of
İzmir Institute of Technology
in Partial Fulfillment of the Requirements for the Degree of

MASTER OF SCIENCE

in Materials Science and Engineering

by
Oylum ÇOLPANKAN

December 2013
İZMİR

We approve the thesis of **Oylum ÇOLPANKAN**

Examining Committee Members:

_____

Prof. Dr. Metin TANOĞLU
Department of Mechanical Engineering, İzmir Institute of Technology

_____

Assist. Prof. Dr. H. Seçil ARTEM
Department of Mechanical Engineering, İzmir Institute of Technology

_____

Prof. Dr. Mehmet POLAT
Department of Chemical Engineering, İzmir Institute of Technology

_____

Prof. Dr. Sacide ALSOY ALTINKAYA
Department of Chemical Engineering, İzmir Institute of Technology

_____

Assist. Prof. Dr. Özgenç EBİL
Department of Chemical Engineering, İzmir Institute of Technology

17 December 2013

_____

Prof. Dr. Metin TANOĞLU
Supervisor, Department of Mechanical Engineering, İzmir Institute of Technology

_____

Assist. Prof. Dr. H. Seçil ARTEM
Co-Supervisor, Department of Mechanical, Engineering, İzmir Institute of Technology

_____

Assoc. Prof. Dr. Mustafa M. DEMİR
Head of the Department of Materials Science and Engineering

_____

Prof. Dr. R. Tuğrul SENGER
Dean of the Graduate School of Engineering and Sciences

ACKNOWLEDGMENTS

I would like to express my gratitude to my advisor, Prof. Dr. Metin TANOĞLU, for his supervision, guidance, support, understanding and encouragement during my study. I would also like to thank to my co-advisor Assist. Prof. Dr. H. Seçil ARTEM for her help and support.

I would like to acknowledge the Undersecretariat for Defence Industries of Turkey (SSM) and BARIŞ ELEKTRİK A.Ş. for financial support to this project and my study.

A special thank go to Fikret ŞENEL and Pınar ERBİL from BARIŞ ELEKTRİK A.Ş. for providing the materials and also for their advice throughout my study.

I am grateful to my project mate Sema YILDIZ for her contribution and help. I am also grateful to my laboratory, office colleagues and my friends İrem İNCE, Bilge Nihan GÜNGÖR for their encouragement, help and patience.

I would also like to thank Prof. Dr. Hürriyet POLAT for the help of DLS analysis and Center of Materials Research staff at Izmir Institute of Technology for their help during my study.

Last, but most importantly, I offer sincere thanks to three important people in my life, my mother Şengül ÇOLPANKAN, my father Recep ÇOLPANKAN and Mehmet Deniz GÜNEŞ for their support and continuous advice, motivation and love in all my life and believing in me. I feel very lucky to have them. I would not have accomplished anything without them by my side. I need them always by my side.

ABSTRACT

DEVELOPMENT OF LIQUID BODY ARMOR SYSTEMS

Body armors consist of fabrics made of high performance fibers which are characterized by low density, high strength, high tenacity and high energy absorption. Soft body armors are produced with lamination of 20-50 layers of fabrics and hard body armors consist of ceramic/metal plates along with the fabric. However, these armors are bulky, heavy, non-flexible. In order to eliminate disadvantages of traditional armors, new armor concept has been come into use with impregnation of shear thickening fluids (STFs) onto soft body armors called as liquid body armors. STFs are used within the fabrics to improve the ballistic and stab resistances due to its flowable behavior under ordinary conditions and become a rigid solid when a strong impact is applied. Objective of this study is to develop flexible, lightweight and high protection level soft body armors with the impregnation of shear thickening fluids onto fabrics.

In this study, for the production of STFs, colloidal and fumed silica nanoparticles were employed. As the carrier fluid polyethylene glycols (PEG) with three different molecular weights were used. The STFs were prepared by sonication of nanoparticles within the carrier fluid. The rheological behaviours of STFs were investigated using a rheometer. Two types of composites were fabricated by impregnating of STFs onto aramid and UHMWPE mat fabrics. The stab resistances (quasi-static and dynamic), flexibility and ballistic features of composites were tested and compared with neat fabrics. The microstructural surface coating features of STF and composites were also characterized by using scanning electron microscope (SEM).

ÖZET

SIVI ZIRH SİSTEMLERİNİN GELİŞTİRİLMESİ

Vücut zırhları yüksek mukavemet, yüksek modül, düşük yoğunluk ve yüksek enerji absorbe edebilme gibi özelliklere sahip olan kumaşlardan oluşmaktadır. Yumuşak vücut zırhları 20-50 katlı kumaşlardan oluşmakta, sert zırhlar ise kumaş ile birlikte rijit metal/seramik levhalardan içermektedir. Geleneksel zırhların ağır, esnek olmayan özelliklerinin iyileştirilmesi amacıyla yumuşak vücut zırhlarına kayma ile kalınlaşan sıvıların (KKS) empreyne edilmesi ile sıvı zırh olarak adlandırılan yeni bir zırh konsepti ortaya çıkmıştır. Normal şartlar altında akışkan özellik gösteren KKSler, güçlü bir darbe ile katı davranış gösterebilme özelliğine bağlıdır. Bu çalışmanın amacı, KKSlerin kumaşlara empreyne edilmesi ile esnek, daha hafif ve balistik dayanımı yüksek vücut zırhlarının geliştirilmesidir.

Bu tez çalışmasında, KKS üretimi için fumed silika ve kolloidal silika dolgu malzemeleri ve üç farklı moleküler ağırlıklı polietilen glikol (PEG) matriks malzemesi kullanılmıştır. KKSler partiküllerin PEG içerisinde ultrasonik teknikler dağıtılması ile elde edilmişlerdir. KKSlerin reolojik özellikleri reometre cihazı ile incelenmiştir., KKSlerin aramid fabrik ve ultra yüksek yoğunluklu PE (UHMWPE) keçelere empreyne edilmesi ile iki tipte kompozit üretilmiştir. Kompozitlerin statik ve dinamik batma dayanımları, esneklik ve balistik özellikleri test edilmiş ve ham kumaşlar ile kıyaslanmıştır. KKS lerin ve kompozitlerin mikroyapıları ve yüzey kaplama özellikleri taramalı elektron mikroskobu (SEM) aracılığı ile karakterize edilmiştir.

TABLES OF CONTENTS

LIST OF FIGURES

Figure **Page**

LIST OF TABLES

CHAPTER 1

INTRODUCTION

Humans throughout recorded history have used various types of materials to protect themselves from injuries. Body armors have been designed to prevent weapons, projectiles, stab threats that comes from knives or sharpened equipments such as spike or needle (Cheeseman and Bogetti 2003, Decker et al. 2007, Rao et al. 2009). For the body armor production, fabrics made of high performance fibers which are characterized by low density, high strength, high tenacity and high energy absorption, such as aramid (Kevlar®, Twaron®, Technora®), ultra high molecular weight polyethylene (Spectra®, Dyneema®) and polybenzoxazole (Zylon®) have been widely used (Tan, Tay, and Teo 2005, Srivastava, Majumdar, and Butola 2012). In order to satisfy the protection requirements of body armors, fabrics approximately 20-50 layers are laminated together or ceramic/steel plates are used along with the fabric structure (Lee, Wetzel, and Wagner 2003, Tan, Tay, and Teo 2005). This laminated fabric structured body armor is called as soft body armor and armor with a rigid ceramic or steel plates is known as hard body armor. They differ from each other in protection level; hard body armors are used for the protection against high speed threats and soft body armors are used for the protection of lower speed threats (Srivastava, Majumdar, and Butola 2012). Besides having a proper protection level against the threats, weight and flexibility are also important and desired design parameters (Duan et al. 2006). However, body armors are bulky, heavy, hard to wear, restrictive the mobility of the wearer due to this laminated structure and heavy plates (Lee, Kim, and Kim 2009). Therefore, there is always need to develop soft body armor materials with flexible, lightweight, higher protection levels against ballistic threats. Recently, shear thickening fluids (STFs) has attracted great interest and it has been started to use within the body armors to meet these requirements and this new armor concept have been started to called as "*liquid body armor*" (Srivastava, Majumdar, and Butola 2011). In addition to body armor application of STFs, adhesives and sealants, flame resistant clothing, motorcycle protective clothing are the other application areas (Suhaimi, Mohamed, and

Faiza 2010). Typical defence/protection applications of shear thickening fluids are presented in Figure 1.1.

Figure 1.1. Typical defence/protection applications of shear thickening fluids (STFs)

Shear thickening is a non-Newtonian flow behavior and defined in the British Standard Rheological Nomenclature as the increase of viscosity with increase in shear rate (Barnes 1989). The flow behaviour of the fluids under steady simple shear stress was introduced by Isaac Newton. He used in his theory two parallel planes with a distance d_y of a fluid which is subjected to a shear by the application of a force F. He proposed that the resulting shear stress is equal to the product of the shear rate (the velocity gradient in the direction perpendicular to that of the shear force) and the viscosity of the fluid medium which is a measure of resistance to flow and synonymous with internal friction (Malkin and Isayev 2006, Chhabra and Richardson 2008). The fluids which obey this rule with a constant viscosity with increasing shear rate are called as Newtonian fluids. Most fluids follow Newton's law. (Lomakin et al. 2011). However, concentrated suspensions do not show a constant viscosity under shear stress and they can be given as an example of non-newtonian fluids (Kalman et al. 2009).

The order-disorder transition and hydrodynamic clustering theories have been the accepted ones in to explain the mechanism of shear thickening fluids (Melrose and Ball 2004). Hoffman et al. (Hoffman 1972) investigated the microstructural details

during shear thickening phenomena by using light diffraction combined with shear rheology. He proposed that shear thickening is related to an order–disorder transition, layered structure becomes unstable beyond a critical shear rate (Kaldasch, Senge, and Laven 2008, Chellamuthu, Arndt, and Rothstein 2009). In subsequent years, researchers have simulated and experimentally studied to investigate the validity of the proposed order to disorder transition. For this aim Boersma et al. (Boersma, Laven, and Stein 1990) proposed a new model which explains the shear thickening phenomena with the balance between hydrodynamic shear forces and stabilizing electrostatic force. The schematic illustration of mechanism of shear thickening is shown in Figure 1.2. (Egres et al. 2003).

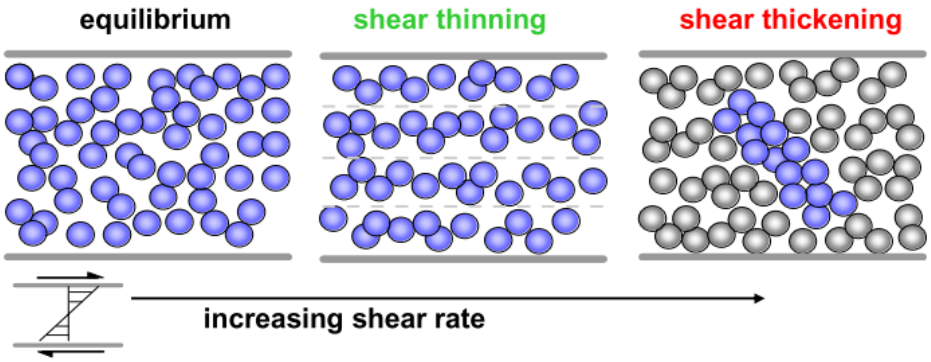

Figure 1.2. Schematic illustration of shear thickening pheomena
(Source: Egres et al. 2003)

The shear thickening fluids consist of two phase; nano-scale particles such as silica (Raghavan and Khan 1997, Lee and Wagner 2003, Kang, Kim, and Hong 2012), calcium carbonate (Wetzel et al. 2004), PMMA particles (Kalman et al. 2007) and medium fluid inwhich the particles are dispersed such as polypropylene glycol (PPG) (Galindo-Rosales and Rubio-Hernández 2010), polyethylene glycol (PEG) (Mahfuz, Clements, and Stewart 2006, Hassan, Rangari, and Jeelani 2010) etc.

The motivation of the study to develop lighter body armors as compared to armors already used in the army. This study focused on the development of shear thickening fluids (STFs) which consist of two different filler materials; fumed silica, colloidal silica and three different molecular weight carrier fluid; polyethylene glycol (PEG) 200, 300, 400 MW. One of the objective of the study was the fabrication of STF impregnated Fabric composites with aramid fabrics and UHMWPE mat. The flow

behaviours of prepared STFs and PEGs were investigated by steady-shear rheological measurements. STF impregnated fabrics' mechanical properties; quastatic and dynamic stab resistances were characterized and compared with those for the neat fabrics. For the evaluation of flexibility of STF/Fabric composites and neat fabrics, flexibility test was applied.

CHAPTER 2

ARMOR MATERIALS

2.1. Armor

Armor is generally defined as a protective equipment to provide protection from a specific form of attack and can be classified according to the intended applications as (Meyers 1994).

- Body armor (personal armor)
- Light armor (vehicular and aircraft armor)
- Heavy armor (tank armor)

Body armor is defined *"an item of personal protective equipment that provides protection against specific ballistic threats within its coverage area"* according to Ballistic Resistance of Body Armor NIJ Standard-0101.06 (NIJ Standart-0101.06 2008).

Seats in helicopters, light vehicles and airplanes can be examples of light armor applications. In order to develop light armors, a variety of materials have been used such as, monolithic metals, ceramic composite armor, polymer composite armor and laminated armor. For vehicular and aircraft applications, ceramic armor and ductile organic composites are laminated together. Ceramic plates have been used to break and deform the projectile in front and ductile composites have been used to absorb the kinetic energy of projectile behind of the armor (Meyers 1994).

Heavy armors systems constructed with rigid plates that are typically designed to provide protection against rifle threats. Heavy armors are defined as rigid armors according to the Ballistic Resistance of Body Armor NIJ Standard-0101.06 (NIJ Standart-0101.06 2008). Heavy armor is usually intended for tanks (Meyers 1994).

2.2. Body Armor

Protection of the personal from the damages has always been an important issue for mankind. From ancient times, humans have used various types of materials to protect their body and all of these materials can be named as body armors. Initially,

protective coverings that made from animal skins (such as; grecian shields) were used and with the developing of civilizations, the wooden shields and metal shields (such as; chain mail and suits in the Middle Ages) came into use (Kang, Kim, and Hong 2012, Cheeseman and Bogetti 2003). At the end of the Middle ages in Japan, the first soft body armor made of layered silk has been developed and the idea that these kind of materials can be use as an armor material has been come up (Cheeseman and Bogetti 2003). Body armors have been designed to provide head and torso protection against ballistic threats such as weapons or projectiles. It is extremely important to protect the head and the torso from the damages because life supporting organs are in these areas (Clements and Mahfuz 2007, Decker et al. 2007).

In addition to ballistic resistance feature of body armors, recent attention has been given to use body armors to provide stab threats comes from knives or sharpened equipments such as spike or needle, physical contact with debris, broken glass (Rao et al. 2009). Stab threats can be grouped into two categories: puncture and cut. The penetration by instruments having sharp tips and no cutting edge, such as awl, spike or needle is included to the puncture threat. Cut threats are related with knives having continuous cutting edge. This continuous cutting edge causes a continuous source of damage initiation during the stab event; therefore these kind of knive threats are more difficult to stop than puncture threats (Decker et al. 2007).

As the threats are developed, new armor concepts are introduced that can defeat the developed threats (DEF STAN 05-101 2005). For example, the metal shields have been used for cut protection but did not provide puncture ballistic resistance. Other armor concepts consists of rigid metal, ceramic, or composite plates. These rigid plates can offer excellent stab protection but they are bulky, heavy, hard to wear, and inflexible (Decker et al. 2007). In addition to these disadvantages, with the advent of firearms, most of the traditional protective devices were no longer used and the need to lightweight, having ballistic and stab resistances armor materials were improved. In the 1970s para-aramid synthetic fiber, Kevlar® which is a trade mark of Du Pont was the developed as a ballistic fabric of body armor and with this development a newera of body armor has been ushered (Kang, Kim, and Hong 2012) and later on many other important types of polymeric fibers have been developed. These high performance polymer fibers are characterized by low density, high strength, high tenacity and high energy absorption. Aramid (Kevlar®, Twaron®, Technora®), ultra high molecular weight polyethylene (Spectra®, Dyneema®) and polybenzoxazole (Zylon®) fibers has

been widely used as ballistic fabric of body armor (Grujicic et al. 2008, Tan, Tay, and Teo 2005, Srivastava, Majumdar, and Butola 2012). The history of the body armors is shown in Figure 2.1.

Figure 2.1. Body armors from (a) layered silk, (b) chain mail, (c) metal shiels, (d) high performance fibers (Source: "The History of Armor Protection, Mobility, and Fashion, Scientia Review, e-journal)

2.2.1. Types of Body Armors

Conventionally, body armors are classified into two groups; hard body armors and soft body armors according to their protection level. Hard body armors are typically used for military officers in high-risk regions for torso and head protection against high speed threats, whereas soft body armors are used for routine wear of police officers and security personnel for the protection against lower speed threats such as handguns, shotguns, hand grenades (Srivastava, Majumdar, and Butola 2012).

2.2.1.1. Soft Body Armors

Soft body armors are light and flexible fabric structures made from high performance fibers (Lee, Kim, and Kim 2009). Fabrics made with these high performance fibers have desirable properties for ballistic applications. These fibers are elastic in tension and not sensitive to strain rate. They also have very high tensile modulus and relatively low tensile failure strain. These behaviours of fibers can cause absorbing more energy per unit volume before failing and becoming ideal materials for body armors. Hundreds of these fibers are grouped together to make a yarn and yarns

are woven to produce a single layer ballistic fabric (Gopinath, Zheng, and Batra 2012, Duan et al. 2006). However, they are relatively expensive and in order to satisfy the protection requirements of body armors, lamination of approximately 20-50 layers of fabrics makes the armor heavy and bulky. This bulkiness also restricts the mobility, agility and comfort of the wearer (Carrillo et al. 2012, Lee, Wetzel, and Wagner 2003). The soft body armor should be design to reduce the amount of required fabric layers without compromising the effectiveness of the armor (Carrillo et al. 2012) with preventing both the projectile from penetrating and the impact inducing significant bulge at the back face which can also cause severe injuries. The ballistic performance of a body armor should be improved with increasing the number of yarns engage the projectile directly (primary yarns) absorb most of the energy during impact and fail at first. The secondary yarns which do not directly contact the projectile absorb the energy, confinedly. Therefore, improving the ballistic performance of a body armor require not only more primary yarns but also disperse stress waves away from the point of contact (Gopinath, Zheng, and Batra 2012).

2.2.1.1.1. Aramid Fibers

Among the high performance polymer fibers used as a body armor materials which are listed above, the most succesful and commonly used one is aramid fibers.

The term “aramid” is a short name of “aromatic polyamide”. Aramid fibers are synthetic high-performance fibers and they are prepared from stiff polymer molecules, aromatic polyamides, which are linked by strong hydrogen bonds each other and having highly ordered morphologies (Çay et al. 2007, Kalantar, Drzal, and Grummon 1990). Chemical composition of aramid is shown in Figure 2.1. Amide group shown in red rectangle in the Figure 2.2.

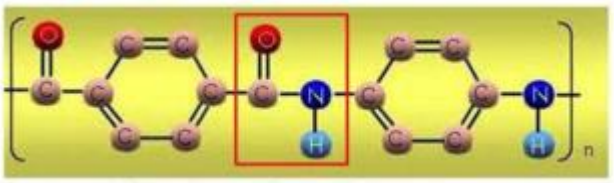

Figure 2.2. Chemical composition of aramid
(Source: Utracki 2010)

Aramid fibers has some specific characteristics that separate them from other synthetic fibers:

- High strength
- Good resistance to abrasion
- Good resistance to organic solvents
- Non-conductive
- No melting point
- Low flammability
- Good fabric integrity at elevated temperatures ("What is aramid?", Teijin Company Industrial Inc.,)

Aramid fibers have been manufactured with a different trade names such as Kevlar®, Twaron® and Technora® by different companies. Kevlar® is a product of Du Pont company, USA, Twaron® and Technora® are products of Teijin Company, Japan.

2.2.1.1.1.1. Kevlar®

Kevlar® has been used for a variety of applications such as, bullet-proof vests, protective clothing, high-performance composites for aircrafts and the automotive industry, mountaineering rope, sporting good apparels (Fan et al. 2012).

The new method was utilized to develop a fiber of poly-para-phenylene terephthalamide by the help of Kevlar®'s rod-like molecular structure, in 1971 by Du Pont. Kevlar® is produced by spinning method. The schematic illustration of the polymer alignment during the spinning process is shown in Figure 2.3. Spinning process initially requires the dissolving of polymer in an appropriate solvent and preparing liquid crystalline polymer solution which involves rod-like molecules. Increasing the concentration increases the number of molecules but doesn't make them align. Under shear forces, solution is passed through a spinneret and it causes the rods fully oriented. After the spinning, fibers comes to the coagulation bath and fiber is produced. The produced fibre is washed and dried, and then it is heat treated and drawn (Tecnical Guide-Kevlar® 2013, Wardman and Mather 2011).

Kevlar® has a unique combination of high strength, high modulus, toughness and thermal stability (Tecnical Guide-Kevlar® 2013). This excellent thermal stability over a wide range of temperatures is due to the aromatic rings in its structure. The fibers

do not melt or support combustion and decomposing starts at about 427°C. The rigid *para*-aramid molecules gives crystalizability to the feature Kevlar® and rod-like molecular structure feature. They are stronger and stiffer in the axial direction than in those the transverse direction (Utracki 2010, Kalantar, Drzal, and Grummon 1990). Kevlar® also has excellent dimensional stability with a negative coefficient of thermal expansion (-0.2 10-6/°C) (Utracki 2010).

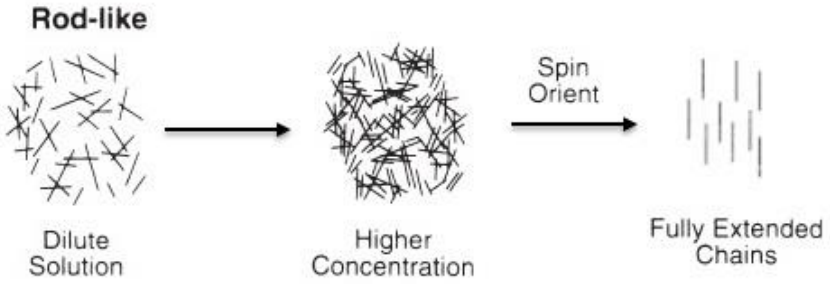

Figure 2.3. Behaviour of polymer during spinning process.
(Source: Tecnical Guide - Kevlar® 2013)

2.2.1.1.1.2. Twaron®

Twaron® has been developed in 1984 by Teijin company. It has 100% paracrystalline structure with molecular chains preferentially oriented along the fiber axis and due to this structure. Twaron® offers a unique combination of characteristics of mechanical properties (high strength, excellent strength-to-weight properties, and high modulus), chemical resistance, excellent durability and thermal stability (no melting point ,degradation only starts at 500°C, and low flammability). Twaron® has many application areas such as ballistic-protection products, civil engineering products, composites etc. Filament yarn, staple fiber, short-cut fiber, powder, pulp, fabrics and laminate types of Twaron® are also available to suit different applications (Twaron Product Brochure 2012).

Production of Twaron® has three main steps: polymerization, filament yarn spinning and conversion. The production schema is shown in Figure 2.4.

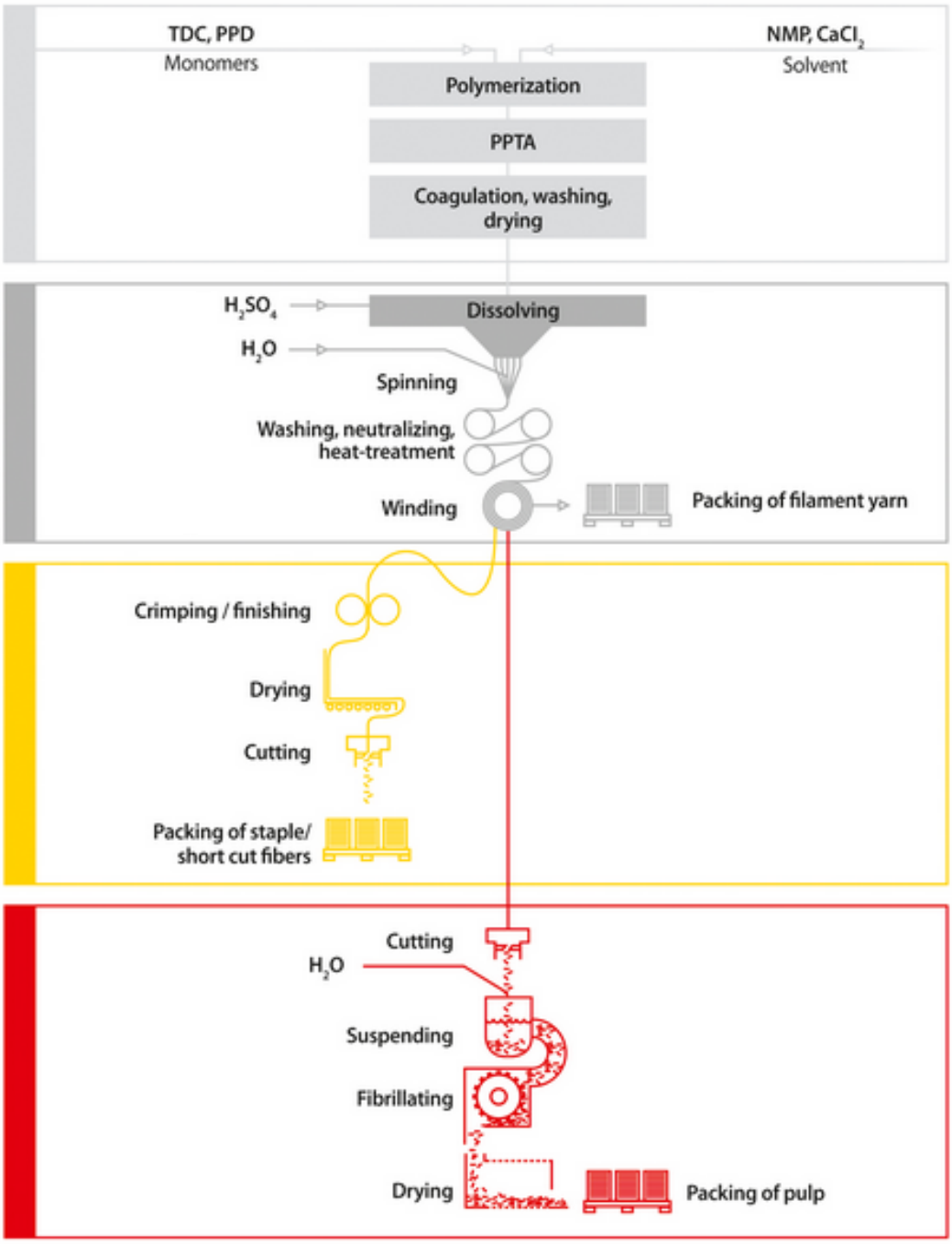

Figure 2.4. Production schema of Twaron® fibers
(Source: Twaron Product Brochure 2012)

In the polymerization step; monomers are converted into a firm fine-grained polymer powder. Thermal and chemical properties of prepared powder are same as properties of para-aramid but it can only be used as is to improve the properties of plastic components.

In the second stage (filament yarn spinning) polymer dissolves in sulfuric acid to produce a liquid crystalline solution. This solution is spun into fine, natural yellow or

dope-dyed black filament yarn. The structure of the yarn is virtually 100% paracrystalline, with molecular chains oriented parallel to the axis of the fiber.

The last step is the conversion and the conversion to staple or short cut fiber and pulp are different from each other. To produce staple or short-cut fibers, the yarn is crimped and then treated with a finishing agent. After drying, the fibers are cut to the desired length and then packaged. To produce pulp, the yarn is first cut, then suspended in water and fibrillated. To obtain wet pulp, yarn is packed directly. However, yarn is packed after dehydration and drying processes to obtain dry pulp (Twaron Product Brochure 2012).

2.2.1.1.1.3. Technora®

Technora® is a para-aramid fiber made from co-polymers (paraphenylene/0,4-diphenylether terephthalamide) (Kalantar, Drzal, and Grummon 1990). It was independently developed by Teijin and has been commercially available since 1987 (Technora, Teijin Company Industrial Inc,)

Technora® has some specific properties, including:

- High tensile strength – weight for weight, Technora is eight times stronger than steel
- Good fatigue resistance
- Long-term dimensional stability
- Excellent resistance to corrosion, heat, chemicals and saltwater (Technora, Teijin Company Industrial Inc,)

2.2.1.1.2. Ultra High Molecular Weight Polyethylene (UHMWPE) Fibers

An UHMWPE molecule is constructed of numerous repeating units of ethylene monomers and has C–C covalent bond backbone structure. UHMWPE molecules are arranged in both ordered, crystalline, and disordered, amorphous, regions. In the crystalline region, the chains are folded with the chain axis, (C–C direction). In the amorphous region, there is no regular chain folding but adjacent chains are

interconnected each other with random mechanical entanglements and chemical crosslinks. The connections between crystalline and amorphous regions are provided by tie molecules. The structure of this molecule is shown in Figure 2.5. (Gordon, D'Lima, and Colwell 2006, Wang et al. 1998).

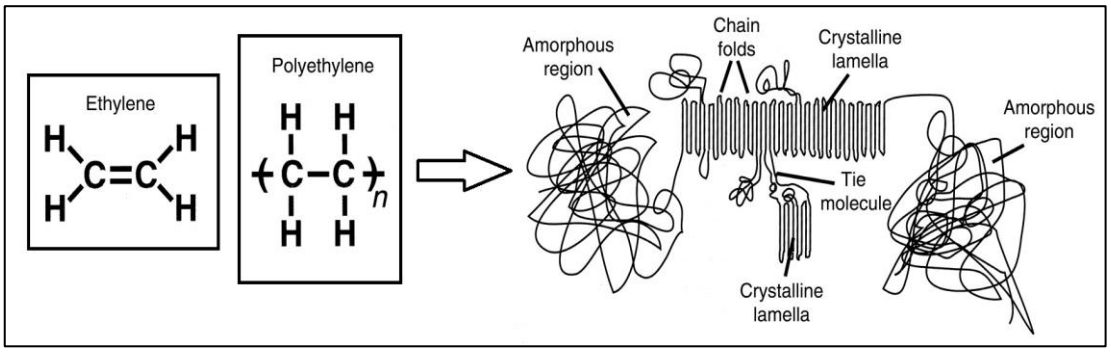

Figure 2.5. Structure of UHMWPE
(Source: Gordon, D'Lima, and Colwell 2006)

This polymer has many unique properties such as;

- Abrasion resistance that is higher than of any known other thermoplastic,
- Highest impact toughness of all polymer materials, even at cryogenic temperatures,
- A good corrosion resistance,
- An excellent environmental stress-crack resistance,
- A low coefficient of surface friction (Visjager 2001).

UHMWPE has many demanding applications, ranging from liners for hoppers and pipes in the food industry to medical and sport products. UHMWPE is produced by gel-spinning method due to the molecular weight (Mw) of the solvents is lower than the molecular weight between chain entanglements (Me) (Visjager 2001).

2.2.1.1.2.1. Dyneema ®

In the 1990's, DSM patented a method of "gel-spinning" of polyethylene fibers. These fibers were exceptionally light, durable and have high strength, low density, low elongation at break, and resistance to most chemicals characteristics and this product was named as Dyneema®. It has been adapted in fiber, tape and uni-directional (UD) sheets forms for use in a wide range of products, from fishing line and nets, medical

implants, to body armors. ("The Dyneema® Brand", Dyneema Company Industrial Inc, Utracki 2010,).

2.2.1.1.2.2. Spectra ®

After DSM sold the gel-spinning technology used to make Dyneema®, Honeywell developed Spectra® Fiber which is the expanded version of their Spectra® ballistic products This fiber is very similar with Dyneema® and so it can be used for many of the same uses. It has a low density and due to his feature, it exhibits a very high specific strength and modulus at room temperature. It has also excellent radar transparency, low dielectric constant and limited temperature capability almost 290 °C due to polyethylene molecular structure (Campbell 2006, "Advanced Fibers and Composites" Honeywell Company Industrial Inc).

2.2.1.1.3. Polybenzoxazole Fibers

Poly(benzobisoxazole), PBO, was invented at the USAF (*United States Air Force*) research lab in the 1980s. PBO fibers have high tensile strength, achieving better penetration resistance than the UHMWPE fibers, but low compressive strength. The decomposition temperature of PBO is about 550°C, which is higher as compared to 450°C for aramid (Utracki 2010).

2.2.1.1.3.1. Zylon®

Zylon® is the brand name of poly(p-phenylene-2,6-benzobisoxazole), which is a synthetic polyurethane fiber manufactured by Toyobo, a Japanese corporation in 1998. It consists of rigid-rod chain molecules of poly(p-phenylene-2,6-benzobisoxazole. The chemical structure of Zylon® is shown in Figure 2.6. (Utracki 2010, "What is Zylon®?", Toyoba Company Industrial Inc.).

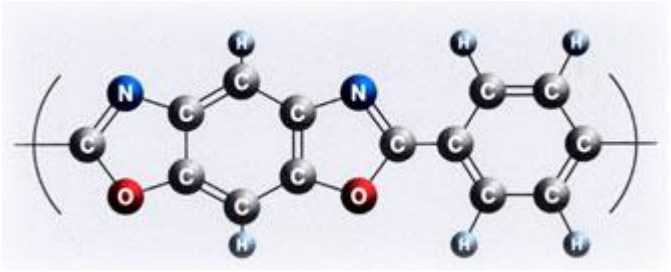

Figure 2.6. Chemical structure of Zylon®
(Source: “What is Zylon®?”, Toyoba Company Industrial Inc.)

2.2.1.2. Hard Body Armors

Soft body armors’ ballistic protection level is limited and if protection against high-level threats is required, hard body armors are used which have rigid ceramic or metal plates along with the fabric in the front and in the back (Srivastava, Majumdar, and Butola 2012).

Traditionally, the metallic plates, generally hard hardness steels have been used widely in armor applications for a long time, because of the cheaper cost, large technological database and mechanical properties in a very wide range. However, due to its high density, steel is not proper material for the body armor design (Übeyli, Yıldırım, and Ögel 2007, Majumdar et al. 1997).

In recent years, due to the this high density disadvantage of steel armor and the demand for lightweight armor for personal protection, alternative materials to product lightweight armor with the same level of protection in defense systems of that steel armors (Übeyli, Yıldırım, and Ögel 2007). For his purpose, the non-metallic materials, such as ceramics and composites, have been started to use in the design of hard body armor (Feli and Asgari 2011).

Ceramic materials have been applied in armor systems for their low density, high hardness and compressive strength features. While the projectile impacts to the ceramic platel, the nose of the projectile is shattered or blunted and the projectile loss its mass and energy. However, their brittle behavior and poor tensile strength cause failure and prevent them from absorbing significant amount of energy (Wang, Chen, and Chen 2013).

2.2.1.2.1. Lightweight Armor

In order to obtain the same ballistic protection level with lower weight, ceramic plates have been used with a ductile back-up plate such as laminated composite plate. The design is known as lightweight integral armor as shown in Figure 2.7.

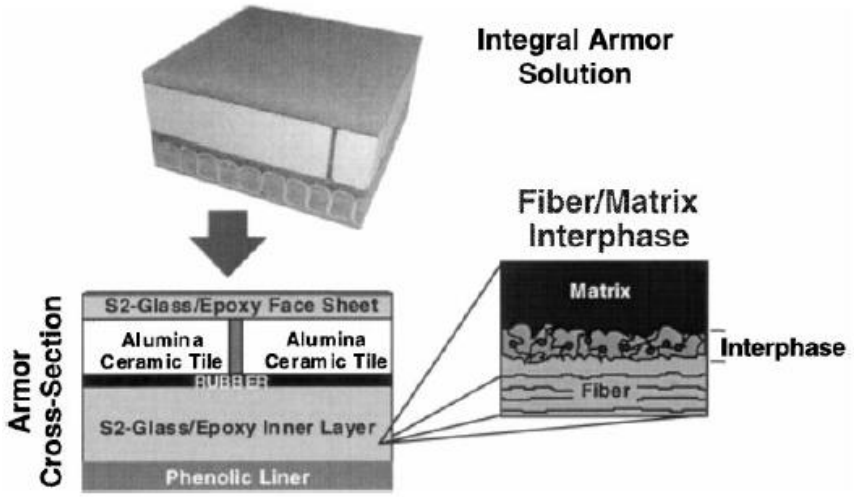

Figure 2.7. Repsentative of integral armor design
(Source: Tanoglu et al. 2001)

This includes multiple layers of glass fiber reinforced-polymeric composites and oxide ceramics (mostly alumina or alumina–mullite ceramics) and non-oxide ceramics based on carbides, nitrides, borides and some others, as well as their combinations, with homogeneous and heterogeneous structures (Tanoglu et al. 2001, Medvedovski 2010, Wang, Chen, and Chen 2013).

Lightweight integral armor shows effective protection against low and high velocity impact, because they combine low density, high hardness, high rigidity, strength in compression and low fracture toughness, predisposition to fracture when subjected to high tensile stresses of ceramics and the lightweight and ductility of composite laminated (Shokrieh and Javadpour 2008, Feli and Asgari 2011). This type of protection, 60% lighter than the steel armours, is composed of a tile of ceramic material that receives the impact, and a metal backplate. The two components are normally joined by a thin layer of adhesive (Fernández-Fdz and Zaera 2008).

The main role of the ceramic plate in the armor is the erosion and rupture of the projectile. When a projectile impact into such an armor, it is gradually slowed down and

caught by the hard plate (Duan et al. 2006, Feli and Asgari 2011). The projectile is first eroded by the hard ceramic plate and the reflected tensile wave breaks the ceramic in tension and this impact increases the contact surface of the metallic plate via forming a hard cone reducing the local pressure in the backup. The backing composite layer deforms to absorb the remaining kinetic energy of the projectile, about 20–40% of energy (Wang, Chen, and Chen 2013, Übeyli, Yıldırım, and Ögel 2007). It delays the initiation of tensile failure in the ceramic and backing plate interface, and allowing more projectile erosion (Chocron Benloulo and Sánchez-Gálvez 1998, Shokrieh and Javadpour 2008).

2.2.1.3. Liquid Body Armor Systems

The design of armor systems should be focused on its protective capacity, cost, areal density (weight/area) and the application area. The armors which are used for defensive walls weight is not a determining factor, laminated low-cost materials with larger thicknesses can be used to increase the ballistic resistance. However, weight is a key factor for body armor. Besides the weight in everyday operational use, factors such as comfort and wearability become extremely important (Fernández-Fdz and Zaera 2008, Horsfall, Champion, and Watson 2005). Hard body armors with rigid ceramic or metal plates can provide higher ballistic protection against the threats, on the other hand these plates makes the armors bulky, heavy, and restrictive to movement. In addition, soft body armors have also many layers of fabrics which affects the wearability and the comfort in a bad way (Carrillo et al. 2012, Lee, Kim, and Kim 2009).

These disadvantages have directed the researchers to investigate different types of armor satisfying the equivalent ballistic protection with keeping or even reducing its weight and rigidity (Srivastava, Majumdar, and Butola 2012, Duan et al. 2006).

To achieve these attributes, a new armor concenpt which is known as “liquid body armor” has been introduced. The key component of the liquid body armor is a shear thickening fluids (STFs) (Kang, Kim, and Hong 2012).

CHAPTER 3

SHEAR THICKENING FLUIDS

3.1. Classification of Fluid Behaviour

3.1.1. Definition of a Newtonian Fluid

The flow behaviour of solids and fluids under steady simple shear flow were developed by Robert Hooke and Isaac Newton, respectively. In 1678, Robert Hooke developed his *"True Theory of Elasticity"* which proposes *"the power of any spring is in the same proportion with the tension".* In other words, *if you double the tension you double the extension.* In 1687 Isaac Newton published a hypothesis associated with the steady simple shearing flow of fluids in the *"Principia"* which proposes *"the resistance which arises from the lack of slipperiness of the parts of the liquid, other things being equal, is proportional to the velocity with which the parts of the liquid are separated from one another"* (Barnes, Hutton, and Walters 1989, Shenoy 1999).

In order to analyse the hypotesis of Newton two parallel planes having each of surface area A and a distance d*y* apart from each other and the intervening space being filled with a thin layer of a fluid could be considered as shown in Figure 3.1.

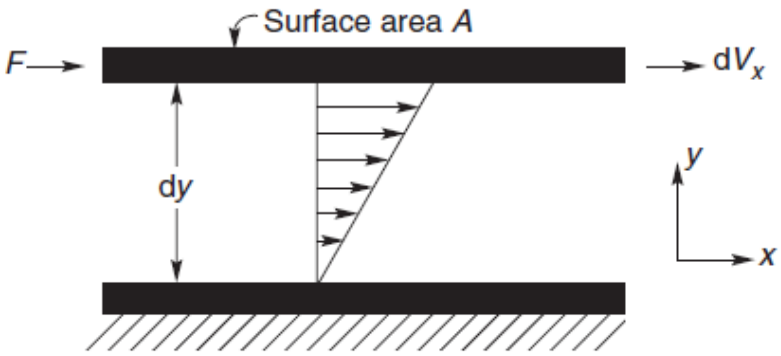

Figure 3.1. Schematic representation of unidirectional shearing flow
(Source: Chhabra and Richardson 2008)

If under steady state conditions, the fluid is subjected to a shear by the application of a force *F* and the force per unit area required to produce the motion of upper plane with relative velocity dV_x. The resulting shear stress (τ_{yx}) is equal to the product of the shear rate and the viscosity of the fluid medium (η). Viscosity is the lack of slipperiness which proposed in the hypothesis of Newton in Principia and it is also synonymous with internal friction and a measure of resistance to flow. The shear rate ($\dot{\gamma}$) may be expressed as the velocity gradient (dV_x/d_y) (Barnes, Hutton, and Walters 1989, Chhabra and Richardson 2008). The Newton's law of fluid flow under steady simple shear condition is shown in Equation 3.1.

$$\frac{F}{A} = \tau_{xy} = \eta\left(\frac{dV_x}{d_y}\right) = \eta\dot{\gamma} \tag{3.1}$$

Fluids with flow properties obeying the Newton hypothesis is called as *Newtonian Fluid*. This equation suggests that the shear stress is proportional to the deformation rate (shear rate), and such fluid is a linear rheological medium. For most fluids shear stress is proportional to the deformation rate. They follow Newton's law with the constant viscosity (Malkin and Isayev 2006, Lomakin et al. 2011).

3.1.2. Definition of a non-Newtonian Fluid

Newton's Law for liquids have been thought as universal law for two centuries after their developments. It was in the nineteenth century that scientists began to have some doubts. In 1835, Wilhelm Weber carried out experiments on silk threads and found out that they were not perfectly elastic. He proposed that "A longitudinal load produced an immediate extension. This was followed by a further lengthening with time. On removal of the load an immediate contraction took place, followed by a gradual further decrease in length until the original length was reached". This material was a solid-like material, whose behaviour cannot be described by Hooke's law alone (Barnes, Hutton, and Walters 1989, Malkin 1994). The existance of non-Newtonian (liquid-like) and non-Hookean (solid-like) materials was the crystal-clear fact after the development of Weber. Navier and Stokes independently developed a consistent three-

dimensional theory and formed in a modern form of Newtonian Law (Barnes, Hutton, and Walters 1989).

Non-Newtonian fluids, such as concentrated colloidal dispersions do not obey the hypotesis and shear stress is not proportional to the shear rate, the ratio of these terms is called apparent viscosity, which is not constant (Barnes, Hutton, and Walters 1989, Kalman et al. 2009).

Non-Newtonian fluids can be grouped into three categories;

- Visco-elastic fluids,
- Time-dependent non-Newtonian fluids,
- Time-independent non-Newtonian fluids (Chhabra and Richardson 2008).

3.1.2.1. Visco-elastic Fluid Behaviour

Many materials in practical interest such as polymer melts, polymer and soap solutions, synovial fluid show both ideal fluids and elastic solids' characteristics. The response of these kind of materials depend on its structure and on the conditions (kinematic) to which it has been subjected; thus the distinction between ' solid ' and ' fluid ' and between ' elastic ' and ' viscous ' is to some extent arbitrary and subjective (Chhabra and Richardson 2008, Goodwin and Hughes 2008).

3.1.2.2. Time-dependent Fluid Behaviours

In more complex fluids, the relationship between shear stress and shear rate depends on their kinematic history upon the duration of shearing. The viscosities of time dependent non-Newtonian fluids decrease r increase with time under conditions of constant shear rate as the ' internal ' structure of the material is progressively broken down or linked up. Thixotropy and rheopexy are two time-dependent fluid behaviours (Viswanath 2007, Chhabra and Richardson 2008, Kazemian, Prasad, and Huat 2010).

Thixotropic fluids shows a decrease in viscosity with time when it is sheared at a constant shear rate as shown in Figure 3.2. Concentrated suspensions, laponite and bentonite clay suspensions, emulsions, drilling fluids, waxy crude oils, protein solutions

and foodstuffs, are some examples of these fluids (Viswanath 2007, Chhabra and Richardson 2008).

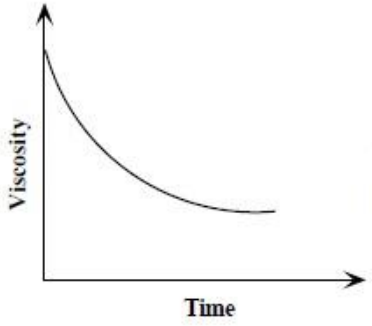

Figure 3.2. Txiotropic fluid behaviour
(Source: Viswanath 2007)

Rheopectic fluids' viscosity increases with the time as it is sheared at a constant rate on the contrary of thixotropic fluids, therefore Rheopectic fluids are also known as negative thixtropy. The rheopexy fluid behaviour is shown in Figure 3.3. (Viswanath 2007, Kazemian, Prasad, and Huat 2010).

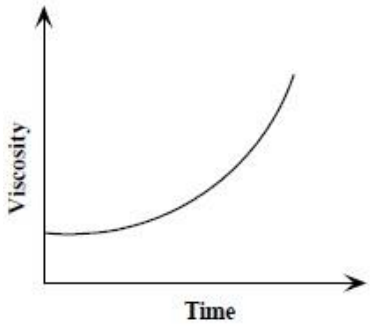

Figure 3.3. Rheopexy fluid behaviour
(Source: Viswanath 2007)

3.1.2.3. Time-independent Fluid Behaviour

Time-independent non-Newtonian fluids are the fluids for which the rate of shear at any point is determined only by the value of the shear stress at that point at that instant. When the shear rate is varied, the shear stress does not vary proportionally for these kinds of fluids. Three types of time-independent non-Newtonian fluids (Shear-

thinning (pseudoplastic), Viscoplastic (Bingham plastic), Shear-thickening (dilatant) and the Newtonian fluid are shown in Figure 3.4. (Chhabra and Richardson 2008).

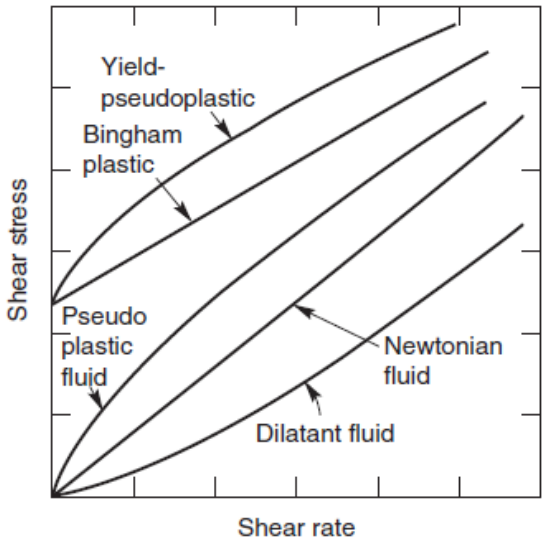

Figure 3.4. Various types of fluids based on viscosity
(Source: Chhabra and Richardson 2008)

3.1.2.3.1. Shear-thinning (Pseudoplastic)

This type of fluid displays a decreasing apparent viscosity with an increasing shear rate. Both at very low and at very high shear rates, most shear-thinning plots become straight lines. The resulting values of the apparent viscosity at very low and high shear rates are known as the zero shear viscosity, η_0 , and the infinite shear viscosity, η_∞ respectively. Thus, the apparent viscosity of a shear-thinning fluid decreases from η_0 to η_∞ with increasing shear rate (Chhabra and Richardson 2008).

Shear thinning of suspensions is associated with formation of particle layers. In equilibrium position, particles are dispersed randomly and this makes them naturally resists the flow, but as the shear stress or shear rate increses, particles organize in flow direction, and this phenemona decreases the viscosity (Wagner and Brady 2009, Cheng et al. 2011).

Filled polymer systems, polymer melts, polymer solutions, printing inks are the typical examples of shear-thinning fluids and these fluids have been used into a range of products such as; shampoos, paints, liquid detergents (Chhabra and Richardson 2008, Wagner and Brady 2009).

3.1.2.3.2. Viscoplastic (Bingham plastic)

The viscoplastic fluids were first defined by Professor Eugene Bingham who invented the term 'Rheology' as study of the deformation and flow of matter. For these type of fluids a critical level of stress must be reached in order to initiate the flow, yield stress (τ_0). Below this critical stress, the material behaves as a solid as critical stress has been reached, the material yields to flow. Particulate suspensions, emulsions, foodstuffs, blood and drilling mud are the common examples of viscoplastic fluids (Viswanath 2007, Chhabra and Richardson 2008).

3.1.2.3.3. Shear-thickening (Dilatant)

Shear thickening is a non-Newtonian flow behavior and defined in the British Standard Rheological Nomenclature as the increase of viscosity with increase in shear rate (Barnes 1989).

The term, diladant, is also used in practice to mean shear thickening. However, this usage is not completely correct as diladant is a property often associated with suspensions of irregularly shaped particles, in which the liquid exhibits an increase in volume while being sheared (Chhabra and Richardson 2008).

In order to explain the causes of shear thickening phenomena several theories have been proposed. ‘Order-disorder theory’ and ‘hydrodynamic clustering’ are the two widely accepted theories (Frith et al. 1996). Hoffman (Hoffman 1972) was the first scientist who was investigated the microstructural details during shear thickening phenomena by using light diffraction. He proposed that shear thickening is related to an order–disorder transition, where an odered, layered structure becomes unstable above a critical shear rate (Boersma, Laven, and Stein 1990, Kaldasch, Senge, and Laven 2008, Chellamuthu, Arndt, and Rothstein 2009). In subsequent years, researchers have allowed simulations of a large number of hard spheres under shear by the immense progress in computer technology. They have simulated and experimentally studied to investigate the validity of the proposed order to disorder transition. For this aim Boersma (Boersma, Laven, and Stein 1990) proposed a new model which explains the shear thickening phenomena with the balance between hydrodynamic shear forces and stabilizing electrostatic force, they proposed that short-range lubrication forces are

responsible for the formation of shear induced hydroclusters causing shear thickening. Formation of hydrodynamic clusters and hydrodynamic lubrication forces, which dominate all other colloidal forces in the shear thickening suspension were provided by rheo-optical experiments (Bender and Wagner 1996) and small angle neutron scattering measurements (Laun et al. 1992). Bossis (Bossis and Brady 1984) supported Boersma's model with the dynamic simulation for the hydrodynamic clustering of particles. Figure 3.5 indicates the hydroclustering mechanism of shear thickening with changes in viscosity with incresing shear rate. In equilibrium, At rest, the voidage is minimum and there is a random distributions of particles in the fluid. This distribution makes the fluid resistant to flow. But as increasing shear rates, the liquid lubricates the motion of each particle past others, particles become organized in the direction of the flow which reduces the viscosity; this step is called as shear thinning. At high shear rates, the material expands slightly and hydrodynamic interactions between the particles dominate over stochastic ones. so that there is no longer sufficient liquid to fill the increased void space and the difficulty of particles following around each other in a flow requires the higher energy dissipation and increases the viscosity. This region is a shear thickening region (Chhabra and Richardson 2008, Wagner and Brady 2009).

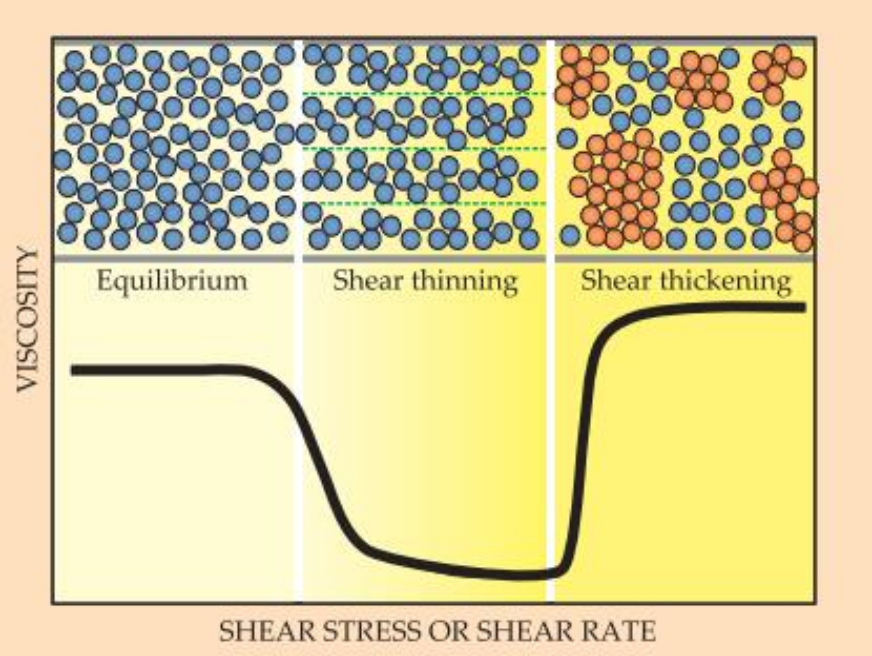

Figure 3.5. Schematic illustration of shear thickening pheomena
(Source: Wagner and Brady 2009)

Shear thickening has been observed for a wide variety of suspensions (Barnes 1989). The majority of work has been conducted on colloidal suspensions (Hoffman 1972, Barnes, Hutton, and Walters 1989, Franks et al. 2000). This increase occurs at a critical shear rate. Shear thickening behaviour is also observed in non-colloidal suspensions with larger solid phase particle sizes, where these mechanisms are inappropriate to describe the behaviour of these coarser suspensions. In general, the shear thickening fluids consist of two phases; nano-scale particles such as fumed silica (Raghavan and Khan 1997, Hassan, Rangari, and Jeelani 2010), colloidal silica (Lee and Wagner 2003, Houghton et al. 2007), calcium carbonate (Wetzel et al. 2004, Egres and Wagner 2005), PMMA particles (Kalman et al. 2007), and medium fluid in which the particles are dispersed within a liquid medium such as polypropylene glycol (PPG) (Galindo-Rosales and Rubio-Hernández 2010), polyethylene glycol (PEG) etc. (Mahfuz, Clements, and Stewart 2006, Egres Jr et al. 2004)

In recent years, shear thickening fluid (STF) has attracted much interest and it has been started to be used within the systems such as adhesives and sealants, flame resistant clothing, body armor, motorcycle protective clothing etc. (Suhaimi, Mohamed, and Faiza 2010). As a body armor material, shear thickening fluid (STF) is used within the fabrics to improve the ballistic and stab resistances due to its flowable behavior under ordinary conditions and become a rigid solid when a strong impact is applied (Srivastava, Majumdar, and Butola 2011).

CHAPTER 4

EXPERIMENTAL

4.1. Materials

In this study, for the synthesis of shear thickening fluids (STFs), various materials such as hydrophobic fumed silica nanoparticles CAB-O-SIL® M-5 and colloidal silica MP 1040 were used. The details of the nanoparticles used are given in Table 4.1.

Table 4.1 Details of the filler materials used in STF synthesis process

Materials / **Properties**	**CAB-O-SIL® M-5**	**MP 1040**
BET Surface Area (m^2/g)	200	-
Average Particle Size (nm)	200-300	70-100
Density (g/cm^3)	2.2	1.298
Purity	> 99.8 wt. %SiO_2	40.7 wt. %SiO_2
Supplier	Cabot Corporation, USA	Nissan Chemicals, Japan

Polyethylene glycol (PEG) with three different molecular weights (200, 300 and 400 g/mole) were used as a medium fluid in shear thickening fluids and purchased from Acros Organics, Belgium. Physical properties of the polymers are given in Table 4.2. PEG is non-toxic and easy to handle in addition to that it is thermally stable and easily available in bulk quantities which make it useful for bulk production.

In order to obtain stable dispersions, ethyl alcohol was used as a solvent and it was purchased from Tekkim Laboratory Chemicals, Turkey.

Table 4. 2. Physical properties of the polymers used in STF synthesis process

Materials / Properties	PEG 200	PEG 300	PEG 400
Molecular Weight (g/mole)	200	300	400
Density (g/mL)	0.9640	1.12	1.1275
Melting Point (T_m) (^oC)	-65	-15	8
Flash Point (^oC)	171	180	235

For the processing of composite aramid fabrics (Twaron® CT709), PE mat and ultra high molecular weight polyethylene (UHMWPE) (Dyneema® SB71) were used. Dyneema SB71 has specific gravity of 0.97g/cm³ and areal density 185-195 g/m^2. PE mat has areal density of 245 g/m^2. The specifications of the aramid fabric is given in Table 4.3.

Table 4.3. Specifications of the aramid fabrics used within the study

Properties	
Weave	Plain
Areal density (g/m^2)	200
Yarn	930f1000 dtex
Type Warp-Weft	Twaron 2040
Fabric sett (ends and picks per 10 cm)	105x105
Supplier	Teijin Company, Japan

4.2. Synthesis of Shear Thickening Fluids (STFs)

The procedure of colloidal silica based and fumed silica based STFs are different each other due to the structural difference of the materials. Colloidal silica is in

a liquid form, whereas fumed silica is in a powder form. The following sections describe the procedures for synthesis of STFs with different approaches.

4.2.1. Fumed Silica Based STFs

Fumed silica particles were dispersed in a liquid medium. There are three main steps in the fumed silica based STFs synthesis as shown in Figure 4.1.

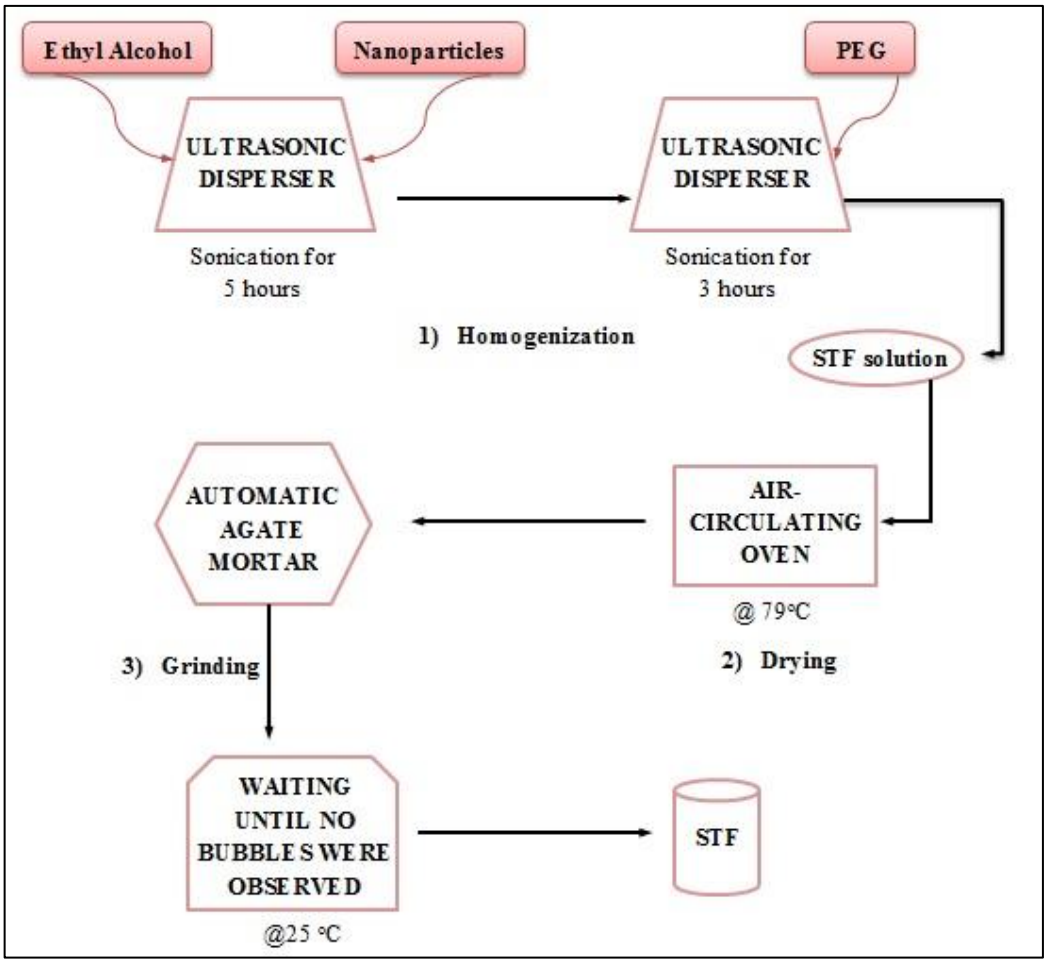

Figure 4.1. Schematic illustration of synthesis of shear thickening fluids (STFs) with fumed silica

In this procedure, the first step is homogenization in which sonochemical method using a Hielscher UP400S ultrasonic disperser with a titanium sonotrode with 25 mm diameter (Figure 4.2) was carried out to disperse nanoparticles in medium fluid, PEG. A various amount of nanoparticles were added to ethyl alcohol with a 1:5 weight ratio of STF:ethyl alcohol and they were sonicated for 5 hours at 70% amplitude, 50 Hz

and 28 kWh. PEG was added to the prepared solution and sonication was maintained for 3 hours with the same process parameters described above. The weight fractions of fumed silica nanoparticles were adjusted for all STFs from 5 wt. % to 30 wt. %.

Figure 4.2. Ultrasonic disperser

The second step is drying of homogenized STF solution. This drying process was performed within an air-circulating oven shown in Figure 4.3 at ethyl alcohol evoporation temperature (79 ºC). The drying process was continued until STFs weight became stable.

Figure 4.3. Air-circulating oven used in drying process

The last step is grinding and in this step STF was grinded with the aid of Retsch RM 200 an automatic agate mortar (Figure 4.3) at 250 watt and 100 rpm. A viscous liquid was obtained from dried solid particles of STFs after this step. The images of STF before and after grinding process is shown in Figure 4.5.

In order to eliminate the bubbles, STF was waited at room temperature until no bubbles were observed.

Figure 4.4. Automatic agate mortar used for grinding dried particles

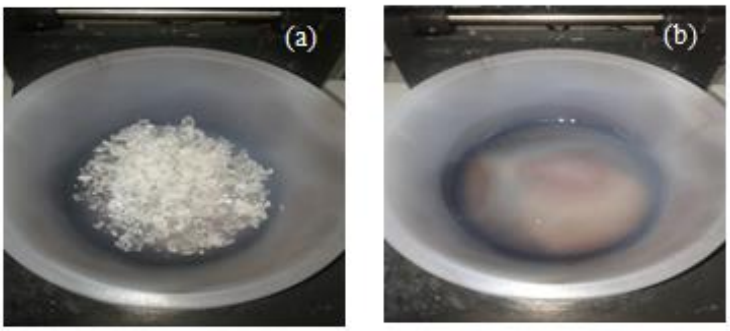

Figure 4.5. The images of STF (a) before and (b) after grinding process

4.2.2. Colloidal Silica Based STFs

Colloidal silica (MP 1040) that contains 40 wt.% SiO_2 and 60 wt.% water was also used for STF synthesis. Four different concentrations of STF was prepared with 40, 50, 60 and 70 wt.% SiO_2. The STF preparation procedure with colloidal silica has some

similarity with those prepared with fumed silica. There are three main steps (homogenization, drying, grinding) for the synthesis of STFs as shown in Figure 4.6.

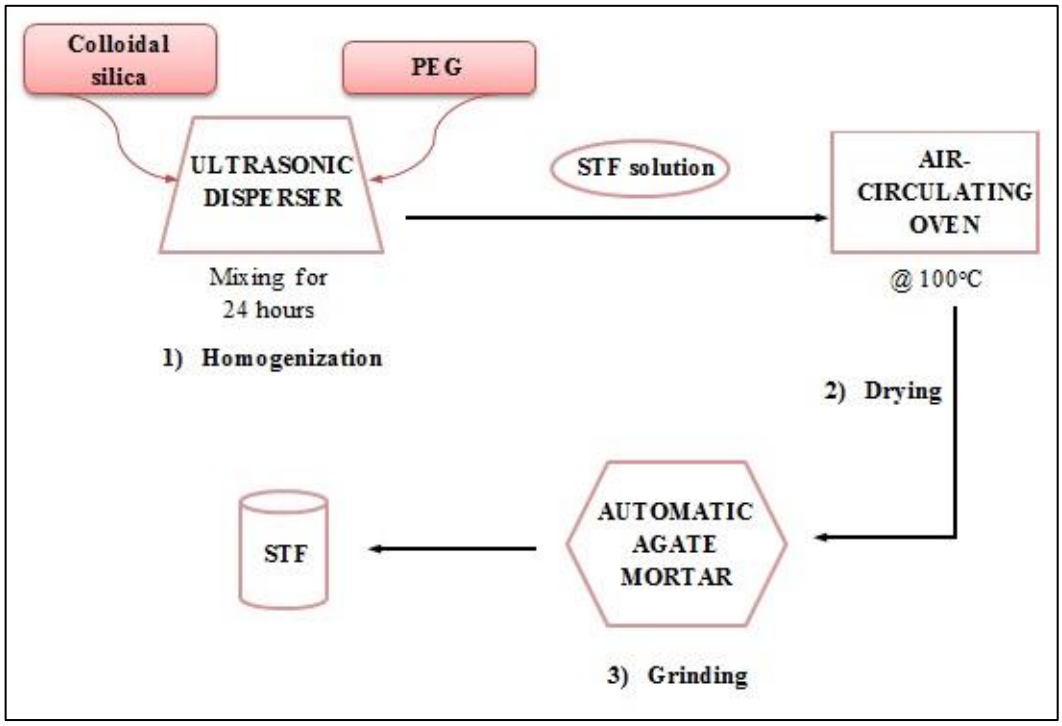

Figure 4.6. Schematic illustration of synthesis of shear thickening fluids (STFs) with colloidal silica

In the homogenization step colloidal silica and PEG were mixed by magnetic stirrer as shown in Figure 4.7 for 24 hours. The water within the homogenized STF solution was evaporated using an air-circulating oven at 100 ºC and this process was continued until STF's weight became stable. The last step was grinding and dried STF particles were grinded along this stage with the help of an automatic agate mortar (Retsch RM 200) at 250 watt and 100 rpm.

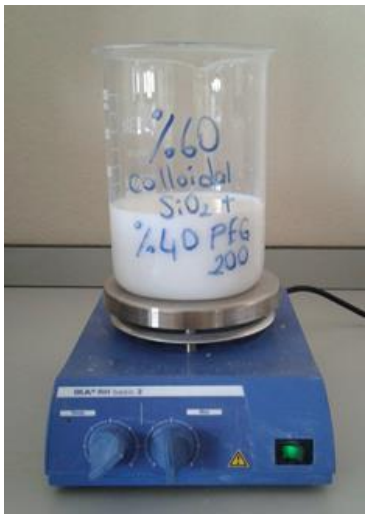

Figure 4.7. Homogenization of colloidal silica and PEG by magnetic stirrer

4.3. Fabrication of STF/Fabric Composites

In order to fabricate STF/Fabric composites, impregnation by soaking method was used. The schematic illustration of the procedure is shown in Figure 4.8. In this method, STF corresponding to 30 wt. % of the total fabric mass was diluted within 200 ml ethyl alcohol. The 30 wt. % of STF was obtained as the value in order to reach the final concentration of 15 wt. % of STF impregnated on the fabrics. The solution was poured into a impregnation pool, aramid and PE mat fabrics soaked and impregnated with STF solution, individually. Each fabric was held in the pool for 30 seconds in order to obtain homogeneous impregnation and then they hanged vertically for 10 seconds in order to remove the excess amount of solution. Fabrics were dried in an air-circulating oven at 79 ºC until their weights become stable. After the drying step, STF/Fabric composites were sealed in a laminated polyethylene pouch which has the sizes of 25 cm x 25 cm by means of vacuum packing machine at 760 mmHg pressure for 40 seconds. The image of the machine is shown in Figure 4.9.

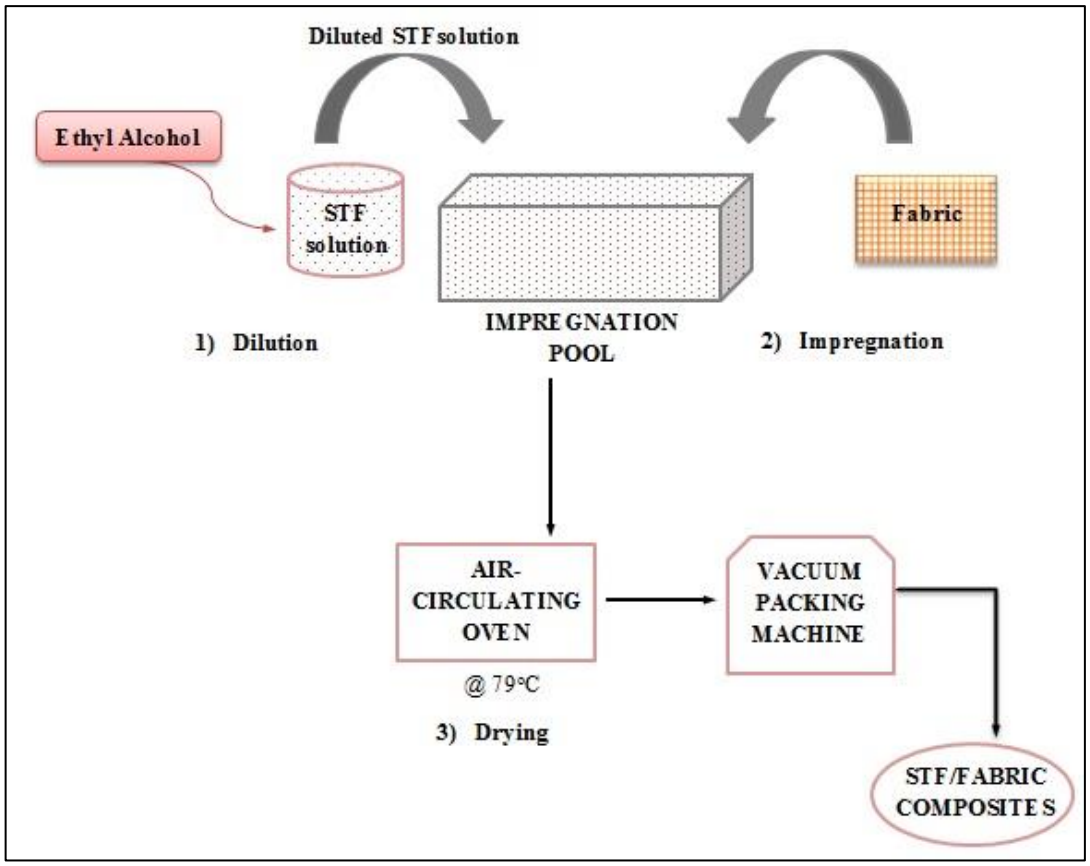

Figure 4.8. Schematic illustration of fabrication of STF/Fabric composites via soaking impregnation method

Figure 4.9. Packing machine used for STF/aramid composite packaging.

4.4. Characterization of Nanoparticles

4.4.1. Microstructural Features

4.4.1.1. X-Ray Diffraction (XRD)

The crystallinity of hydrophobic fumed silica nanoparticle (CAB-O-SIL® M-5) was characterized by X-ray Diffraction (XRD) analysis using a Phillips™ Xpert diffractometer with Cu Kα as a radiation source. Powdered sample was scanned in the interval of a $2\theta = 5°\text{-}70°$ at 40 kV and 30 mA. The XRD analysis of colloidal silica (MP 1040) was also performed after all liquid medium in it was evaporated. The same XRD parameters were used for the colloidal silica analysis.

4.4.1.2. Scanning Electron Microscopy (SEM)

The microstructures of nanoparticles were investigated with Scanning Electron Microscopy (SEM), Phillips™ XL-30S FEG. A 5 gram of silica nanoparticles were dispersed in 20 ml ethyl alcohol and sonochemical method was applied for half an hour for the dispersion of the samples. The solution was dried in an air-circulating oven at 79 ^{o}C in order to evaporate ethyl alcohol in the solutions. Similarly, 2 ml of colloidal silica MP 1040 was dried in an air-circulating oven at 100 ^{o}C in order to evaporate water. All the sample surfaces were gold-coated by a sputtering apparatus before SEM examination to eliminate charging.

4.4.1.3. Dynamic Light Scattering (DLS)

The average particle sizes as a function of volume % and particle size distributions of nanoparticles were measured with Zetasizer 3000HS by using Dynamic Light Scattering (DLS) technique with a laser light which has 633 nm wavelength. In order to analyze the particle size distribution, dispersion of nanoparticles with 5 gram of each in 20 ml ethyl alcohol were prepared by sonochemical method for half an hour.

4.4.2. Thermal Properties

4.4.2.1. Thermogravimetric Analysis (TGA)

Thermogravimetric analysis (TGA) was performed with Perkin Elmer Diamond Thermogravimetric Analyzer in order to analyze the weight loss of nanoparticles as a function of temperature. The experiments were carried out from 25^{o}C to 1000^{o}C at a heating rate of 10 ºC/min in a 50 ml/min nitrogen flow.

4.5. Characterization of Medium Fluids (PEGs)

4.5.1. Thermogravimetric Analysis (TGA)

In order to analyze the weight loss of PEGs as a function of temperatures, thermogravimetric analysis (TGA) was performed by using Perkin Elmer Diamond Thermogravimetric Analyzer at the range of temperature of 30 ^{o}C to 800 ^{o}C at a heating rate of 10 ºC/min in a 50 ml/min nitrogen flow.

4.6. Characterization of Shear Thickening Fluids (STFs)

4.6.1. Rheological Properties

A TA Instruments AR2000ex oscillatory rheometer was used to analyze the rheological properties of shear thickening fluids. The rheological measurements of STFs were repeated three times and the average of the values were taken. The rheometer is shown in Figure 4.10.

For higher concentrated materials (above 20 wt. % particle content) cone plate geometry with a 168 micrometer gap, 25 mm plate diameter, 0.1 radian (~6º) cone angle was used. For lower concentrated materials, cone plate geometry with a 55 micrometer gap, 40 mm plate diameter, 2º cone angle was used. Experiments were performed in steady (continuous ramp) mode. By this mode, steady shear viscosities of STFs as a

function of shear rate was obtained and shear rate varied between 10^{-2} to 10^{3} s^{-1} during the experiments and all rheological experiments were carried out at room temperature.

In order to remove loading effects, a preshear of 1 s^{-1} for 60 s and equilibrium for 2 minutes were applied prior to all rheological measurements.

Figure 4.10. TA Instruments AR2000ex oscillatory rheometer used within the experiments

4.6.2. Microstructural Features

4.6.2.1. Scanning Electron Microscopy (SEM)

Dispersion of the nanoparticles in the organic phase was identified by the help of scanning electron microscope (SEM) (Phillips™ XL-30S FEG). Before SEM analyses, STFs were diluted in ethyl alcohol at a 3:1 weight ratio of ethyl alcohol:STF. After evaporation of all ethyl alcohol with STF blends, they were gold-coated by a sputtering apparatus.

4.6.2.2. Dynamic Light Scattering (DLS)

Dynamic light scattering analysis of STFs were performed to determine the average particle sizes and particle size distributions of STFs.

4.6.3. Thermal Properties

4.6.3.1. Thermogravimetric Analysis (TGA)

In order to determine the weight percentage of silica and PEG in STF samples, thermogravimetric analysis (TGA) was performed by using Perkin Elmer Diamond Thermogravimetric Analyzer within the range of temperature range of 30 to 800 ^{o}C at a heating rate of 10 ºC/min in a 50 ml/min nitrogen flow.

4.7. Characterization of STF/Fabric Composites

4.7.1. Scanning Electron Microscopy (SEM)

The microstructural characterization of neat fabrics and STF-impregnated fabric surfaces were performed by the help of scanning electron microscope (SEM) (Phillips™ XL-30S FEG). SEM analysis of STF/fabric composites was used to investigate the impregnation level of STFs within the Twaron and PE mat fabrics. Before the analysis, sample surfaces were gold-coated in order to obtain electrically conductive surfaces to prevent charging.

4.7.2. Mechanical Property Characterization

4.7.2.1. Quasi-static Stab Resistance Testing

The quasi-static stab tests were performed based on the 'NIJ Standard-0115.00 stab resistance of personal body armor' by using Schimadzu AGS-J universal test

machine with a 5 kN load cell. The targets with 10 layers and having sizes of 20 cm x 20 cm were placed on a backing material which consists of four layers of 5.8 mm-thick neoprene sponge, one layer of 31 mm-thick polyetylene foam, two 6.4-mm-thick layers of rubber. This backing materials that is specified by the NIJ test standart is illustrated in Figure 4.11.

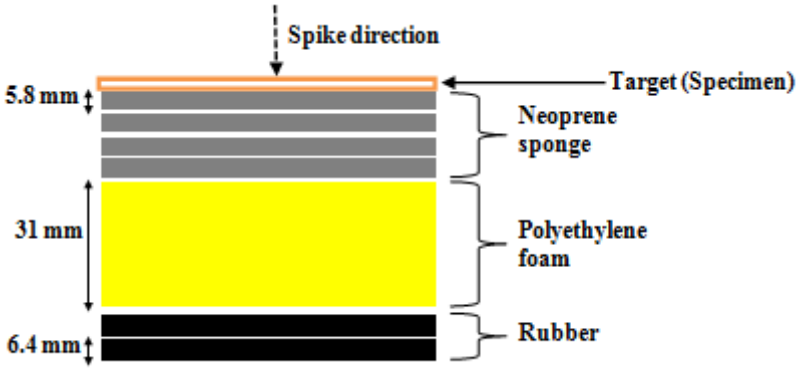

Figure 4.11. Schematic illustration of quastatic stab testing backing material

As a stab threat, spike was used and stab resistance of STF/Fabric composites were evaluated and compared with those mode with neat fabrics. The test setup is presented in Figure 4.12. The spike rate was adjusted to 500 mm/min and it was pushed into the target until 30 mm displacement was achieved. Load values as a function of displacement for neat fabrics and STF/Fabric composites were obtained and compared with each other. Tests were repeated for three times for all prepared composites and the average values were taken.

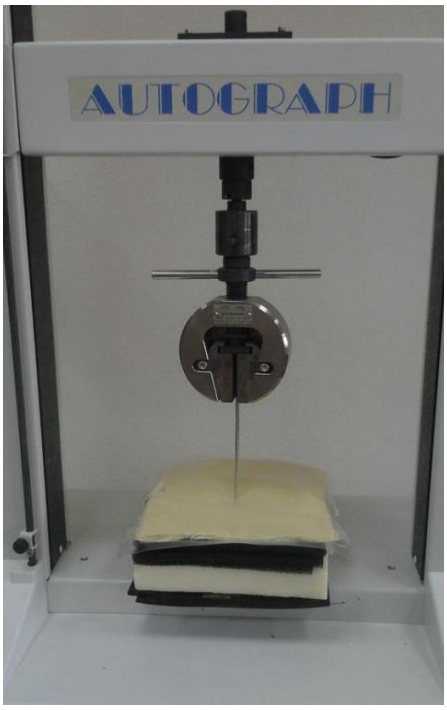

Figure 4.12. Quasi-static stab resistance test setup

4.7.2.2. Dynamic Stab Resistance Testing

Dynamic stab resistance of neat fabrics and STF/Fabric composites were determined by drop tower test by means of MATEŞ Electronic stab and impact test machine located in BARIŞ Electrical Industry Inc., Ankara. The test set up is shown in Figure 4.13. As a threat, spike having 9 mm diameter and 3020 g weight was used. The targets with 10 layers and having sizes of 20 cm x 20 cm were placed on a glass cement having a 55 mm thickness. Spike heights were adjusted to 250, 500 and 750 mm. The impact velocities of 2.21, 3.13 and 3.83 m/sec were calculated based on the heights according to potential and kinetic energy balance equation (Equation 4.1). From these measurements penetration depth versus impact velocity graphs were obtained. Tests were repeated for three times for all prepared composites and the average values were taken.

$$mgh = 0.5mV^2 \tag{4.1}$$

With the equation above, m, g, h, V are the spike weight (g), acceleration of gravity (m/sec^2), spike height (m), impact velocity (m/sec), respectively.

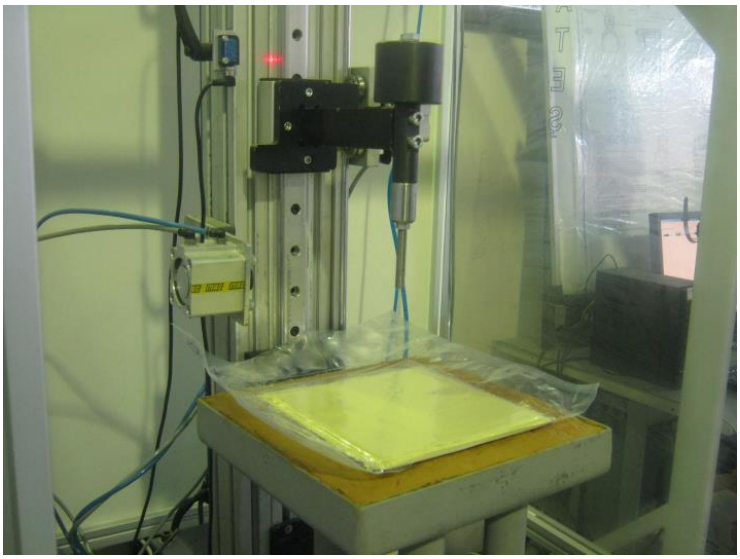

Figure 4.13. Dynamic stab resistance test setup

4.7.3. Flexibility Testing

Flexibility is the another critical feature for body armor besides the high stab resistance properties. Therefore, the flexibility test was performed to determine the effect of STF addition on the fabric flexibility by using Schimadzu AGS-J universal test machine. Schematic test set up for flexibility testing is shown in Figure 4.14. The test rate was adjusted as 20 mm/min and test was maintained until the force of 6N was achieved. Bending at the end of the sample is measured, bending angle is calculated by dividing this extension to target adge (10 cm). Bending angle is reported as a measure of target flexibility, with larger angles indicating greater flexibility. Tests were repeated for three times for all prepared composites and the average values were taken.The images of neat fabric before and after flexibility test are shown in Figure 4.15. a and b, respectively.

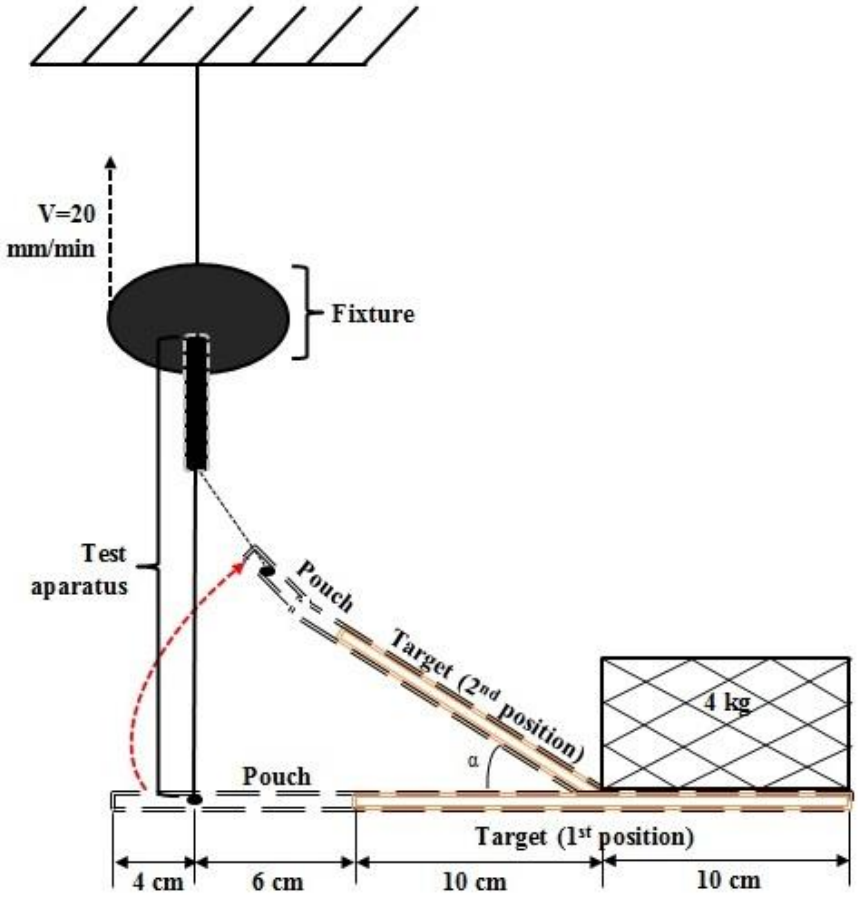

Figure 4.14. Schematic illustration of flexibility test setup

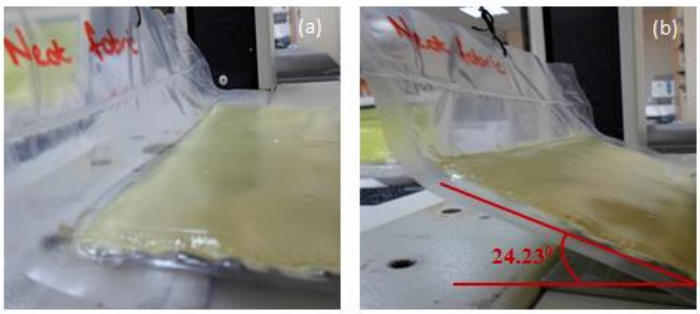

Figure 4.15. Images of neat fabric (a) before and (b) after flexibility test

4.7.4. Ballistic Testing

Ballistic testing on neat fabrics and STF/Fabric composites was conducted using 9 mm parabellum FMJ projectile and 1.1 gr. fragment-simulating projectiles (FSPs) in accordance to NATO Standart 2920. These ballistic tests were preformed in 8th Major

Maintenance Center Command, Afyon and according to '*NIJ-0101. 04 Ballistic Resistance of Personal Body Armor'* (NIJ Standart-0101.04 1987).

The schematic test setup for 9 mm parabellum test is seen in Figure 4.16. The exact impact velocity of projectile was measured with a chronograph immediately before impacting the target. The glass cement was used as a backing material of the targets and deformation of target was measured from this backing material after test was applied.

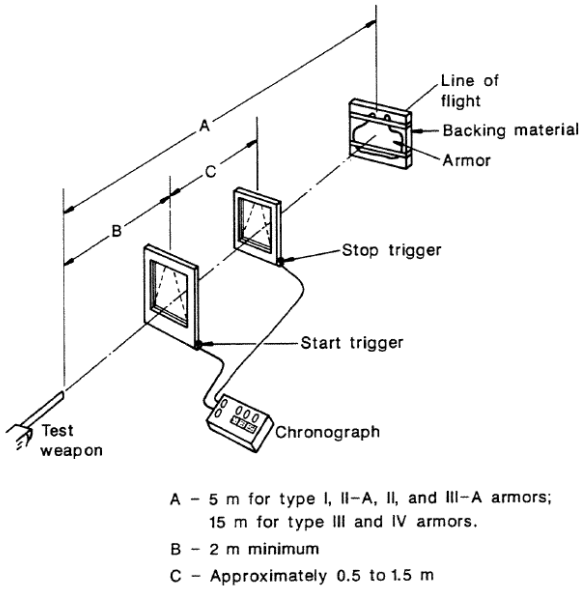

Figure 4.16. 9 mm parabellum test setup
(Source: NIJ Standart-0101.04 1987)

V_{50} ballistic limit test was applied onto the neat fabrics and STF/Fabric composites by using ,1.1 ± 0,03 gr (17 grain) fragment-simulating projectiles (FSPs) according to STANAG standard. The FSP used in the ballistic test is seen in Figure 4.17.

After each projectile, the target was controlled, noted that the penetration is full or partial. The test was continued until at least three full and three partial penetration were observed.

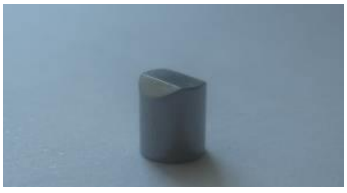

Figure 4.17. 1,1 ± 0,03 gram (17grain) fragment-simulating projectile

CHAPTER 5

RESULTS AND DISCUSSIONS

In this chapter, rheological, thermal and microstructural features of shear thickening fluids (STFs) syntesized within the study is given. Characterization of filler materials (fumed silica nanoparticles and colloidal silica) and medium fluids (polyethlyene glycol) used to prepare STFs are also reported. In addition, microstructure, flexibility, mechanical properties (quasistatic and dynamic stab resistances) and ballistic features of STF/fabric composites prepared by impregnation of STFs onto aramid and UHMWPE fabrics are reported.

5.1. Characterization of Nanoparticles

5.1.1. Microstructural Features

5.1.1.1. X-Ray Diffraction (XRD)

X-ray diffractograms of fumed silica nanoparticles (CAB-O-SIL® M-5) and colloidal silica (MP 1040) are shown in Figure 5.1 and 5.2.respectively. XRD patterns of fumed silica nanoparticles exhibited no sharp peaks but a broad peak at $2\theta = 23°$ suggesting that the silica used in the study is highly amorphous. The colloidal silica had also amorphous structure with a broad peak at $2\theta = 23°$. The peak for colloidal silica is more apparent with higher intensity value compared to those for the fumed silica.

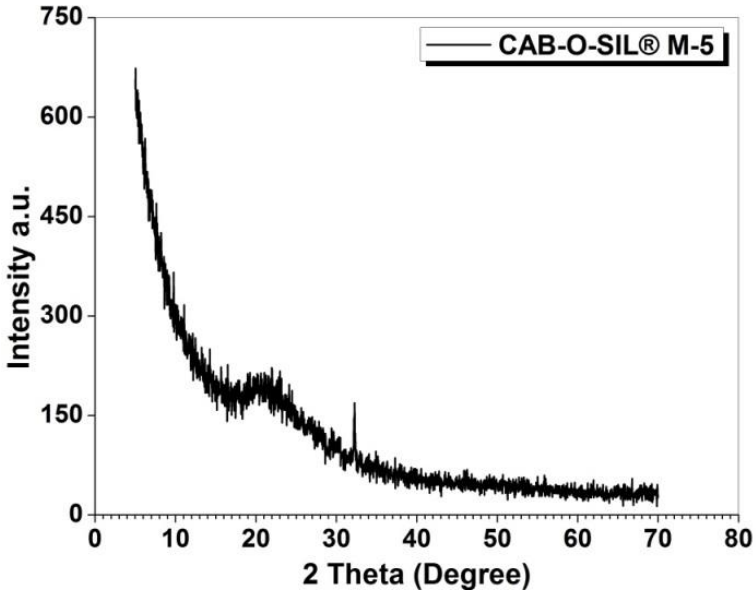

Figure 5.1. XRD pattern of fumed silica nanoparticles

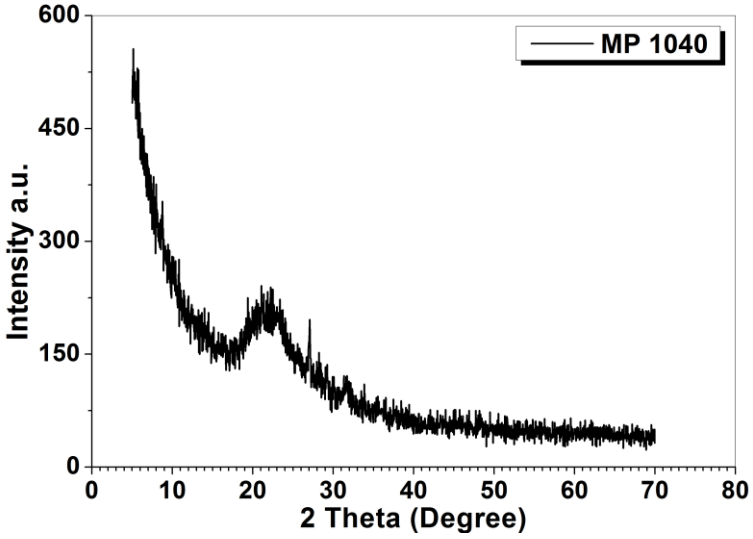

Figure 5.2. XRD pattern of colloidal silica MP 1040

5.1.1.2. Scanning Electron Microscopy (SEM)

SEM images of hydrophobic fumed silica and colloidal silica nanoparticles at high magnifications are shown in Figure 5.3 and 5.4, respectively. Fumed silica nanoparticles were found to have irregular shape and some aggregates. Colloidal silica particles have certain spherical shapes and their average size was measured to be around 100 nm as shown in Figure 5.5.

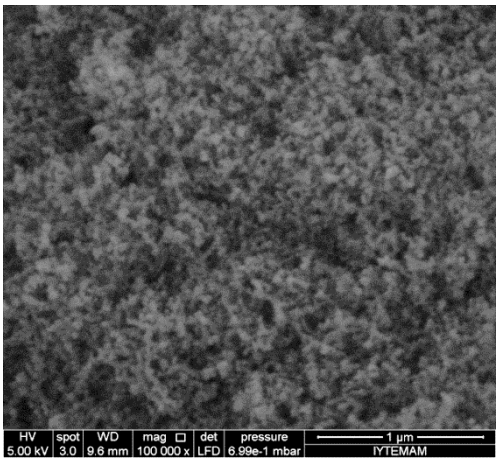

Figure 5.3. SEM image of fumed silica (100000X magnification)

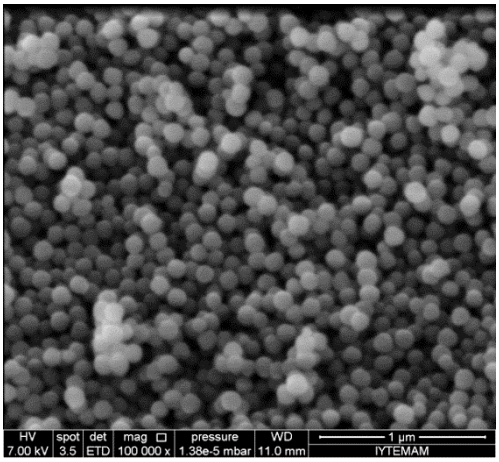

Figure 5.4. SEM image of colloidal silica (100000X magnification)

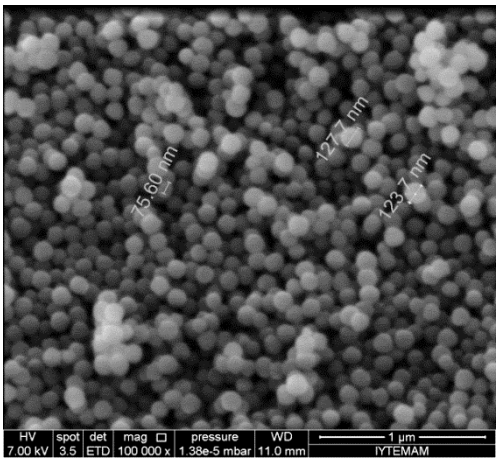

Figure 5.5. SEM image of colloidal silica with average particle size (100000X magnification)

5.1.1.3. Dynamic Light Scattering (DLS)

The volume % and particle size distributions of fumed silica and colloidal silica nanoparticles are shown in Figure 5.6 and 5.7, respectively. Particle sizes of fumed and colloidal silica were found as between 40-240 nm and 60-160 nm, respectively.

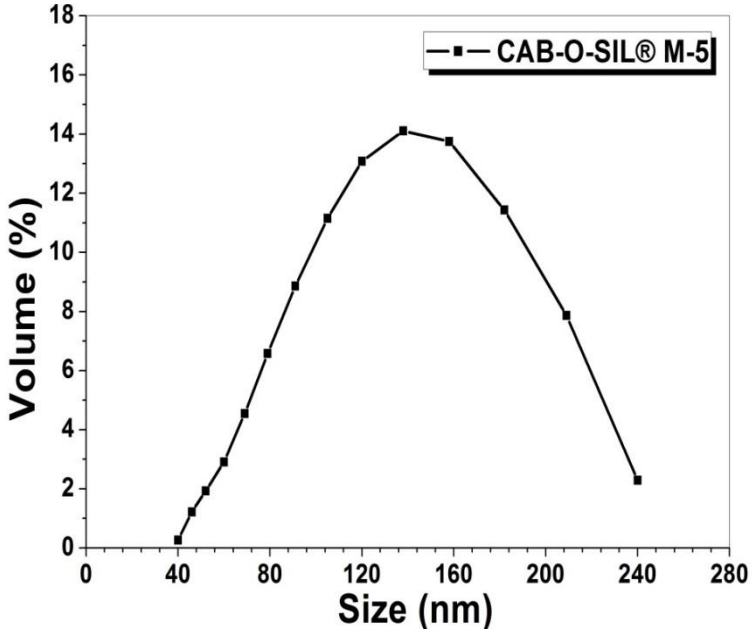

Figure 5.6. Size distributions of fumed silica nanoparticles as a function of volume %

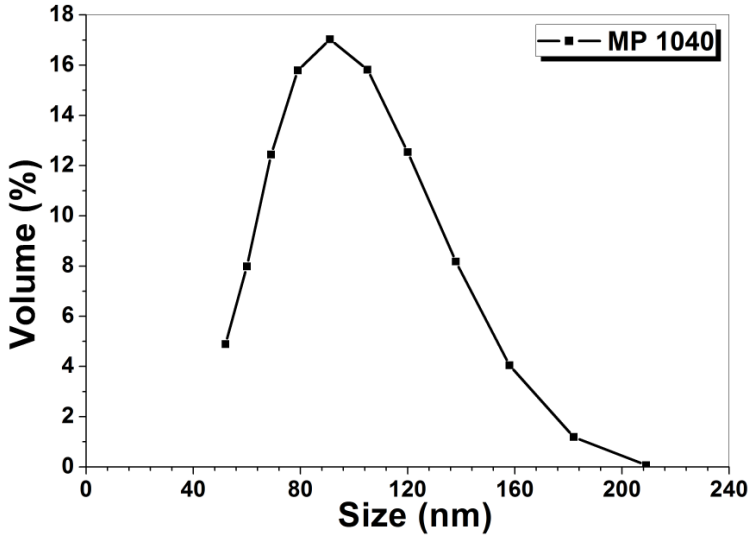

Figure 5.7. Size distributions of colloidal silica nanoparticles as a function of volume %

5.1.2. Thermal Properties

5.1.2.1. Thermogravimetric Analysis (TGA)

Figure 5.8 and 5.9 show typical thermogravimetric analysis (TGA) weight loss curves of fumed silica and colloidal silica, respectively. Total weight loss of fumed silica was found to be around 8 wt. % and 5 wt. % for colloidal silica.

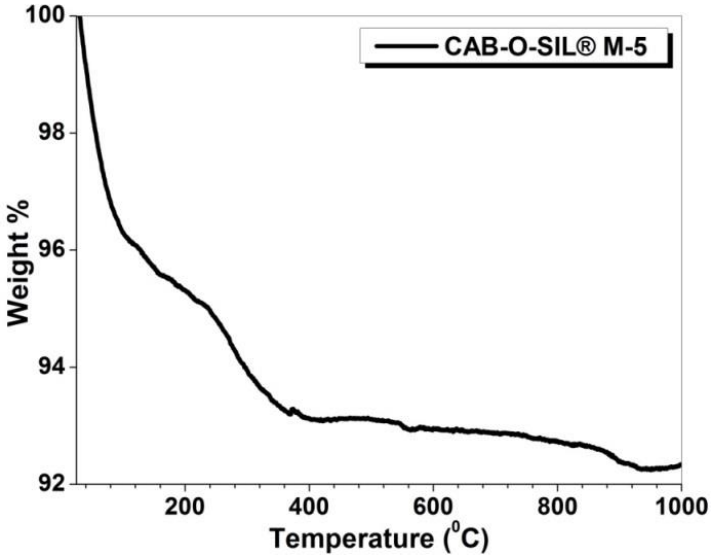

Figure 5.8. TGA thermogram of fumed silica nanoparticles

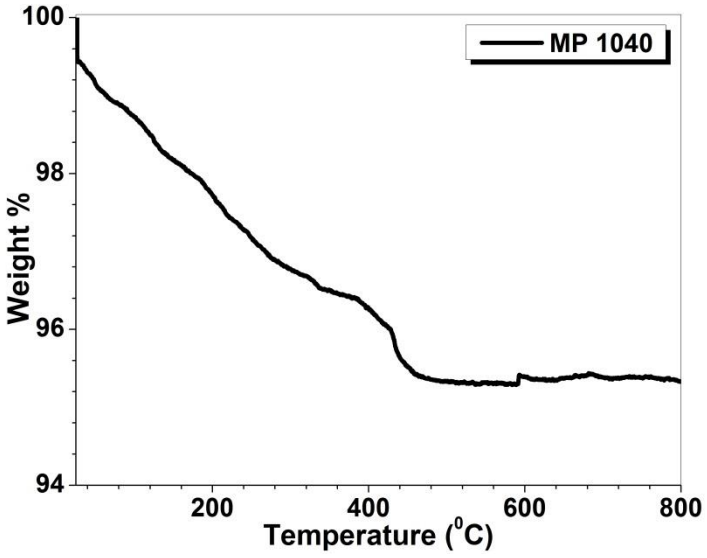

Figure 5.9. TGA thermogram of colloidal silica nanoparticles

5.2. Properties of Medium Fluids (PEGs)

5.2.1. Thermogravimetric Analysis (TGA)

Figure 5.10 shows typical thermogravimetric analysis (TGA) weight loss curves of three PEG samples (PEG 200, PEG 300 and PEG 400). The huge weight loss of the samples within the TGA curves indicating the total decomposition of the PEGs. As seen in the figure, PEG 200 was the first one start to decompose at around 150°C where a major weight loss was seen. The others (PEG 300 and PEG 400) start to decompose at higher temperatures at around 230 °C. The decomposition temperatures were measured as 150 - 350 °C, 230 - 420 °C and 230 - 440°C for PEG 200, PEG 300 and PEG 400, respectively.

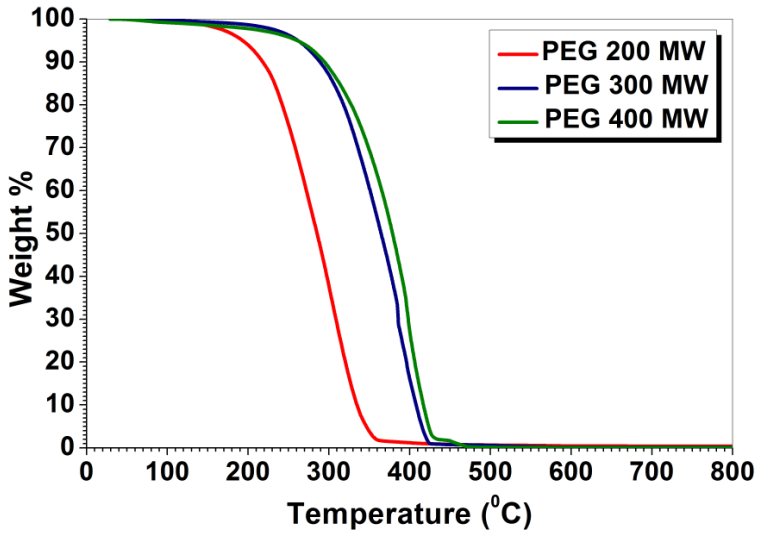

Figure 5.10. TGA thermograms of PEG 200, PEG 300 and PEG 400

5.3. Properties of Shear Thickening Fluids (STFs)

5.3.1. Rheological Properties

5.3.1.1. Fumed Silica Based STFs

In order to investigate the optimum synthesis conditions of fumed silica based STFs three different methos were used and rheological mesaurements of prepared STFs were applied. These methods are explained below.

- *Method I,* polyethylene glycol (PEG) and fumed amorphous silica nanoparticles were sonicated together for 8 hours in ethyl alcohol with a 1:5 weight ratio of STF:ethly alcohol together.
- *Method II,* nanoparticles were added to ethyl alcohol with a 1:5 weight ratio of STF:ethly alcohol and they were sonicated for 5 hours and PEG was added to the prepared solution and sonication was maintained for 3 hours.
- *Method III,* polyethylene glycol (PEG) and ethyl alcohol with a 1:5 weight ratio of STF:ethly alcohol were sonicated for an hour and then fumed silica nanoparticles were added into the prepared solution and they were sonicated together for 7 hours.

For all samples, after the homogenization step, prepared STF solution were dried within an air-circulating oven shown at ethyl alcohol evoporation temperature (79 ºC) until STFs weight became stable. The dried STFs were grinded with the aid of an automatic agate mortar. After the elimination of the bubbles, STFs were obtained. Prepared STFs were carried to rheological measurements in order to determine the shear thickening behaviour. The steady shear viscosity values as a function of shear rate for the STFs prepared based on the three procedures described above is shown in Figure 5.11.

As seen in Figure 5.9 STF sample prepared with *Method III* did not show a shear thickening effect. The sample prepared with *Method I* showed an increament in viscosity as increasing shear rate. The sample prepared with *Method II* is the most effective one among the others such that they exhibited a clear thickening effect with sudden and continuous increase in viscosity with increasing shear rate. Based on this result, *Method II* was selected to use in further experiment.

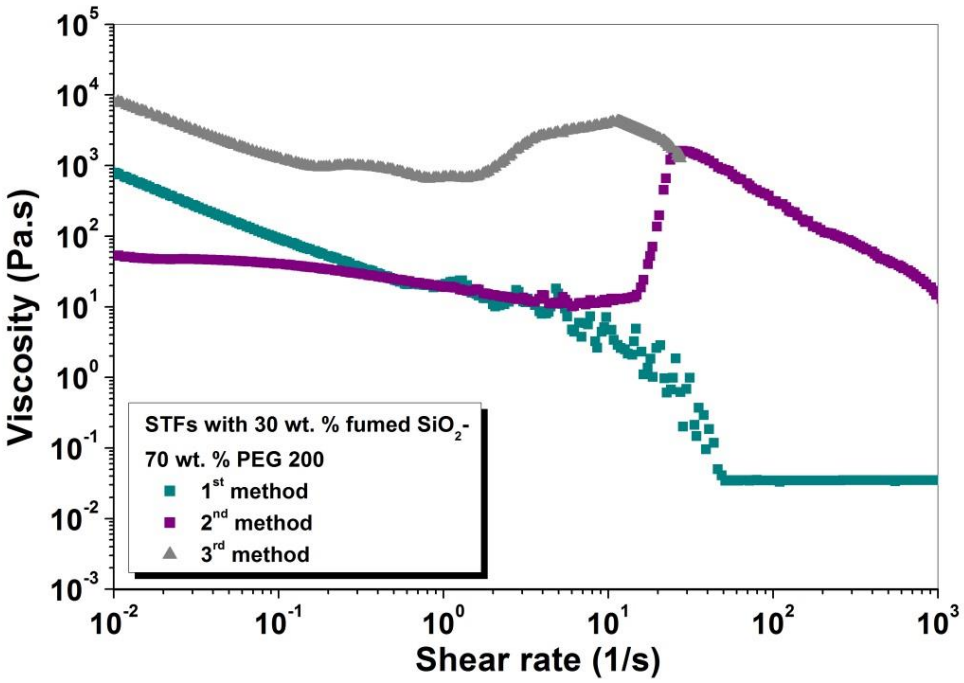

Figure 5.11. Steady shear viscosity vs. shear rate graph of STFs prepared with 30 wt. % fumed silica - 70 wt. % PEG 200 prepared based on three methods

Figure 5.12 shows the steady-shear rheological behavior of neat PEG 200 and STFs prepared with various fractions of fumed silica together with PEG 200. As seen in the graph, PEG 200 exhibits Newtonian fluid behavior with constant viscosity as a function of increasing shear rate. The addition of silica nanoparticles into the PEG results with the increase of the viscosity over the entire range of shear rates and STFs exhibit shear thickening behaviour. However, the STF sample containing 5 wt. % fumed silica does not show a shear thickening effect due to the lower silica content in the fluid.

It was also observed from the graph, the silica suspensions are glassy at rest and yield at low shear rates. This manifests as shear thinning. It is a desired feature for the body armor application areas. As increasing shear rate the viscosity begins to plateau, followed by a transition to shear thickening behavior at high shear rates. The second shear thinning regime is visible at higher shear rates after the shear thickening transition and this behavior is known as reversible shear thickening. This is an important issue for multishots. The sudden increase in the viscosity of silica dispersions and the shear thickening transitions are due to microstructural changes in the fluid along with the hydrocluster mechanism. The formation of particle clusters increases the hydrodynamic stress in the shear thickening fluid that leads to the dramatic increase in the viscosity. It was also seen that the viscosity of the STF samples increased with increasing silica

weight fraction. As it is known, the shear rate at which shear thickening behavior observed is a critical shear rate. It was found that the critical shear rate values decreases as particle loading increases. The range of shear rates at which shear thickening behaviour was observed and the viscosity values at these ranges are tabulated in Table 5.1 for STFs prepared with fumed silica and PEG 200. The sample containing 30 wt. % silica exhibited the highest thickening effect with sudden and continuous increament in viscosity.

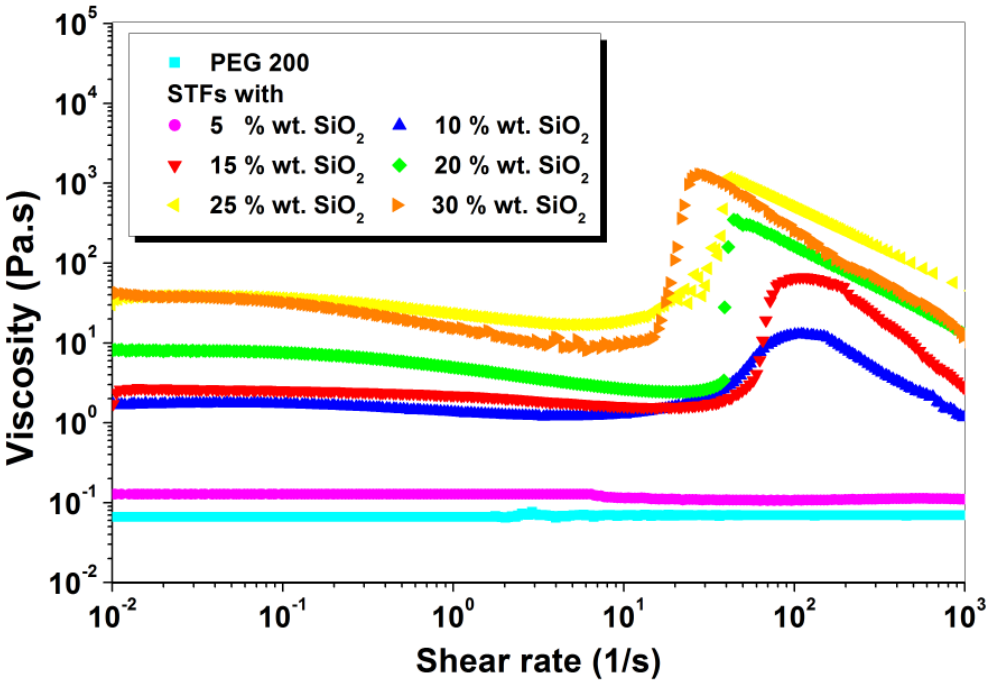

Figure 5.12. Steady shear viscosity vs. shear rate graph of STFs prepared with PEG 200 and various weight fractions of fumed silica

Table 5.1. Range of shear rates and viscosity values of STFs prepared with fumed silica and PEG 200

Silica content in STFs (wt. %)	**Range of shear rates (s^{-1})**	**Viscosity values (Pa.s)**
5	-	-
10	31.58 - 109.9	2.145 - 12.89
15	22.8 - 112.8	1.624 - 66.81
20	21.22 - 44.08	2.434 - 350.3
25	18.28 - 41.21	33.68 - 1185
30	15.79 - 27.36	18.87 - 1297

The steady-shear viscosity as a function of shear rate graphs for fumed silica based STFs composed of PEG 300 and PEG 400 are shown in Figure 5.13 and 5.14, respectively. These graphs exhibit similar trend in viscosity for those containing PEG 200. Viscosity values of PEG 300 and PEG 400 remain constant as increasing shear rate. In addition, STF samples containing 5 wt. % of fumed silica also does not show any increament in viscosity as a function of shear rate. As silica particle concentration increased, the interparticle forces increased and so the friction between particles greatly increased, causing an enhanced shear thickening property of the STFs. It could be simply demonstrated with the calculation of distance between particles for STFs prepared with various weight fractions of silica and it could also associated with the Van der waals forces between particles. These critical shear rates decrease and the maximum viscosity values after thickening increase as molecular weight of medium fluids decrease. Among the STFs prepared with fumed PEGs, the shear thickening behaviour was more significant in STFs prepared with PEG 200. The shear thickening effect started earlier in this system as compared to those prepared with PEG 300 and PEG 400.

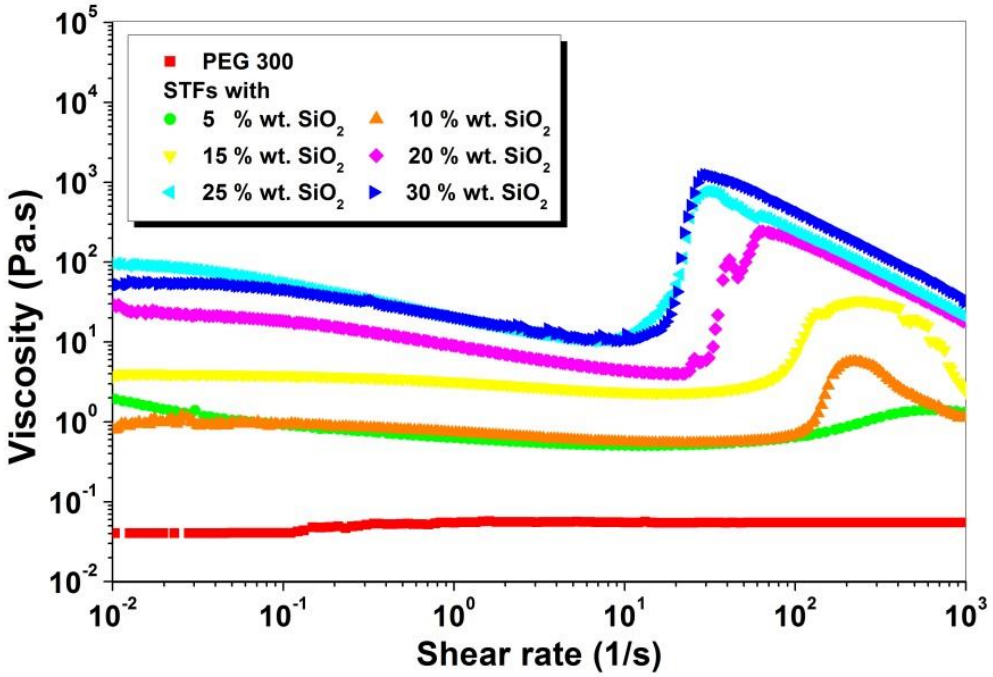

Figure 5.13. Steady shear viscosity vs. shear rate graph of STFs composed of PEG 300 and various weight fractions of fumed silica

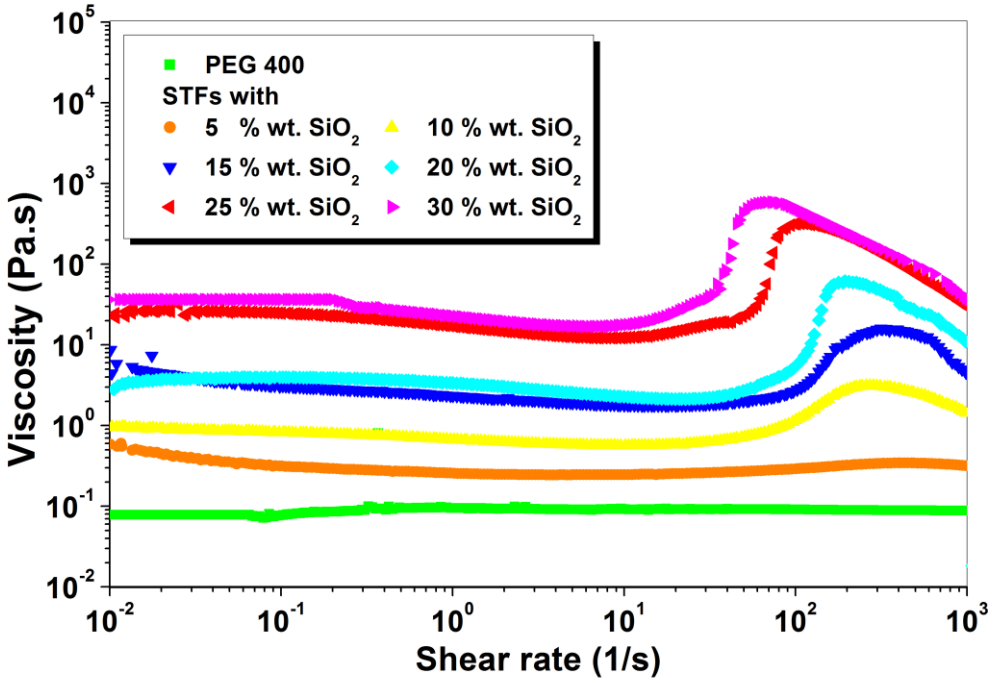

Figure 5.14. Steady shear viscosity vs. shear rate graph of STFs prepared with PEG 400 and various weight fractions of fumed silica

The range of shear rates in the shear thickening transition region and the viscosity values at these ranges for STFs prepared with various weight fractions of fumed silica together with PEG 300 and PEG 400 are given in Table 5.2 and 5.3, respectively.

Table 5.2. Range of shear rates and viscosity values of STFs prepared with fumed silica and PEG 300

Silica content in STFs (wt. %)	**Range of shear rates (s^{-1})**	**Viscosity values (Pa.s)**
5	-	-
10	119.2 - 219.5	0.8538 - 5.681
15	94.03-247.6	5.517 - 33.35
20	22.56 - 64.26	4.021 - 243.6
25	19.27 - 30.57	41.05 - 773.9
30	16.84 - 29.28	16 - 1241

Table 5.3. Range of shear rates and viscosity values of STFs prepared with fumed silica and PEG 400

Silica content in STFs (wt. %)	**Range of shear rates (s^{-1})**	**Viscosity values (Pa.s)**
5	-	-
10	79.59 - 271.2	0.9355 - 3.129
15	74.9 - 314.6	2.275 - 15.94
20	72.16 - 194.4	3.636 - 61.58
25	65.36 - 99.3	42.95 - 315.7
30	37.74 - 74.72	75.68 - 586.1

5.3.1.2. Colloidal Silica Based STFs

The steady-shear viscosity graphs of STFs containing colloidal silica together with PEG 200, PEG 300 and PEG 400 are shown in Figure 5.15, 5.16 and 5.17, respectively. Four different concentrations of STFs were prepared with 40, 50, 60 and 70 wt.% silica. Among these concentrations, the STF containing 70 wt. % silica was obtained in a solid like form after the grinding step. Therefore, the rheological mesurement were not be able to performed on these systems. As seen in the graphs, none of STFs containing of 40 and 50 wt. % colloidal silica do not show a shear thickening behaviour. STF samples prepared with 60 wt. % colloidal silica and together with PEG 300 and PEG 400 also do not show a thickening effect. Only, the STF containing 60 wt. % colloidal silica showed a minor increament in viscosity with 60 Pa.s maximum value. Colloidal silica is a spherical shaped and sphere silica does not form aggregates. Hence, the branch-shaped aggregates made up of fumed silica lead to a large increase in the viscosity of its STF. Therefore, the formation of hydrocluster happened easier in the STF consisting of fumed silica rather than in the STF consisting of sphere silica. In addition to that there might be some chemicals in the colloidal silica suspension to obtain a stable dispersion. Therefore, hydroclustering may not be easy for STFs prepared with colloidal silica.

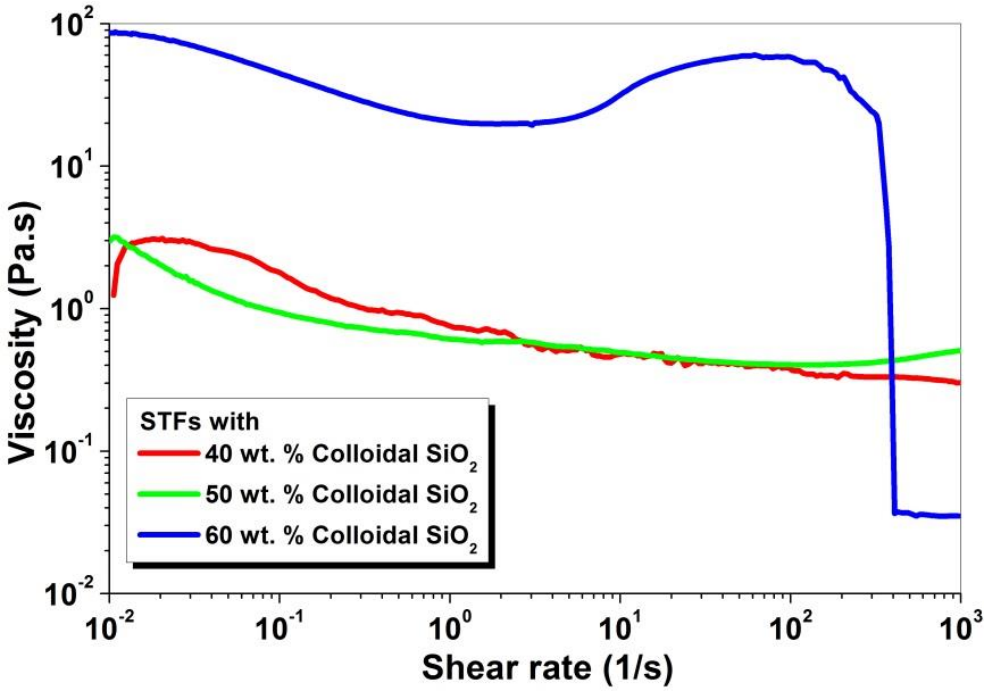

Figure 5.15. Steady shear viscosity vs. shear rate graph of STFs prepared with PEG 200 and varying weight fractions colloidal silica

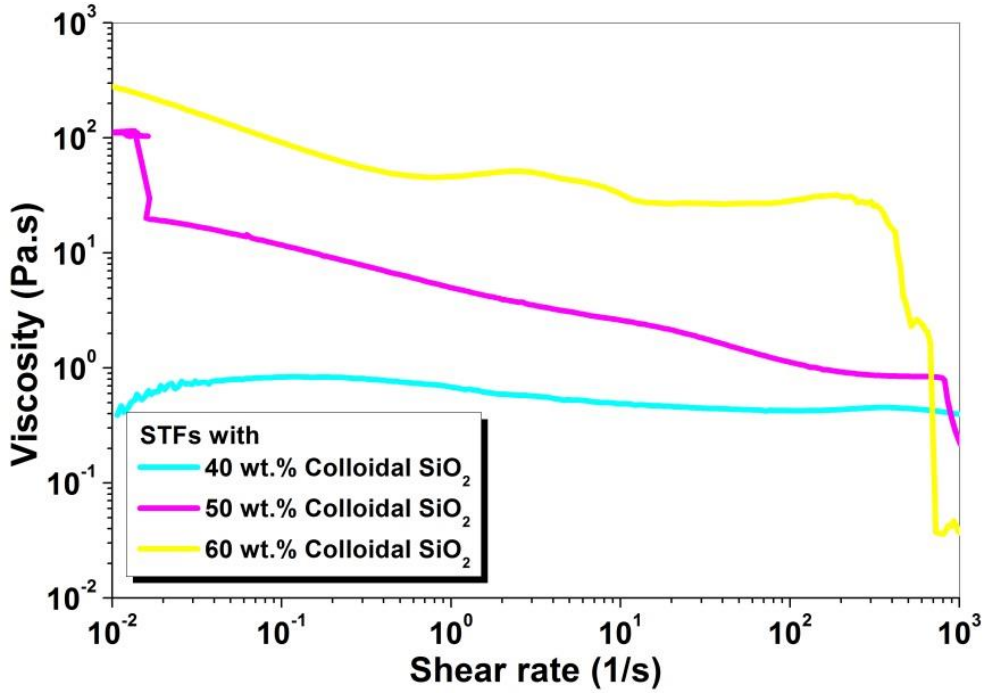

Figure 5.16. Steady shear viscosity vs. shear rate graph of STFs prepared with PEG 300 and varying weight fractions colloidal silica

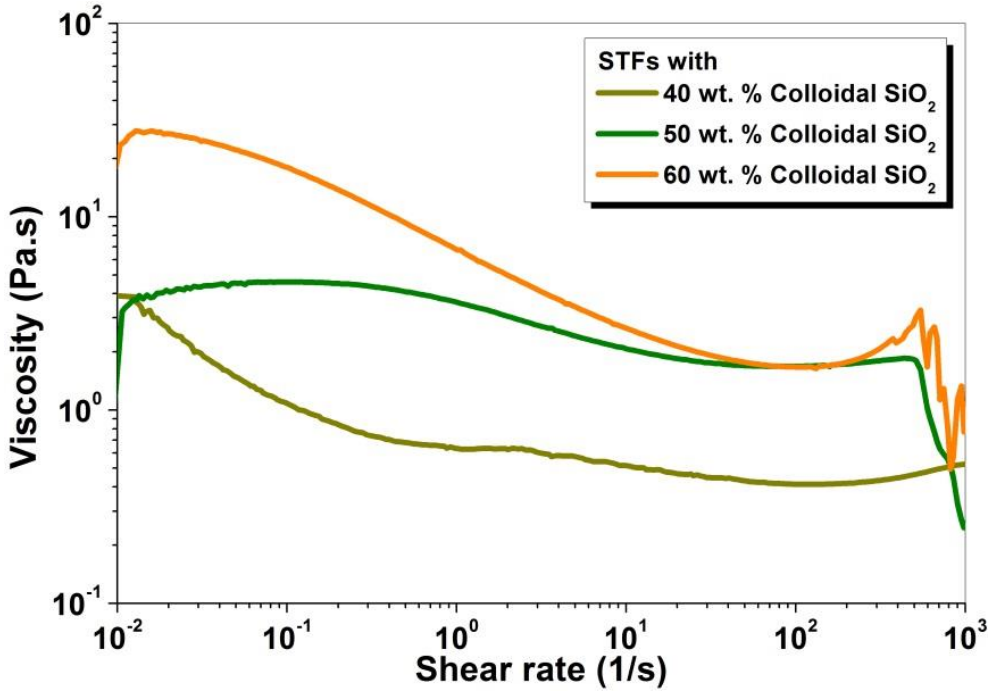

Figure 5.17. Steady shear viscosity vs. shear rate graph of STFs prepared with PEG 400 and varying weight fractions colloidal silica

5.3.2. Microstructural Features

5.3.2.1. Scanning Electron Microscopy (SEM)

The SEM image of STF containing 30 wt.% of fumed silica and 70 wt. % PEG 200 is shown in Figure 5.18. The image shows that silica nanoparticles were well coated with PEG and the silica nanoparticles were well dispersed in the solution.

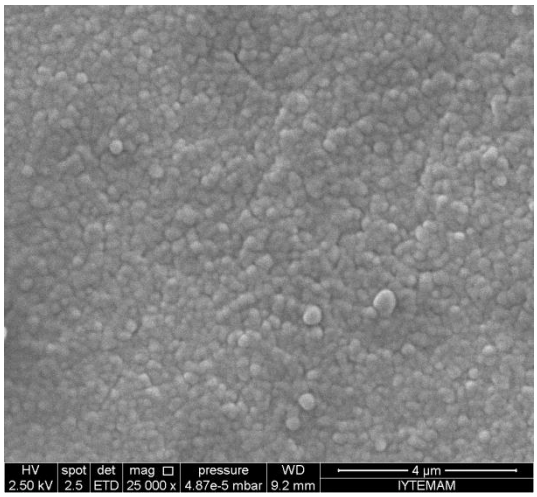

Figure 5.18. SEM image of STF containing 30 wt.% of fumed silica –70 wt. % PEG 200 (25000x magnification)

SEM image of STF containing of 30 wt. % of fumed silica – 70 wt. % PEG 300 is given in Figure 5.19. This image is at same magnification with the previous one. When the two images are compared, it seems that the STFs prepared with PEG 300 has larger grain as compared to those prepared with PEG 200. This might be due to the higher molecular weight of PEG 300.

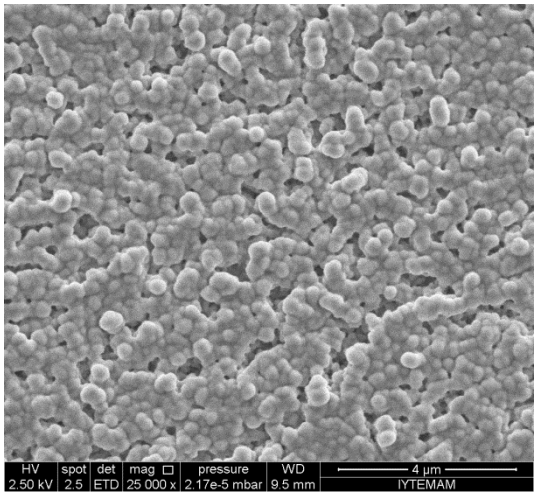

Figure 5.19. SEM image of STF containing 30 wt.% of fumed silica –70 wt. % PEG 300 (25000x magnification)

STF containing 10 wt.% of fumed silica – 90 wt. % PEG 400 was also subjected to microstructural characterization to reveal the effect of silica concentration on the dispersibility of STFs. The SEM image of this system at 2500x magnification is shown in Figure 5.20. It was difficult to capture an SEM image without charging on the

surface. Therefore, the highest magnification obtained was 2500X. SEM image shows that silica nanoparticles are relatively well dispersed within the PEG

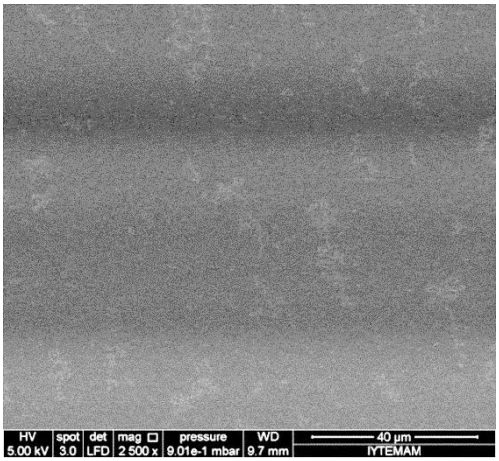

Figure 5.20. SEM image of STF containing 10 wt.% of fumed silica – 90 wt. % PEG 400 (2500X magnification)

SEM image of STF containing 60 wt.% of colloidal silica and 40 wt. % PEG 200's is shown in Figure 5.21. Different from fumed silica nanoparticles, colloidal silica nanoparticles seems well dispersed in the solution and they form a homogenized suspensions in the solution.

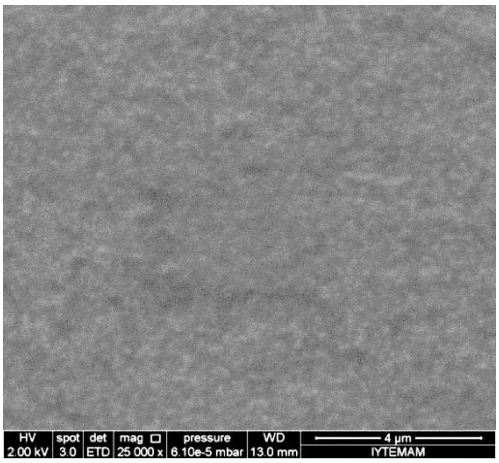

Figure 5.21. SEM image of STF containing 60 wt.% of colloidal silica – 40 wt. % PEG 300 (25000X magnification)

5.3.2.2. Dynamic Light Scattering (DLS)

The average particle sizes graphs of STF samples containing 30 wt. % fumed silica – 70 wt. % PEG 200 and 70 wt. % colloidal silica – 30 wt. % PEG 200 are shown Figure 5.22 and 5.23, respectively. The average particle size of STFs prepared with 30 wt. % fumed silica and PEG 200 and with 70 wt. % colloidal silica and PEG 200 was measured as 185 nm and 112 nm.

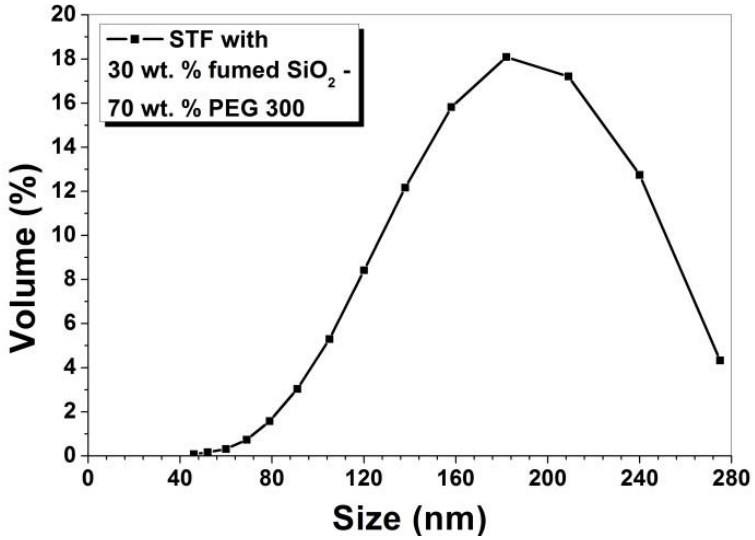

Figure 5.22. Size distributions of STF containing 30 wt. % fumed silica – 70 wt. % PEG 200 as a function of volume %

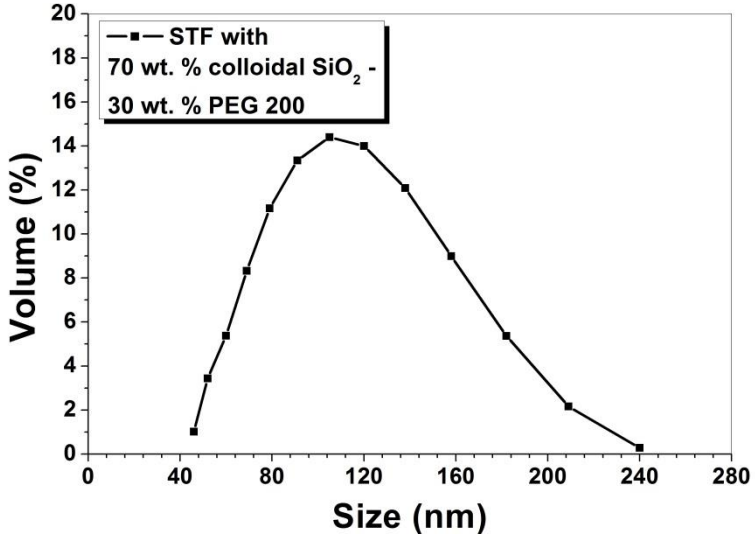

Figure 5.23. Size distributions of STF containing 70 wt. % colloidal silica – 30 wt. % PEG 200 as a function of volume %

5.3.3. Thermal Properties

5.3.3.1. Thermogravimetric Analysis (TGA)

Figure 5.24 shows typical thermogravimetric analysis (TGA) weight loss curves of neat PEG 300 and STFs containing 5 to 30 wt % of the fumed silica and PEG 300. As seen in the graph, neat PEG 300 starts to decompose at around 230 °C and the weight loss of the STFs continues after this temperature. At around 420 °C the decomposition of PEG is completed and no residue is observed. Figure 5.22 also shows the TGA thermograms of STFs prepared with various silica content. As the silica content increase, the decomposition of the PEG starts at lower temperatures. The graph shows that the decomposition of the PEG is completed the residue is silica added into the system. There is slight differences between the amount of the residual and the prepared concentration of STFs. This difference may be associated with the loss of some minimal amount of silicas during the syntesis of STFs. The residual weight percentage of silica was about 8, 11, 15, 18, 24 and 28 wt % for the corresponding concentrations of 5, 10, 15, 20, 25 and 30 wt %, respectively. These results also confirm the validity of STF sample preparations.

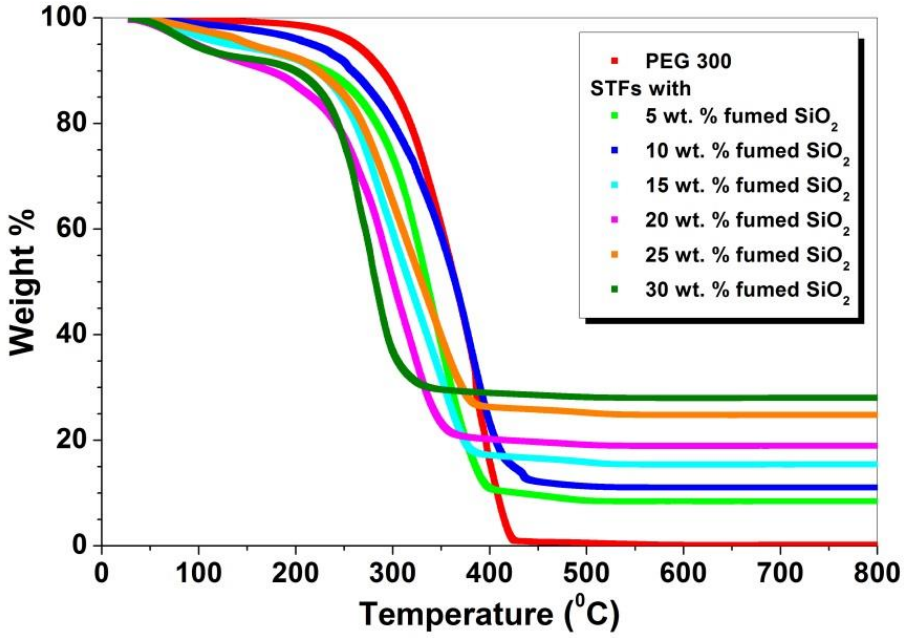

Figure 5.24. TGA thermograms of neat PEG 300 and STF samples prepared with fumed silica and PEG 300

5.4. Properties of STF/Fabric Composites

5.4.1. Scanning Electron Microscopy (SEM)

The SEM image of neat woven aramid fabric at 60X magnification and neat UHMWPE mat used within the experiment at 120X magnification are shown in Figure 5.25 and 5.26, respectively.

In order to characterize the impregnation of STFs on the fabric surfaces, microstructural characterization was applied onto the aramid and UHMWPE fabrics impregnated with STFs. As an example, Figure 5.27, 5.28 and 5.29 show the SEM images of aramid fabrics and Figure 5.30, 5.31 and 5.32 show UHMWPE fabrics impregnated with STFs containing 30 wt.% of fumed silica- 70 wt. % of PEG 300 at various magnifications, respectively. It was observed that fabric surfaces are well impregnated with STF solutions. The higher magnification SEM images better illustrates that the aramid fabrics were coated with STFs uniformly.

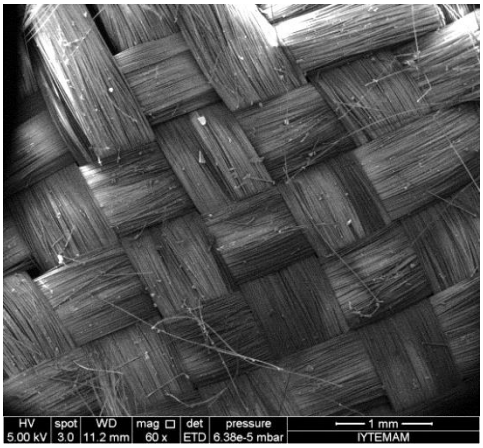

Figure 5.25. SEM image of neat woven aramid fabric (60X magnification)

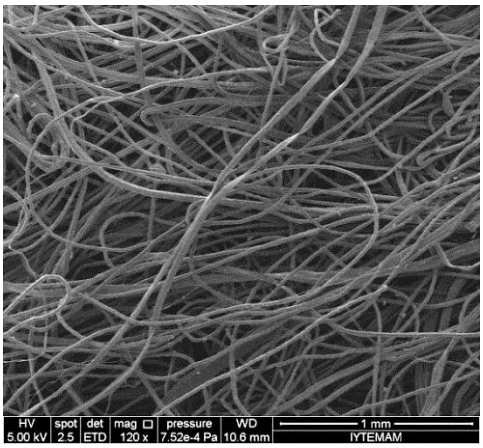

Figure 5.26. SEM image of neat UHMWPE mat (120X magnification)

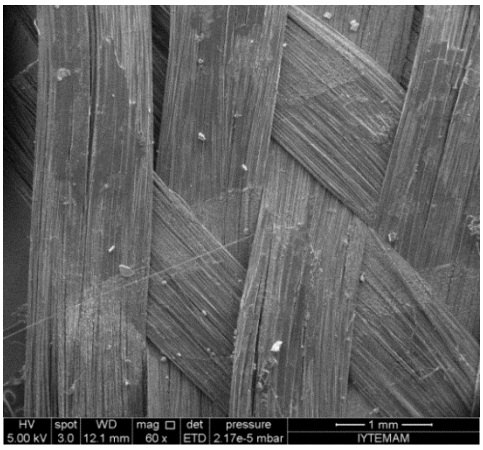

Figure 5.27. SEM image of aramid fabric impregnated with STFs containing 30 wt.% fumed silica - 70 wt. % of PEG 300 (60X magnification)

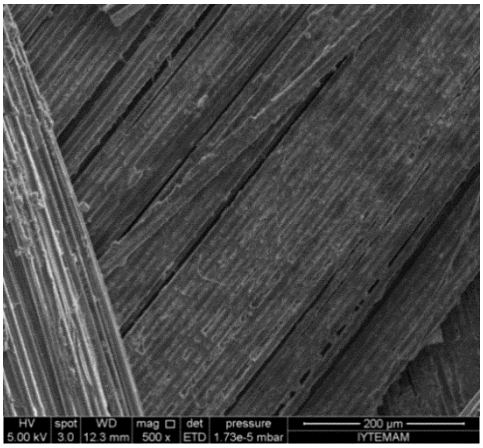

Figure 5.28. **S**EM image of aramid fabric impregnated with STFs containing 30 wt.% fumed silica - 70 wt. % of PEG 300 at (500X magnification)

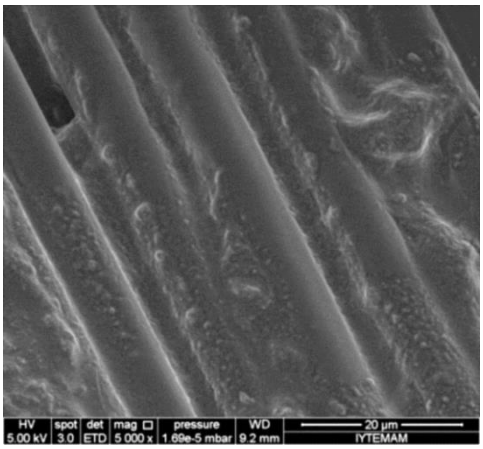

Figure 5.29. SEM image of aramid fabric impregnated with STFs containing 30 wt.% fumed silica - 70 wt. % of PEG 300 at (5000X magnification)

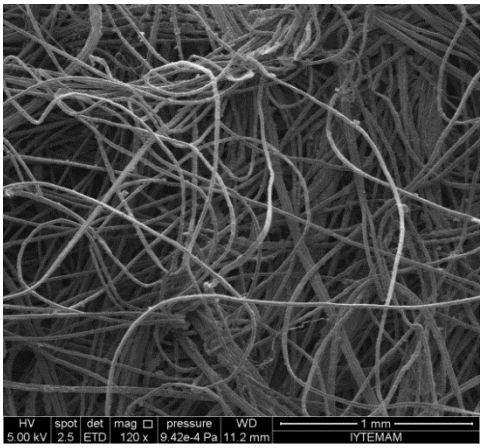

Figure 5.30. SEM image of UHMWPE mat impregnated with STFs containing 30 wt.% fumed silica - 70 wt. % of PEG 300 (120X magnification)

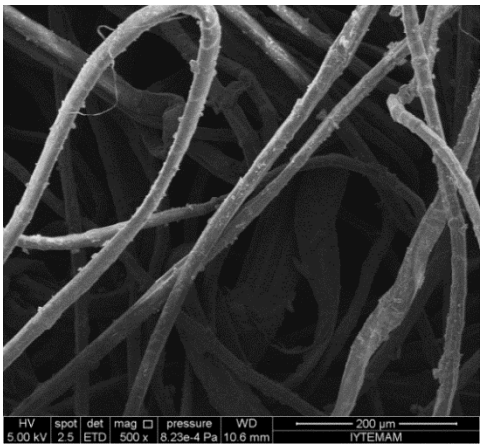

Figure 5.31. SEM image of UHMWPE mat impregnated with STFs containing 30 wt.% fumed silica - 70 wt. % of PEG 300 (500X magnification)

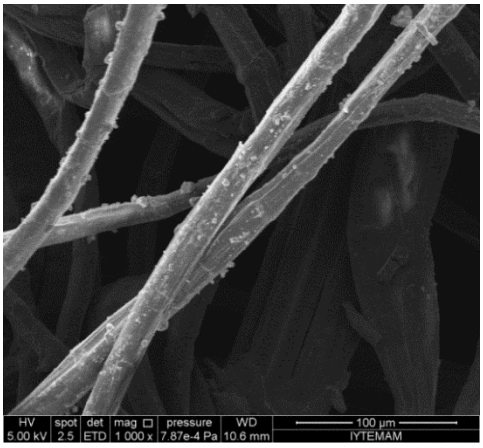

Figure 5.32. SEM image of UHMWPE mat impregnated with STFs containing 30 wt.% fumed silica - 70 wt. % of PEG 300 (1000X magnification)

The microstructural characterization was also performed with the aramid fabrics impregnated with STFs containing 70 wt.% colloidal SiO_2 - 30 wt. % of PEG 300. The SEM images of for this system at various magnifications are shown in Figure 5.33 and 5.34. The aramid fabrics were found to be coated uniformly by STF solutions in these figures. The STFs with colloidal silica forms a relatively thicker layer on the fabric surface, as compared to those with fumed silicas. The higher magnification image reveals the silica nanoparticles on the fabrics.

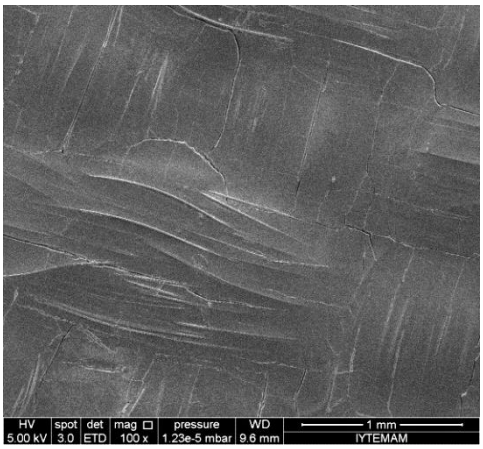

Figure 5.33. SEM image of aramid fabric impregnated with STFs containing 70 wt.% colloidal silica - 30 wt. % of PEG 300 (100X magnification)

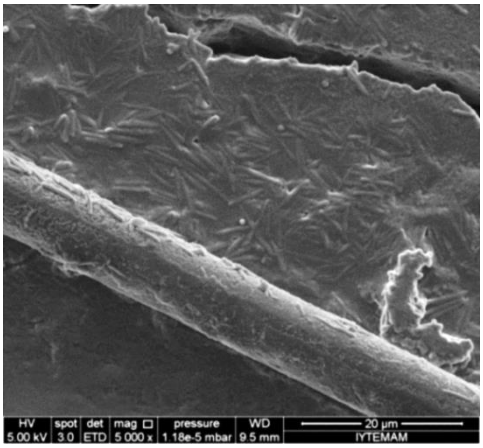

Figure 5.34. SEM image of aramid fabric impregnated with STFs containing 70 wt.% colloidal silica - 30 wt. % of PEG 300 (5000X magnification)

5.4.2. Mechanical Property Characterization

5.4.2.1. Quasi-static Stab Resistance

5.4.2.1.1. Fumed Silica Based STFs/Fabric Composites

The quasi-static stab resistance tests were applied onto the neat aramid fabrics and STF/aramid fabric systems prepared with fumed silica together with PEG 200, PEG 300, PEG 400. The load as a function of stab penetration depth graphs were obtained based on this test. The quasi-static test results are illustrated in Figure 5.35, 5.36 and

5.37 for fumed silica based STF/aramid systems prepared with PEG 200, PEG 300 and PEG 400, respectively. As seen from the graphs, all prepared STF/fabric targets exhibited significantly higher penetration load as compared to those for the neat fabric targets. The increament in silica content of the fluid improve the quasi-static stab resistance of STF/fabric systems due to more effective shear thickening behaviour.

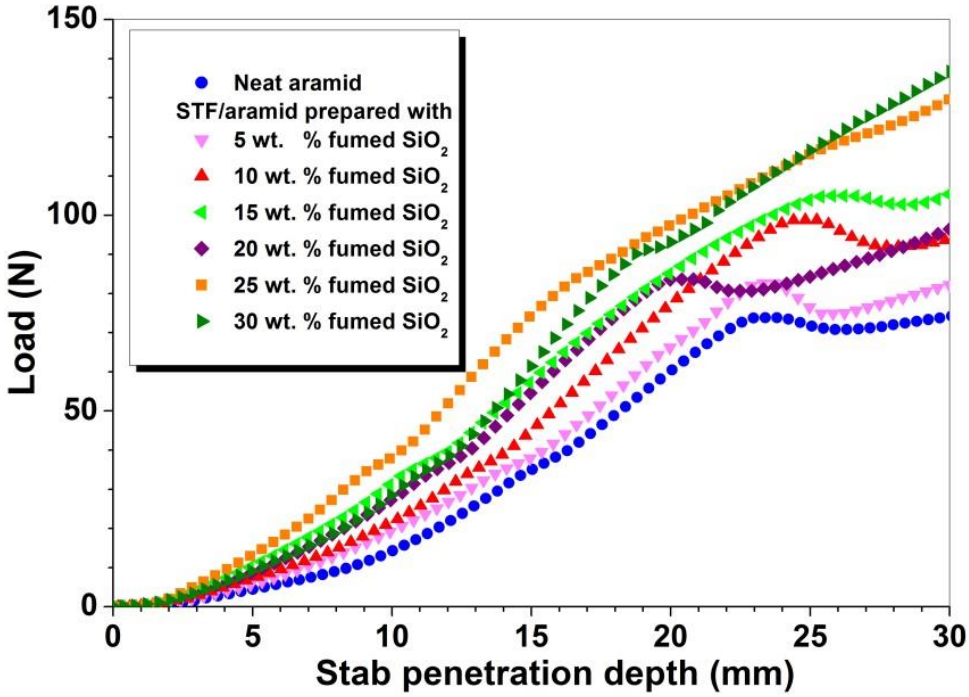

Figure 5.35. Load as a function of stab penetration depth graph of neat aramid fabric and STF/aramid composites containing STFs prepared with fumed silica and PEG 200

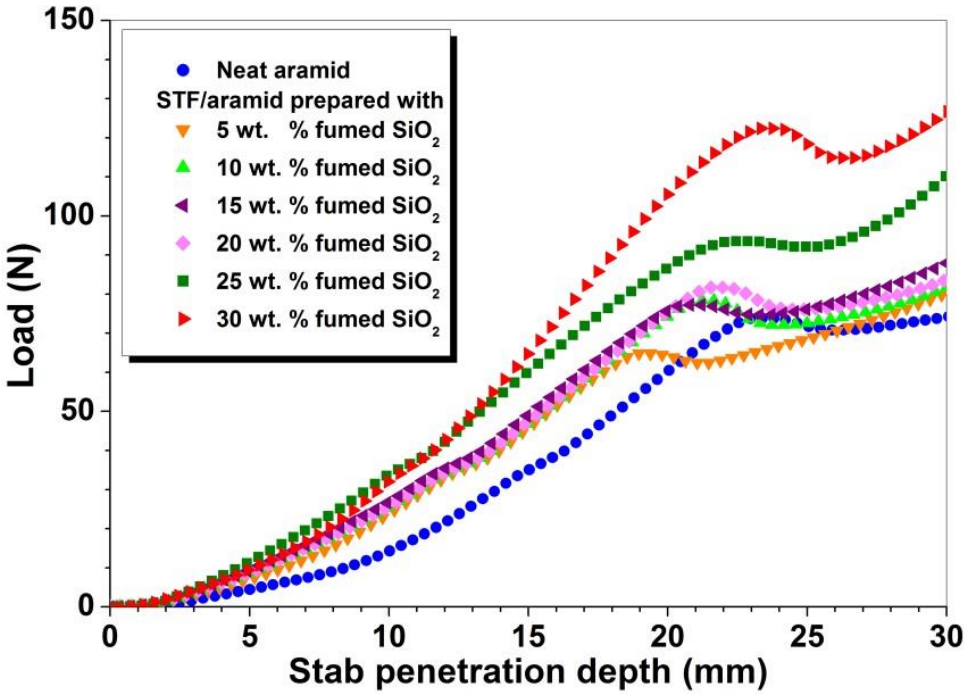

Figure 5.36. Load as a function of stab penetration depth graph of neat aramid fabric and STF/aramid composites containing STFs prepared with fumed silica and PEG 300

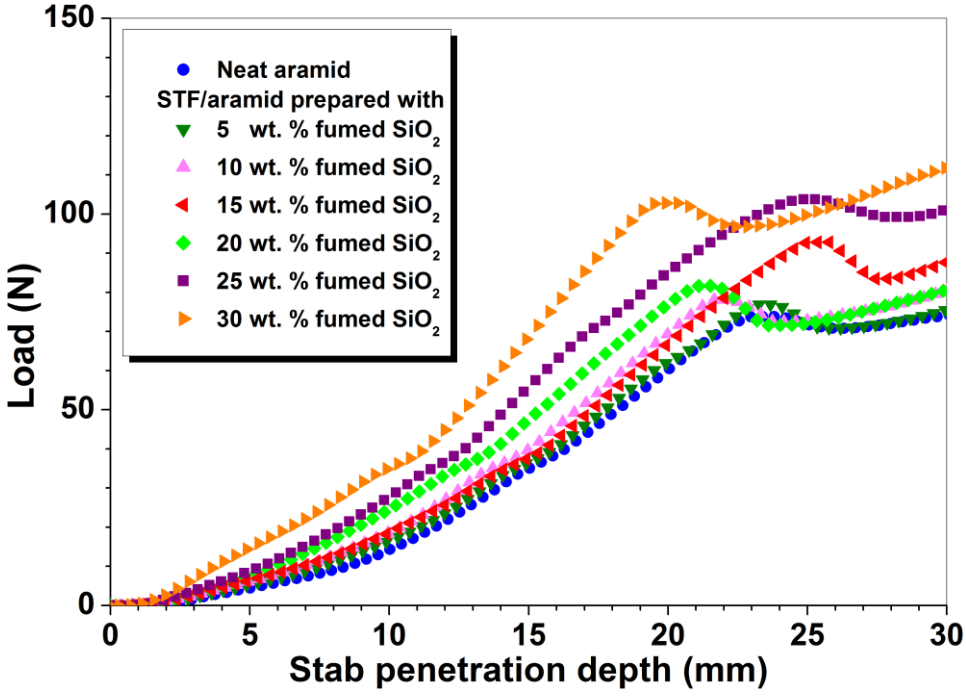

Figure 5.37. Load as a function of stab penetration depth graph of neat aramid fabric and STF/aramid composites containing STFs prepared with fumed silica and PEG 400

The quasi-static test results of neat aramid fabrics and STF/aramid fabric systems prepared with fumed silica together with PEG 200, PEG 300, PEG 400 are summarized in Table 5.4, 5.5 and 5.6, respectively. It was observed that the neat aramid fabric resists to load of 74 N at 30 mm stab penetration depth. Among the three different group (STFs prepared with PEG 200/PEG 300/PEG 400) fumed silica based STF/fabric composite samples, aramid fabric impregnated with STF containing 30 wt.% fumed silica and 70 wt. % of PEG 200 exhibited the highest quasi-static stab resistance with highest stab penetration load of 136.7 N at 30 mm penetration. This can be related with the highest shear thickening effect observed from this system based on the rheological measurements.

Table 5.4. Quasi-static stab test results for neat aramid fabric and STF/aramid composites containing STFs prepared with fumed silica and PEG 200

Stab test targets	**Load at 30 mm (N)**
Neat aramid	74.275
5 wt. % fumed SiO_2 – 95 wt. % PEG 200 STF/ aramid	83.125
10 wt. % fumed SiO_2 – 90 wt. % PEG 200 STF/ aramid	94.5
15 wt. % fumed SiO_2 – 85 wt. % PEG 200 STF/ aramid	97.725
20 wt. % fumed SiO_2 – 80 wt. % PEG 200 STF/ aramid	106.975
25 wt. % fumed SiO_2 – 75 wt. % PEG 200 STF/ aramid	131.7
30 wt. % fumed SiO_2 – 70 wt. % PEG 200 STF/ aramid	136.7

Table 5.5. Quasi-static stab test results for neat aramid fabric and STF/aramid composites containing STFs prepared with fumed silica and PEG 300

Stab test targets	**Load at 30 mm (N)**
Neat aramid	74.275
5 wt. % fumed SiO_2 – 95 wt. % PEG 300 STF/ aramid	81.175
10 wt. % fumed SiO_2 – 90 wt. % PEG 300 STF/ aramid	81.8
15 wt. % fumed SiO_2 – 85 wt. % PEG 300 STF/ aramid	84.65
20 wt. % fumed SiO_2 – 80 wt. % PEG 300 STF/ aramid	89.3
25 wt. % fumed SiO_2 – 75 wt. % PEG 300 STF/ aramid	112.925
30 wt. % fumed SiO_2 – 70 wt. % PEG 300 STF/ aramid	126.7

Table 5.6. Quasi-static stab test results for neat aramid fabric and STF/aramid composites containing STFs prepared with fumed silica and PEG 400

Stab test targets	Load at 30 mm (N)
Neat aramid	74.275
5 wt. % fumed SiO_2 – 95 wt. % PEG 400 STF/ aramid	76.325
10 wt. % fumed SiO_2 – 90 wt. % PEG 400 STF/ aramid	80.425
15 wt. % fumed SiO_2 – 85 wt. % PEG 400 STF/ aramid	81.275
20 wt. % fumed SiO_2 – 80 wt. % PEG 400 STF/ aramid	88.7
25 wt. % fumed SiO_2 – 75 wt. % PEG 400 STF/ aramid	101.825
30 wt. % fumed SiO_2 – 70 wt. % PEG 400 STF/ aramid	113.7

5.4.2.1.2. Colloidal Silica Based STFs/Fabric Composites

The quasi-static stab resistance tests were also performed with STF/aramid fabric systems prepared with colloidal silica together with PEG 200, PEG 300, PEG 400. The quasi-static test results are illustrated in Figure 5.38, 5.39 and 5.40 for colloidal silica based STF/aramid systems prepared with PEG 200, PEG 300 and PEG 400, respectively. As seen from these three graphs, the quasi-static stab resistances of aramid fabrics impregnated with 40 and 50 wt. % of colloidal silica are lower and the aramid fabrics impregnated with 60 and 70 wt. % of colloidal silica show higher quasi-static stab resistances as compared to those for neat aramid fabrics.

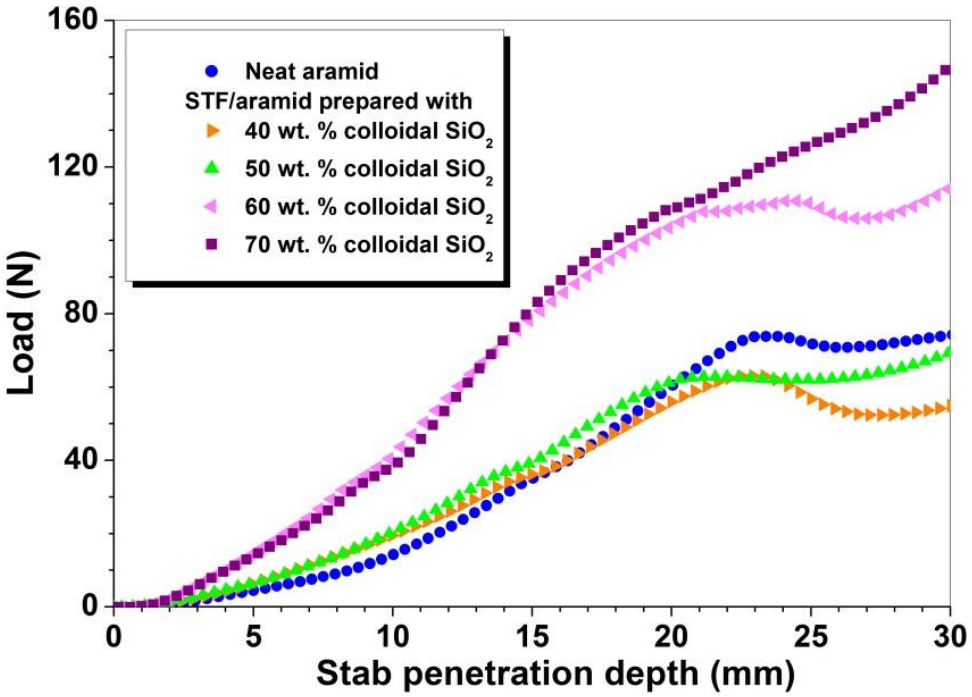

Figure 5.38. Load as a function of stab penetration depth graph of neat aramid fabric and STF/aramid composites containing STFs prepared with colloidal silica and PEG 200

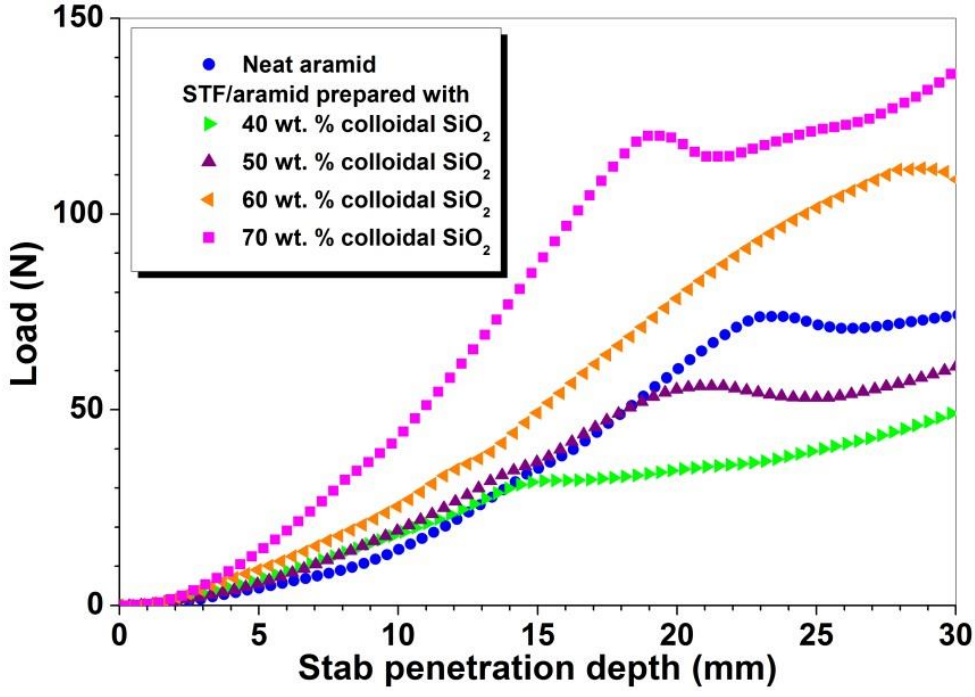

Figure 5.39. Load as a function of stab penetration depth graph of neat aramid fabric and STF/aramid composites containing STFs prepared with colloidal silica and PEG 300

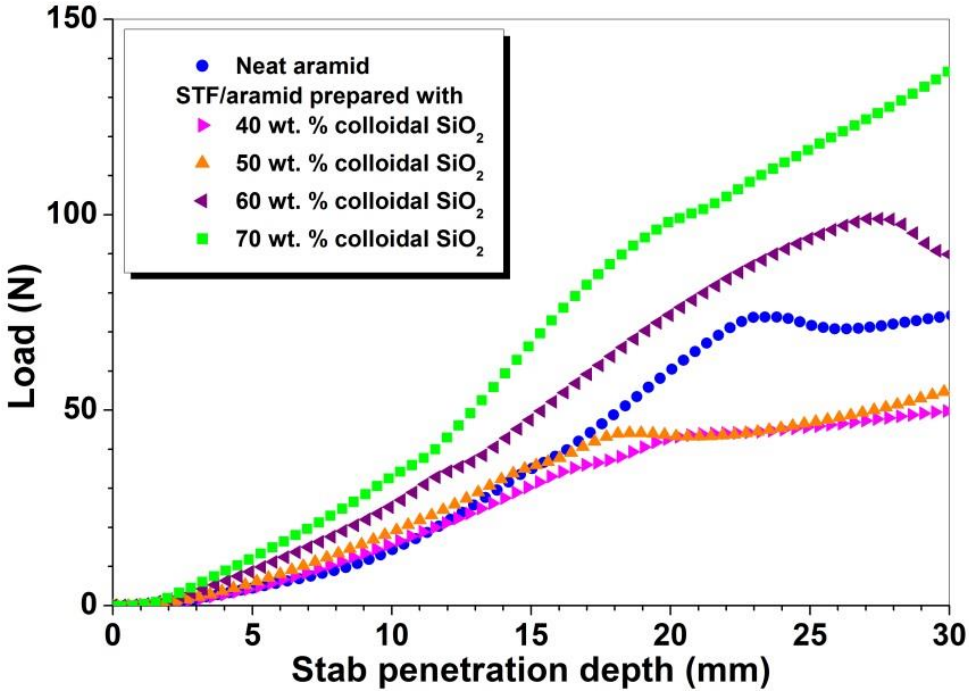

Figure 5.40. Load as a function of stab penetration depth graph of neat aramid fabric and STF/aramid composites containing STFs prepared with colloidal silica and PEG 400

The quasi-static test results of neat aramid fabrics and STF/aramid fabric systems prepared with colloidal silica together with PEG 200, PEG 300, PEG 400 are summarized in Table 5.7, 5.8 and 5.9, respectively. It was observed that as increasing the silica content in the fluids, the quasi-static stab resistances improve. It was also seen from the values, the most effective STF/aramid system is those prepared with PEG 200. Fabric impregnated with STF containing 70 wt.% colloidal silica has load of 149 N. These value is higher as compared to those for fumed silica based STF/aramid fabric systems. This effect could be due to the higher silica content in the fluids. Silica nanoparticles in these fluids restricts their movement which cause the enhancement in stab resistance. The colloidal silica used in the study consist of 40 wt. % silica. the load of STFs containing 40 and 50 wt.% colloidal silica prepared with PEG 200, PEG 300 and PEG 400 that resist are lower as compared to those for neat fabrics due to the lower silica content in the fluid.

Table 5.7. Quasi-static stab test results for neat aramid fabric and STF/aramid composites containing STFs prepared with colloidal silica and PEG 200

Stab test targets	Load at 30 mm (N)
Neat aramid	74.275
40 wt. % colloidal SiO_2 – 60 wt. % PEG 200 STF/ aramid	54.875
50 wt. % colloidal SiO_2 – 50 wt. % PEG 200 STF/ aramid	70.55
60 wt. % colloidal SiO_2 – 40 wt. % PEG 200 STF/ aramid	116.025
70 wt. % colloidal SiO_2 – 30 wt. % PEG 200 STF/ aramid	149.275

Table 5.8. Quasi-static stab test results for neat aramid fabric and STF/aramid composites containing STFs prepared with colloidal silica and PEG 300

Stab test targets	Load at 30 mm (N)
Neat aramid	74.275
40 wt. % colloidal SiO_2 – 60 wt. % PEG 300 STF/ aramid	50.25
50 wt. % colloidal SiO_2 – 50 wt. % PEG 300 STF/ aramid	61.05
60 wt. % colloidal SiO_2 – 40 wt. % PEG 300 STF/ aramid	108.825
70 wt. % colloidal SiO_2 – 30 wt. % PEG 300 STF/ aramid	140.825

Table 5.9. Quasi-static stab test results for neat aramid fabric and STF/aramid composites containing STFs prepared with colloidal silica and PEG 400

Stab test targets	Load at 30 mm (N)
Neat aramid	74.275
40 wt. % colloidal SiO_2 – 60 wt. % PEG 400 STF/ aramid	50.15
50 wt. % colloidal SiO_2 – 50 wt. % PEG 400 STF/ aramid	55.6
60 wt. % colloidal SiO_2 – 40 wt. % PEG 400 STF/ aramid	89.95
70 wt. % colloidal SiO_2 – 30 wt. % PEG 400 STF/ aramid	138.275

5.4.2.2. Dynamic Stab Resistance

5.4.2.2.1. Fumed Silica Based STFs/Fabric Composites

Penetration depth as a function of impact velocity graph for the neat aramid fabric and STF/aramid composites containing STFs prepared with fumed silica and PEG

300 is illustrated in Figure 5.41. The three impact velocities used during the tests are marked on the graph.

For all impact velocities, neat aramid fabric target exhibited the lowest stab resistance with the highest penetration depths. With increasing silica concentration, the resistance to stab of targets improved. It was observed that targets containing STF prepared with 30 wt. % silica exhibited the least penetration depth and the highest stab resistance. However, as expected as, the impact velocity increased, penetration depth of all targets increased. The penetration depth values for the STF/aramid composites prepared with various weight fractions of fumed silica and PEG 300 are given in Table 5.10.

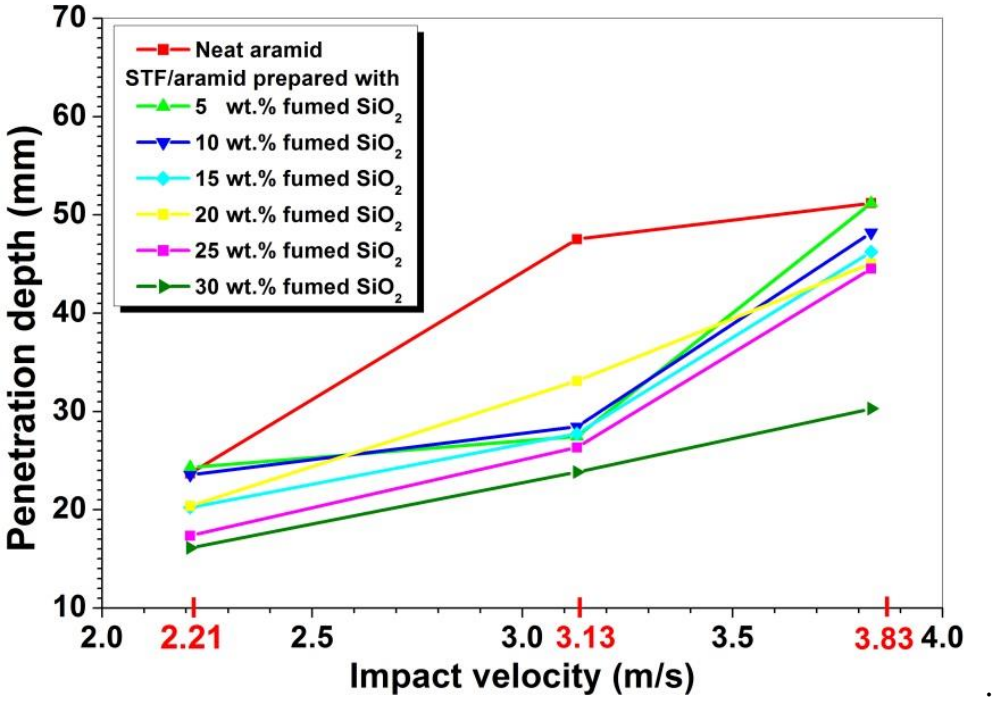

Figure 5.41. Dynamic stab test results for neat aramid fabric and STF/aramid composites containing STFs prepared with fumed silica and PEG 300

Table 5.10. Dynamic stab test results for neat aramid fabric and STF samples prepared with fumed silica and PEG 300

Targets	Impact Velocity (m/s)	Penetration Depth (mm)
Neat aramid	2.21 3.13 3.83	23.68 47.52 51.20
5 wt. % fumed SiO_2 – 95 wt. % PEG 300 STF/ aramid	2.21 3.13 3.83	24.32 27.46 51.20
10 wt. % fumed SiO_2 – 90 wt. % PEG 300 STF/ aramid	2.21 3.13 3.83	23.56 28.45 48.2
15 wt. % fumed SiO_2 – 85 wt. % PEG 300 STF/ aramid	2.21 3.13 3.83	20.22 27.74 46.23
20 wt. % fumed SiO_2 – 80 wt. % PEG 300 STF/ aramid	2.21 3.13 3.83	20.39 33.11 45.04
25 wt. % fumed SiO_2 – 75 wt. % PEG 300 STF/ aramid	2.21 3.13 3.83	17.37 26.33 44.54
30 wt. % fumed SiO_2 – 70 wt. % PEG 300 STF/ aramid	2.21 3.13 3.83	16.12 23.84 30.29

Figure 5.42 shows the example images of neat aramid fabric and STF/aramid composites containing STF with 30 wt.% silica during and after dynamic stab test at a 2.21 m/s spike impact velocity. It was clearly seen that, neat fabrics have higher penetration depth as compared to those for STF/aramid systems.

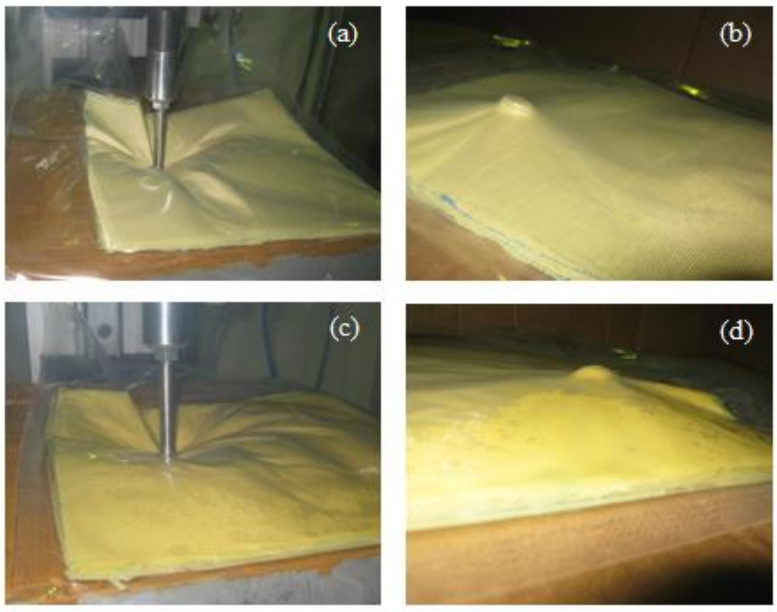

Figure 5.42. Images for neat aramid fabric (a) during, (b) after dynamic stab test and STF/aramid composites containing STF prepared with 30 wt.% fumed silica and 70 wt. % PEG 300 (c) during, (d) after dynamic stab test

5.4.3. Flexibility Properties

In order to obtain the flexibility behaviours of neat aramid fabric, flexibility test was performed onto neat fabric and with the measurements of bending at the end of the sample bending angle was ontained. Bending angle is a measure of target flexibility, with larger angles indicating greater flexibility. The images of neat fabric before and after flexibility test is presented in Figure 5.43. Neat aramid exhibited the highest flexibility with 24^{o} bending angle.

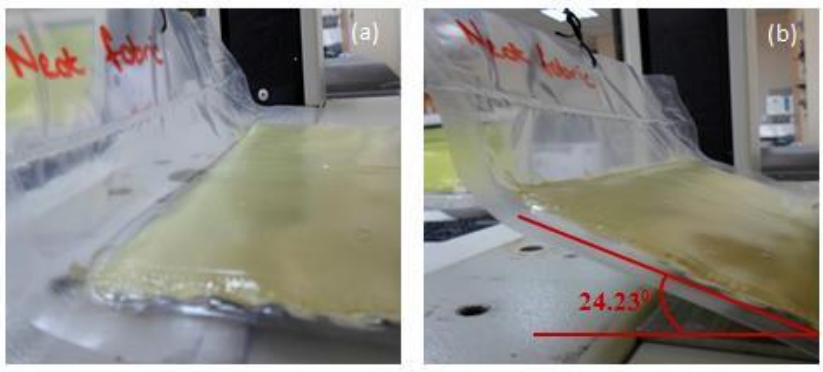

Figure 5.43. Images of neat aramid fabric (a) before and (b) after flexibility test

5.4.3.1. Fumed Silica Based STFs/Fabric Composites

The flexibility tests were also applied onto STF/aramid fabric systems prepared with fumed silica together with PEG 200, PEG 300, PEG 400. The flexibility test results of these STF/aramid fabrics are shown in Figure 5.44, 5.45 and 5.46, respectively. The bending angles of these STF/aramid fabric systems are measured and compared with the neat aramid fabric. As seen from the graphs, the bending angles of STF/aramid fabric systems are lower as compared to this for neat aramid target.

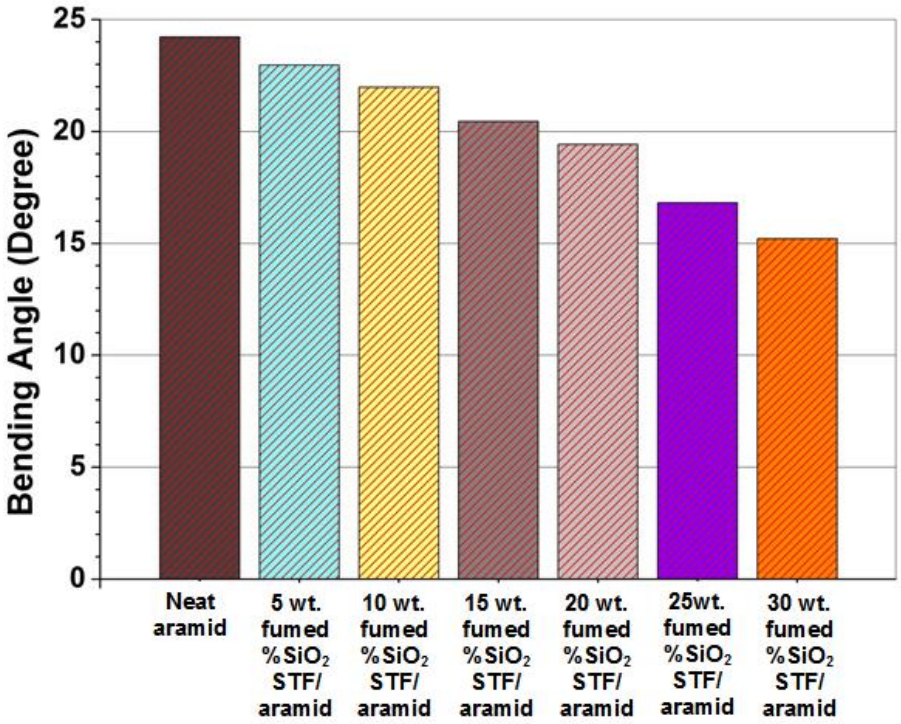

Figure 5.44. Flexibility test results for neat aramid fabric and STF/aramid composites containing STFs prepared with fumed silica and PEG 200

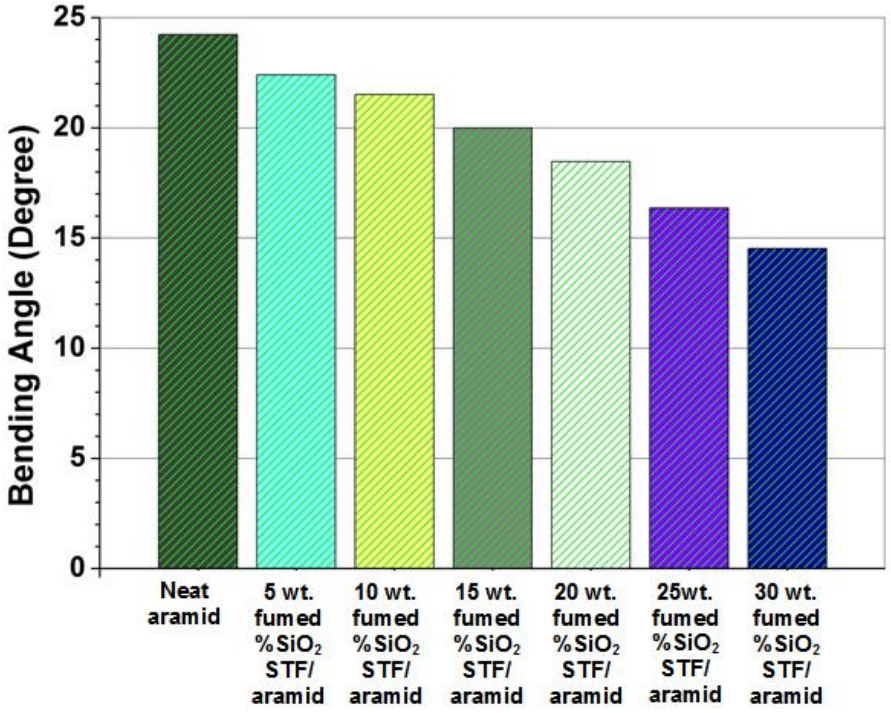

Figure 5.45. Flexibility test results for neat aramid fabric and STF/aramid composites containing STFs prepared with fumed silica and PEG 300

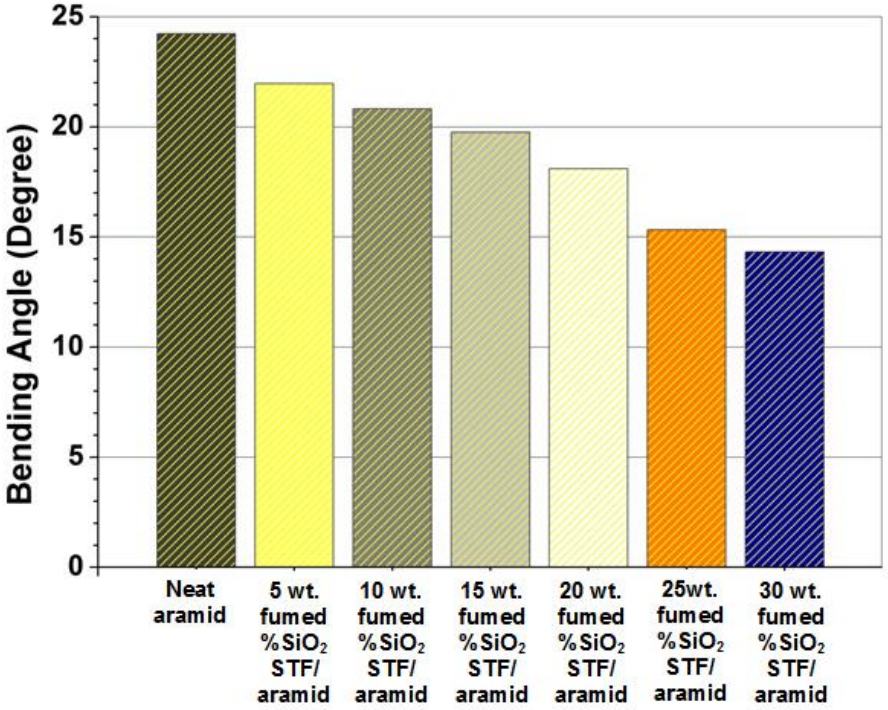

Figure 5.46. Flexibility test results for neat aramid fabric and STF/aramid composites containing STFs prepared with fumed silica and PEG 400

The flexibility test results of neat aramid fabrics and STF/aramid fabric systems prepared with fumed silica together with PEG 200, PEG 300, PEG 400 are summarized in Table 5.11, 5.12 and 5.13, respectively. Among all prepared STF/fabric composites containing fumed silica and PEG 200/PEG 300/PEG 400 and neat fabric, neat fabric was the most flexible target with highest bending angle. With increasing silica concentration and molecular weight of medium fluid, bending angle and flexibility decreased. However, this decreament is in expected limits and can be acceptable. It is important to point out that these fabrics used in the flexibility test are larger as compared to the fabrics used in the literature fabric having sizes of 51 mmx51 mm. (Hassan, Rangari, and Jeelani 2010). Therefore, these test results are more accurate.

Table 5.11. Flexibility test results for neat aramid fabric and STF/aramid composites containing STFs prepared with fumed silica and PEG 200

Targets	**Bending at the end of the sample (mm)**	**(Extension/ 100 mm)**	**Bending angle, α (^{o}) Tan^{-1} (Extension/ 100 mm)**
Neat aramid	45	0.45	24.23
5 wt. % fumed SiO_2 – 95 wt. % PEG 200 STF/ aramid	42.37	0.4237	22.962
10 wt. % fumed SiO_2 – 90 wt. % PEG 200 STF/ aramid	40.35	0.4035	21.974
15 wt. % fumed SiO_2 – 85 wt. % PEG 200 STF/ aramid	37.28	0.3728	20.445
20 wt. % fumed SiO_2 – 80 wt. % PEG 200 STF/ aramid	35.26	0.3526	19.423
25 wt. % fumed SiO_2 – 75 wt. % PEG 200 STF/ aramid	30.23	0.3023	16.82
30 wt. % fumed SiO_2 – 70 wt. % PEG 200 STF/ aramid	27.2	0.272	15.216

Table 5.12. Flexibility test results for neat aramid fabric and STF/aramid composites containing STFs prepared with fumed silica and PEG 300

Targets	**Bending at the end of the sample (mm)**	**(Extension/ 100 mm)**	**Bending angle, α (°) Tan^{-1} (Extension/ 100 mm)**
Neat aramid	45	0.45	24.23
5 wt. % fumed SiO_2 – 95 wt. % PEG 300 STF/ aramid	41.23	0.4123	22.406
10 wt. % fumed SiO_2 – 90 wt. % PEG 300 STF/ aramid	39.41	0.3941	21.509
15 wt. % fumed SiO_2 – 85 wt. % PEG 300 STF/ aramid	36.4	0.364	20.002
20 wt. % fumed SiO_2 – 80 wt. % PEG 300 STF/ aramid	33.38	0.3338	18.459
25 wt. % fumed SiO_2 – 75 wt. % PEG 300 STF/ aramid	29.37	0.2937	16.368
30 wt. % fumed SiO_2 – 70 wt. % PEG 300 STF/ aramid	25.9	0.259	14.521

Table 5.13. Flexibility test results for neat aramid fabric and STF/aramid composites containing STFs prepared with fumed silica and PEG 400

Targets	**Bending at the end of the sample (mm)**	**(Extension/ 100 mm)**	**Bending angle, α (°) Tan^{-1} (Extension/ 100 mm)**
Neat aramid	45	0.45	24.228
5 wt. % fumed SiO_2 – 95 wt. % PEG 400 STF/ aramid	40.34	0.4034	21.969
10 wt. % fumed SiO_2 – 90 wt. % PEG 400 STF/ aramid	38.03	0.3803	20.822
15 wt. % fumed SiO_2 – 85 wt. % PEG 400 STF/ aramid	35.92	0.3592	19.758
20 wt. % fumed SiO_2 – 80 wt. % PEG 400 STF/ aramid	32.67	0.3267	18.092
25 wt. % fumed SiO_2 – 75 wt. % PEG 400 STF/ aramid	27.4	0.274	15.323
30 wt. % fumed SiO_2 – 70 wt. % PEG 400 STF/ aramid	25.33	0.2533	14.322

5.4.3.2. Colloidal Silica Based STFs/Fabric Composites

The flexibility tests were also performed with STF/aramid fabric systems prepared with colloidal silica together with PEG 200, PEG 300, PEG 400. The flexibility test results of these STF/aramid fabrics are shown in Figure 5.47, 5.48 and 5.49, respectively. As seen from the graphs, the bending angles of STF/aramid fabric systems are lower as compared to this for neat aramid target. The STFs consisting of 40 and 50 wt. % colloidal silica have very close bending angles as compared to neat fabrics. However, the STFs with a 60 and 70 wt. % of colloidal silica have very low bending angle. In addition, they are rigid as compared to those for composites prepared with fumed silica.

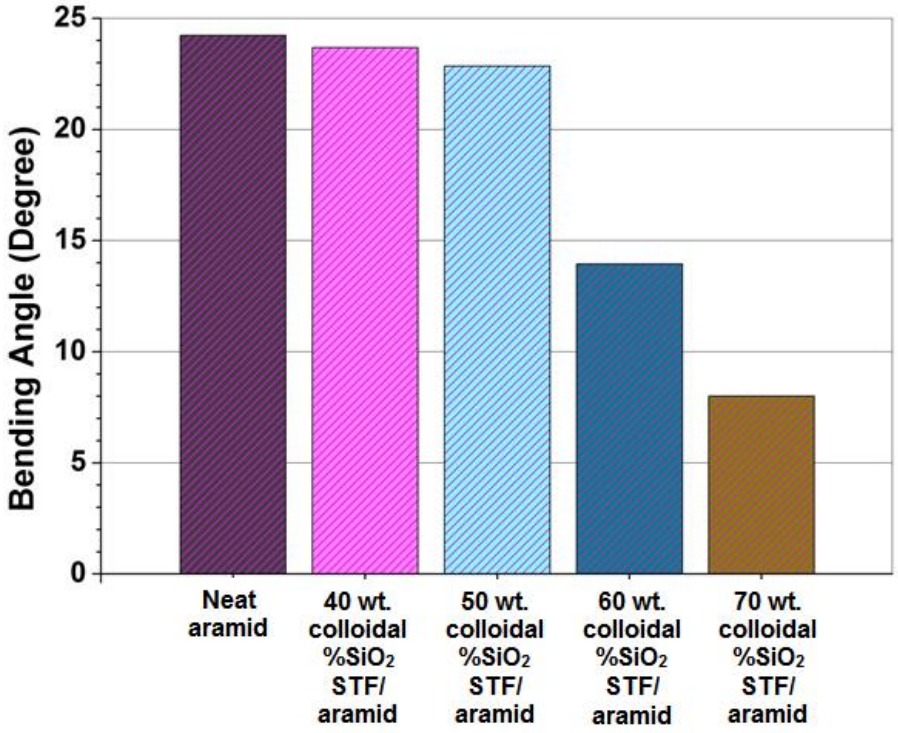

Figure 5.47. Flexibility test results for neat aramid fabric and STF/aramid composites containing STFs prepared with colloidal silica and PEG 200

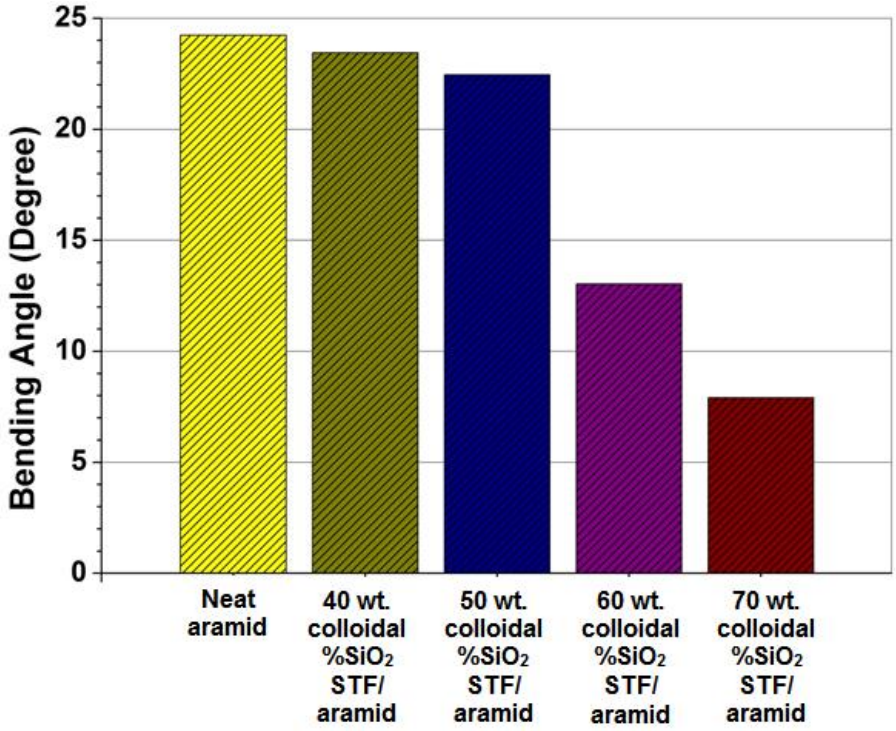

Figure 5.48. Flexibility test results for neat aramid fabric and STF/aramid composites containing STFs prepared with colloidal silica and PEG 300

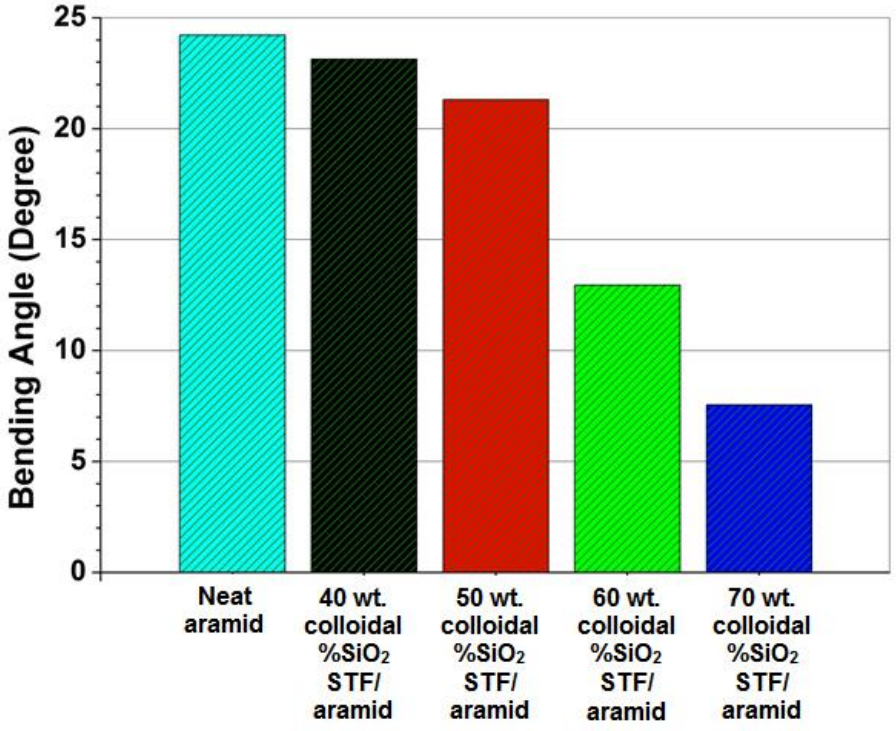

Figure 5.49. Flexibility test results for neat aramid fabric and STF/aramid composites containing STFs prepared with colloidal silica and PEG 400

The flexibility test results of neat aramid fabrics and STF/aramid fabric systems prepared with colloidal silica silica together with PEG 200, PEG 300, PEG 400 are summarized in Table 5.14, 5.15 and 5.16, respectively. Results show that neat fabric exhibits highest bendig angle. STFs consisting of 40 and 50 wt. % of colloidal silica impregnated aramid fabrics, significant decrasing is not observed in bending angle, but when the silica content in the fluid is increased to the 60 and 70 wt. %, the difference in bending angles of neat fabric and these composites become larger.

Table 5.14. Flexibility test results for neat aramid fabric and STF/aramid composites containing STFs prepared with colloidal silica and PEG 200

Targets	**Bending at the end of the sample (mm)**	**(Extension/ 100 mm)**	**Bending angle, α (^{o}) Tan^{-1} (Extension/ 100 mm)**
Neat aramid	45	0.45	24.228
40 wt. % colloidal SiO_2 – 60 wt. % PEG 200 STF/ aramid	43.87	0.4387	23.687
50 wt. % colloidal SiO_2 – 50 wt. % PEG 200 STF/ aramid	42.13	0.4213	22.846
60 wt. % colloidal SiO_2 – 40 wt. % PEG 200 STF/ aramid	24.84	0.2484	13.95
70 wt. % colloidal SiO_2 – 30 wt. % PEG 200 STF/ aramid	14.06	0.1406	8.003

Table 5.15. Flexibility test results for neat aramid fabric and STF/aramid composites containing STFs prepared with colloidal silica and PEG 300

Targets	**Bending at the end of the sample (mm)**	**(Extension/ 100 mm)**	**Bending angle, α (^{o}) Tan^{-1} (Extension/ 100 mm)**
Neat aramid	45	0.45	24.228
40 wt. % colloidal SiO_2 – 60 wt. % PEG 300 STF/ aramid	43.38	0.4338	23.451
50 wt. % colloidal SiO_2 – 50 wt. % PEG 300 STF/ aramid	41.29	0.4129	22.436
60 wt. % colloidal SiO_2 – 40 wt. % PEG 300 STF/ aramid	23.14	0.2314	13.029
70 wt. % colloidal SiO_2 – 30 wt. % PEG 300 STF/ aramid	13.9	0.139	7.913

Table 5.16. Flexibility test results for neat aramid fabric and STF/aramid composites containing STFs prepared with colloidal silica and PEG 400

Targets	**Bending at the end of the sample (mm)**	**(Extension/ 100 mm)**	**Bending angle, α (^{o}) Tan^{-1} (Extension/ 100 mm)**
Neat aramid	45	0.45	24.228
40 wt. % colloidal SiO_2 – 60 wt. % PEG 400 STF/ aramid	42.73	0.4273	23.137
50 wt. % colloidal SiO_2 – 50 wt. % PEG 400 STF/ aramid	39.01	0.3901	21.311
60 wt. % colloidal SiO_2 – 40 wt. % PEG 400 STF/ aramid	23	0.23	12.953
70 wt. % colloidal SiO_2 – 30 wt. % PEG 400 STF/ aramid	13.26	0.1326	7.553

5.4.4. Ballistic Properties

In order to determine the ballistic performance of the composite samples prepared, ballistic test with 9 mm parabellum projecile test and V_{50} ballistic test with FSP projectile were performed.

The 10 layers of neat fabric and STF/aramid fabric composite containing STF prepared with 30 wt. % fumed silica and 70 wt. % PEG 200 having sizes of 20 cm x 20 cm were conducted to 9 mm parabellum test. The projectile was not stopped in neat fabric, the puncture was observed at 454 m/sec projectile velocity and hence the deformation was not measured. Whereas, STF/aramid fabric composite containing STF prepared with 30 wt. % fumed silica and 70 wt. % PEG 200 showed significantly less penetration depth as compared to neat fabric. The composite was not punctured and it was resisted to 454 m/sec projectile velocity with a 55 mm deformation. The image of the neat fabric before ballistic test is seen in Figure 5.50. The front and back side images after ballistic test of neat fabric and STF/aramid fabric composite containing STF prepared with 30 wt. % fumed silica and 70 wt. % PEG 200 are seen in Figure 5.51 and 5.52, respectively.

Figure 5.50. Front image of neat fabric before ballistic test

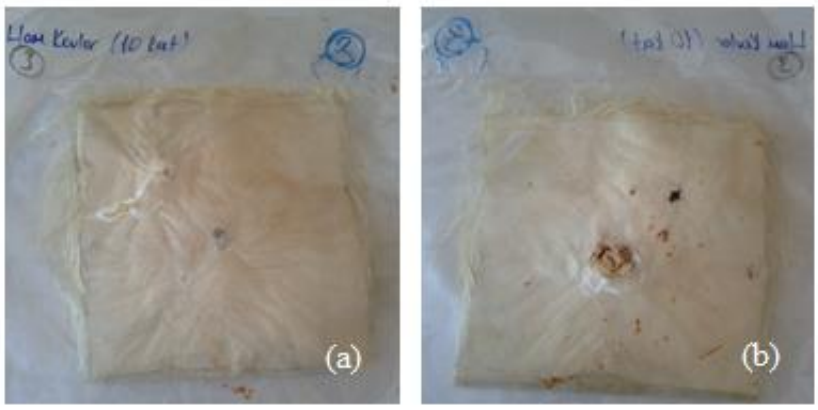

Figure 5.51. Images of 10 layers of neat fabrics from (a) front and (b) back side

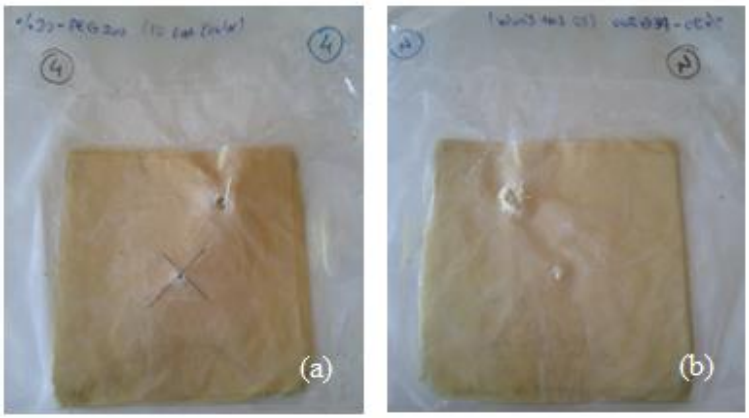

Figure 5.52. Images of 10 layers of STF/aramid fabric composite containing STF prepared with 30 wt. % fumed silica and 70 wt. % PEG 200 from (a) front and (b) back side

15 layers of neat aramids and STF/aramid fabric composite containing STF prepared with 70 wt. % colloidal silica and 30 wt. % PEG 200 having sizes of 30 cm x 40 cm were also conducted to V_{50} ballistic test. The test results of neat aramid and STF/aramid composite were measured as 504.1 m/sec and 529.6 m/sec, repectively. The front and back side images after ballistic test and the projectile marks on the front and back side of neat aramids are seen in Figure 5.53 and 5.54, respectively. In addition, the images after ballistic test and the projectile marks on the front and back side STF/aramid fabric composite containing STF prepared with 70 wt. % colloidal silica and 30 wt. % PEG 200 are seen in Figure 5.55 and 5.56, respectively.

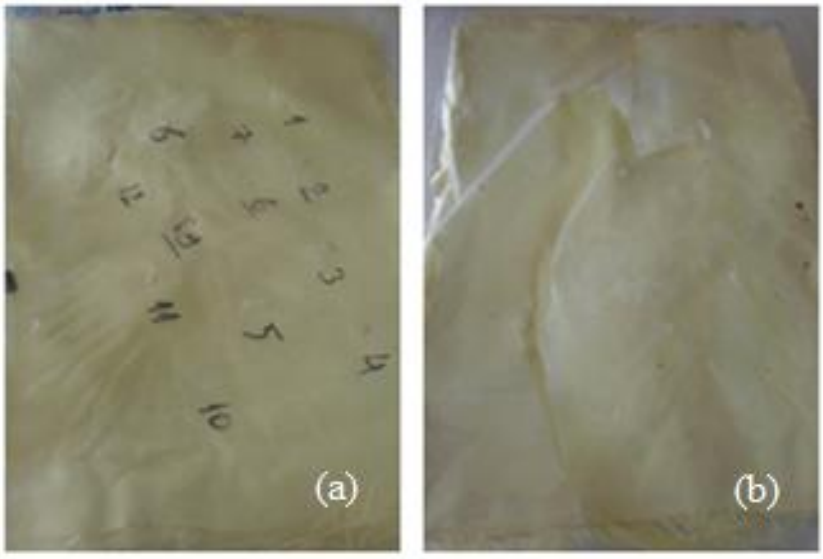

Figure 5.53. Images after ballistic test of 15 layers of neat aramids from (a) front and (b) back side

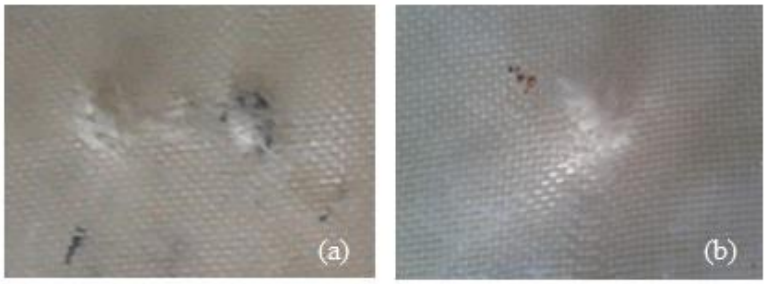

Figure 5.54. The projectile marks on the (a) front and (b) back side of neat aramids

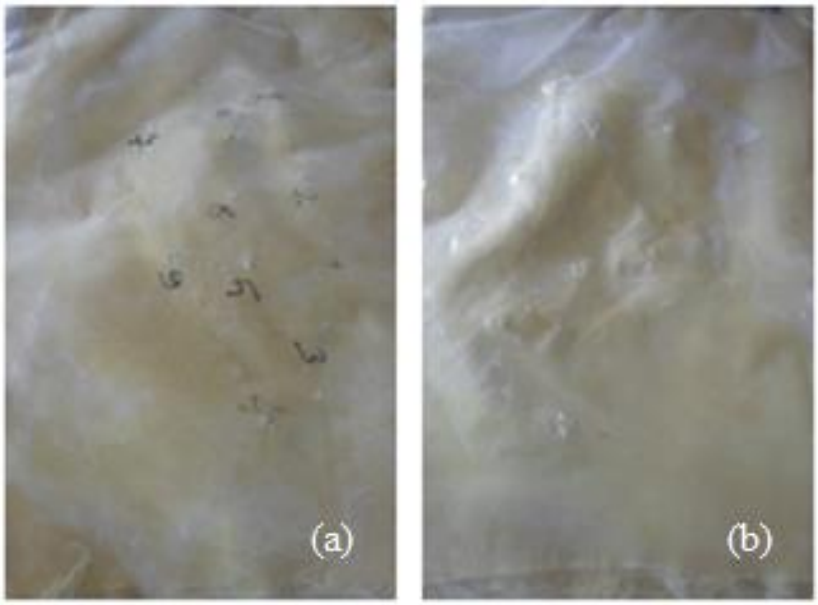

Figure 5.55. Images after ballistic test of 15 layers of STF/aramid fabric composite containing STF prepared with 70 wt. % colloidal silica and 30 wt. % PEG 200 from (a) front and (b) back side

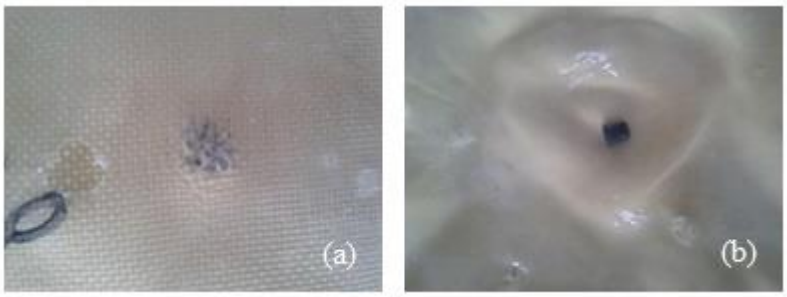

Figure 5.56. The projectile marks on the (a) front and (b) back side of STF/aramid fabric composite containing STF prepared with 70 wt. % colloidal silica and 30 wt. % PEG 200 from (a) front and (b) back side

V_{50} ballistic test was also performed with STF/UHMWPE mat consisting of STF prepared with 30 wt. % fumed silica and 70 wt. % PEG 300 with different configurations. In these configurations UHMWPE sheets were placed in front of mat fabrics and the prepared composites were applied to the ballistic test within the camouflage (Figure 5.57). Figure 5.58 shows front side images of composites before and after ballistic test. Figure 5.59 shows back side images of composites before and after ballistic test.

Figure 5.57. Image of the camouflage used for the composites

Figure 5.58. Images of STF/UHMWPE fabric composite containing STF prepared with 30 wt. % fumed silica and 70 wt. % PEG 300 from front side (a) before and (b) after ballistic test

Figure 5.59. Images of STF/UHMWPE fabric composite containing STF prepared with 30 wt. % fumed silica and 70 wt. % PEG 300 from back side (a) before and (b) after ballistic test

In addition, STF prepared with 30 wt. % fumed silica and 70 wt. % PEG 300 was filled to the PP honeycomb and 8 and 2 UHMWPE sheets were placed in front and back of the prepared STF/honeycomb, respectively. Figure 5.60 shows the images of STF filled PP honeycomb and STF/PP honeycomb/UHMWPE sheet composite. V_{50} test results of prepared composites systems are summarized in Table 5.17.

Figure 5.60. Images of STF/PP honeycomb composite containing STF prepared with 30 wt. % fumed silica and 70 wt. % PEG 300 (a) front and (b) back side

Table 5.17. V_{50} test results of prepared STF/fabric composites systems

V_{50} ballistic test targets	**V_{50} result (m/sec)**
15 layers of neat aramid	504.1
15 layers of STF/aramid with 70 wt. % colloidal silica and 30 wt. % PEG 200	529.6
10 layers of UHMWPE sheet – 7 layers of STF/UHMWPE PE mat with 30 wt. % fumed silica and 70 wt. % PEG 300	580.5
9 layers of UHMWPE sheet – 8 layers of STF/UHMWPE PE mat with 30 wt. % fumed silica and 70 wt. % PEG 300	597.3
9 layers of UHMWPE sheet – 9 layers of STF/UHMWPE PE mat with 30 wt. % fumed silica and 70 wt. % PEG 300	610
STF/Honeycomb	400

These results show that combination of PE mat and UHMWPE sheet give higher results than aramid fabrics. In addition to that, increasing the number of PE mat in the composite give higher ballistic resistance.

CHAPTER 6

CONCLUSIONS

In this study, development of shear thickening fluids (STFs) and fabrication of STF/fabric composites to assess as stab and ballistic proof materials were aimed.

The fumed and colloidal silica nanoparticles employed within the study were charecterized in terms of pyhsical and thermal properties. Physical property characterization include X-Ray Diffraction, Scanning Electron Microscopy (SEM) analysis for microstructural evaluation, dynamic light scattering (DLS) measurement for size distributions. Thermal features of nanoparticles were also investigated by applying thermogravimetric analysis. Thermogravimetric analysis was also applied onto PEGs to analyze the weight loss as a function of temperatures.

Fumed silica and colloidal silica based shear thickening fluids (STFs) with polyethylene glycol (PEG) having different molecular weights (200, 300 and 400 gram/mole molecular weights PEG 200 MW, PEG 300 MW and PEG 400 MW) were developed succesfully. In fumed silica based STFs, the silica concentration varied from 5 to 30 wt. % of silica and these STFs were synthesized by sonochemical method. Colloidal silica based STFs contained 40 to 70 wt. % of silica were prepared. SEM images indicated that sonochemical method provided a better dispersion of fumed silica particles in STFs. TGA test result of STFs indicates that the weight loss % as a function of temprature and after the decomposition of PEG, silica remained in the STF and these remaining silica values associates well with amount of silicas used to prepare.

The rheological behaviour characterization of prepared STFs and neat PEGs indicated that neat PEGs show a Newtonain flow behaviours with a constant viscosity as increasing shear rate. However, with the addition of silica nanoparticles into the PEG, shear thickening behaviour was enhanced and which was more obvious at higher silica concentrations. As silica particle concentration increased, the interparticle forces increased and so the friction between particles greatly increased, causing an enhanced shear thickening property of the STFs. Among fumed silica based STFs prepared with different molecular weights of PEG, the increament in viscosity of STFs prepared with PEG 200 was found to be highest as compared to the other STFs with viscosity jump

from 18.87 to 1297 Pa.s at 15.97 1/s critical shear rate. This viscosity jump was from 16 to 1241 Pa.s and from 75.68 to 586.1 Pa.s at 16.84 1/s and 37.74 1/s critical shear rates for STFs prepared with PEG 300 and 400, respectively. Also, it was observed that there is a general trend such that the onset of shear thickening decreases with increasing silica concentration. Colloidal silica based STFs did not exhibite a obvious shear thickening, however this behaviour were more significant in fumed silica based shear thickening fluids. Colloidal silica is spherical shaped and do not form aggregates. Hence, the branch-shaped aggregates made up of fumed silica lead to a large increase in the viscosity. Therefore, the formation of hydroclusters may took place easier in the STF consisting of fumed silica rather than in the STF consisting of spherical silica. In addition, the density difference between colloidal and fumed silica and the chemicals in colloidal silica dispersion to obtain stable dispersion may not trigger the hydrocluster of particles. Therefore, in the future works various particles could be used to synthesise the STFs such as dry sphere silica and fumed silica nanoparticles with different particle sizes. It is important to understand the effect of particle size effect on the shear thickening mechasim.

STF/aramid and UHMWEPE fabric composites were fabricated with the impregnation of STFs onto the fabrics by soaking method. The impregnation method was standart for all composites. This impregnation method could vary with other materials. In the STF/UHMWPE mat composites, UHMWPE sheets were used in front of the PE mat. The microstructural features of these composites were evaluated by SEM analysis and the images showed that STF is well impregnated over the entire surface on the fabric. It was revelaed that the fabrics were coated with STFs uniformly.

The mechanical property characterization of STF/aramid targets were determined based on quasi-static and dynamic stab resistance tests. STF/aramid targets showed a significant enhancement in stab resistance as compared with neat fabric in both stab tests. Both stab and rheological experiments showed that increasing shear thickening response corresponds to increased stab performance in the STF/aramid targets.

In order to determine the flexibility characters of STF/aramid targets, flexibility tests were applied. It was found that there is no significant difference between the flexibilities of both the neat fabric and STF/aramid targets. However, the literature lacks studies of flexibility tests with fabrics with sizes larger than 20 cm x 20 cm. Therefore,

these test results can be assumed to be more accurate and the decreasing flexibility in composites with higher silica concentration was within the expected limits.

The ballistic tests in terms of 9 mm parabellum and V_{50} test were conducted to STF/aramid and STF/PE mat composites. Results showed that there is increment in the ballistic resistance between neat fabric and STF/aramid composites. However, the increment in STF/PE mat composites is much more as compared to that observed with the aramid fabrics. In this study, STFs prepared with PEG 200 and 300 were used to impregnated the fabrics due to their significant thickening effect. However, with various projectiles the other composites impregnated with STFs consist of PEG 400 could be tried. The higher shear rate values of this composites could be effective for these tests.

REFERENCES

Barnes, HA. 1989. "Shear-thickening ("dilatancy") in suspensions of nonaggregating solid particles dispersed in Newtonian liquids." *Journal of Rheology* no. 33:329.

Barnes, Howard A, John Fletcher Hutton, and Kenneth Walters. 1989. *An introduction to rheology*. Vol. 3: Elsevier.

Bender, Jonathan, and Norman J Wagner. 1996. "Reversible shear thickening in monodisperse and bidisperse colloidal dispersions." *Journal of Rheology* no. 40:899.

Boersma, Willem H, Jozua Laven, and Hans N Stein. 1990. "Shear thickening (dilatancy) in concentrated dispersions." *AIChE journal* no. 36 (3):321-332.

Bossis, Georges, and John F Brady. 1984. "Dynamic simulation of sheared suspensions. I. General method." *The Journal of chemical physics* no. 80:5141.

Campbell, Flake C. 2006. *Manufacturing technology for aerospace structural materials, Chapter 7 Polymer matrix Composites*. 1 ed. Vol. 6: Elsevier Amsterdam.

Carrillo, JG, RA Gamboa, EA Flores-Johnson, and PI Gonzalez-Chi. 2012. "Ballistic performance of thermoplastic composite laminates made from aramid woven fabric and polypropylene matrix." *Polymer Testing* no. 31 (4):512-519.

Cheeseman, Bryan A, and Travis A Bogetti. 2003. "Ballistic impact into fabric and compliant composite laminates." *Composite Structures* no. 61 (1):161-173.

Chellamuthu, Manojkumar, Eric M Arndt, and Jonathan P Rothstein. 2009. "Extensional rheology of shear-thickening nanoparticle suspensions." *Soft Matter* no. 5 (10):2117-2124.

Cheng, Xiang, Jonathan H McCoy, Jacob N Israelachvili, and Itai Cohen. 2011. "Imaging the microscopic structure of shear thinning and thickening colloidal suspensions." *Science* no. 333 (6047):1276-1279.

Chhabra, Raj P, and John Francis Richardson. 2008. *Non-Newtonian flow and applied rheology: engineering applications*. Second ed: Butterworth-Heinemann.

Chocron Benloulo, I. S., and V. Sánchez-Gálvez. 1998. "A new analytical model to simulate impact onto ceramic/composite armors." *International Journal of Impact Engineering* no. 21 (6):461-471.

Clements, F, and Hassan Mahfuz. 2007. Enhancing the Stab Resistance of Flexible Body Armor using Functionalized SiO2 Nanoparticles. Paper read at 16 th Intl. Conference on Composite Materials (ICCM-16), at Kyoto, Japan.

Çay, A, E Kanat, G Süpüren, T Gülümser, and I Tarakçıoğlu. 2007. "Balistik Lifler (Bölüm 1)." *Tekstil ve Konfeksiyon* no. 4:232-236.

Decker, M. J., C. J. Halbach, C. H. Nam, N. J. Wagner, and E. D. Wetzel. 2007. "Stab resistance of shear thickening fluid (STF)-treated fabrics." *Composites Science and Technology* no. 67 (3–4):565-578.

DEF STAN 05-101, (Ministry of Defence, Defence Standard). 2005. "Proof of Ordnance, Munitions, Armour and Explosives".

Duan, Y, M Keefe, TA Bogetti, and B Powers. 2006. "Finite element modeling of transverse impact on a ballistic fabric." *International Journal of Mechanical Sciences* no. 48 (1):33-43.

Dyneema Company Industrial Inc., "The Dyneema® Brand" http://www.dyneema.com/emea/explore-dyneema/the-dyneema%20brand.aspx (accessed October 22, 2013).

Egres Jr, RG, YS Lee, JE Kirkwood, KM Kirkwood, ED Wetzel, and NJ Wagner. 2004. Liquid armor: protective fabrics utilizing shear thickening fluids. Paper read at Proceeding of Industrial Fabrics Associational International Conference on Safety and Protective Fabrics. Pittsburgh.

Egres, RG, YS Lee, JE Kirkwood, KM Kirkwood, ED Wetzel, and NJ Wagner. 2003. Novel flexible body armor utilizing shear thickening fluid (STF) composites. Paper read at Proceedings, 14th Int. Conf. on Composite Materials, San Diego, CA, Soc. Manufacturing Engineers, paper.

Egres, Ronald G, and Norman J Wagner. 2005. "The rheology and microstructure of acicular precipitated calcium carbonate colloidal suspensions through the shear thickening transition." *Journal of Rheology* no. 49:719.

Fan, Jinchen, Zixing Shi, Lu Zhang, Jialiang Wang, and Jie Yin. 2012. "Aramid nanofiber-functionalized graphene nanosheets for polymer reinforcement." *Nanoscale* no. 4 (22):7046-7055.

Feli, S., and M. R. Asgari. 2011. "Finite element simulation of ceramic/composite armor under ballistic impact." *Composites Part B: Engineering* no. 42 (4):771-780.

Fernández-Fdz, D., and R. Zaera. 2008. "A new tool based on artificial neural networks for the design of lightweight ceramic–metal armour against high-velocity impact of solids." *International Journal of Solids and Structures* no. 45 (25–26):6369-6383.

Franks, George V, Zhongwu Zhou, Nanda J Duin, and David V Boger. 2000. "Effect of interparticle forces on shear thickening of oxide suspensions." *Journal of Rheology* no. 44:759.

Frith, William J, P d'Haene, R Buscall, and Joannes Mewis. 1996. "Shear thickening in model suspensions of sterically stabilized particles." *Journal of rheology* no. 40:531.

Galindo-Rosales, FJ, and FJ Rubio-Hernández. 2010. "Static and dynamic yield stresses of Aerosil® 200 suspension in polypropylene glycol." *Applied Rheology* no. 20 (2):22787.

Goodwin, James William, and Roy W Hughes. 2008. *Rheology for chemists: an introduction*: Royal Society of Chemistry.

Gopinath, G, JQ Zheng, and RC Batra. 2012. "Effect of matrix on ballistic performance of soft body armor." *Composite Structures* no. 94 (9):2690-2696.

Gordon, Alexander C, Darryl D D'Lima, and Clifford W Colwell. 2006. "Highly cross-linked polyethylene in total hip arthroplasty." *Journal of the American Academy of Orthopaedic Surgeons* no. 14 (9):511-523.

Grujicic, M, G Arakere, T He, WC Bell, BA Cheeseman, C-F Yen, and B Scott. 2008. "A ballistic material model for cross-plied unidirectional ultra-high molecular-weight polyethylene fiber-reinforced armor-grade composites." *Materials Science and Engineering: A* no. 498 (1):231-241.

Hassan, Tarig A, Vijay K Rangari, and Shaik Jeelani. 2010. "Synthesis, processing and characterization of shear thickening fluid (STF) impregnated fabric composites." *Materials Science and Engineering: A* no. 527 (12):2892-2899.

Hoffman, RL. 1972. "Discontinuous and dilatant viscosity behavior in concentrated suspensions. I. Observation of a flow instability." *Journal of Rheology* no. 16:155.

Honeywell Company Industrial Inc., " Adanced Fiber and Composites" http://www.honeywell-advancedfibersandcomposites.com/ (accessed October 22, 2013).

Horsfall, I, SM Champion, and CH Watson. 2005. "The development of a quantitative flexibility test for body armour and comparison with wearer trials." *Applied Ergonomics* no. 36 (3):283-292.

Houghton, JM, BA Schiffman, DP Kalman, ED Wetzel, and NJ Wagner. 2007. "Hypodermic needle puncture of shear thickening fluid (STF)-treated fabrics." *Proceedings of SAMPE*:3-7.

Kalantar, J, LT Drzal, and DS Grummon. 1990. Structural properties of aramid fibers and their influence on fiber adhesion. Paper read at Third International Conference on Composite Interfaces (ICCI-III).

Kaldasch, Joachim, Bernhard Senge, and Jozua Laven. 2008. "Shear thickening in electrically-stabilized colloidal suspensions." *Rheologica Acta* no. 47 (3):319-323.

Kalman, Dennis P, Richard L Merrill, Norman J Wagner, and Eric D Wetzel. 2009. "Effect of Particle Hardness on the Penetration Behavior of Fabrics Intercalated with Dry Particles and Concentrated Particle− Fluid Suspensions." *ACS applied materials & interfaces* no. 1 (11):2602-2612.

Kalman, DP, JB Schein, JM Houghton, CHN Laufer, ED Wetzel, and NJ Wagner. 2007. "Polymer dispersion based shear thickening fluid-fabrics for protective applications." *Proceedings of SAMPE*:3-7.

Kang, Tae Jin, Chang Youn Kim, and Kyung Hwa Hong. 2012. "Rheological behavior of concentrated silica suspension and its application to soft armor." *Journal of Applied Polymer Science* no. 124 (2):1534-1541.

Kazemian, Sina, Arun Prasad, and Bujang BK Huat. 2010. "Rheological Behavior of Grout in Context of Newtonian and non-Newtonian Fluids." *Electronic Journal of Geotechnical Engineering* no. 15.

Laun, HM, R Bung, S Hess, W Loose, O Hess, K Hahn, E Hädicke, R Hingmann, F Schmidt, and P Lindner. 1992. "Rheological and small angle neutron scattering investigation of shear-induced particle structures of concentrated polymer dispersions submitted to plane Poiseuille and Couette flow." *Journal of Rheology* no. 36:743.

Lee, Bok-Won, Il-Jin Kim, and Chun-Gon Kim. 2009. "The influence of the particle size of silica on the ballistic performance of fabrics impregnated with silica colloidal suspension." *Journal of composite materials* no. 43 (23):2679-2698.

Lee, Young S, Eric D Wetzel, and Norman J Wagner. 2003. "The ballistic impact characteristics of Kevlar® woven fabrics impregnated with a colloidal shear thickening fluid." *Journal of materials science* no. 38 (13):2825-2833.

Lee, Young Sil, and Norman J Wagner. 2003. "Dynamic properties of shear thickening colloidal suspensions." *Rheologica Acta* no. 42 (3):199-208.

Lomakin, EV, PA Mossakovsky, AM Bragov, AK Lomunov, A Yu Konstantinov, ME Kolotnikov, FK Antonov, and MS Vakshtein. 2011. "Investigation of impact resistance of multilayered woven composite barrier impregnated with the shear thickening fluid." *Archive of applied mechanics* no. 81 (12):2007-2020.

Mahfuz, H, F Clements, and J Stewart. 2006. Development of Stab Resistant Body Armor Using Fumed SiO2 Nanoparticles Dispersed into Polyethylene Glycol (PEG) through Sonic Cavitation. Paper read at NSTI-Nanotech 2006.

Majumdar, D, KK Srivastava, SS Purkayastha, G Pichan, and W Selvamurthy. 1997. "Physiological effects of wearing heavy body armour on male soldiers." *International Journal of Industrial Ergonomics* no. 20 (2):155-161.

Malkin, Aleksandr ÏAkovlevich. 1994. *Rheology fundamentals*: ChemTec Publishing.

Malkin, Alexander Ya, and Avraam I. Isayev. 2006. *Rheology: concepts, methods, and applications*: ChemTec Publishing.

Medvedovski, Eugene. 2010. "Ballistic performance of armour ceramics: Influence of design and structure. Part 2." *Ceramics International* no. 36 (7):2117-2127.

Melrose, John R, and Robin C Ball. 2004. "“Contact networks” in continuously shear thickening colloids." *Journal of Rheology* no. 48:961.

Meyers, Marc Andre 1994. *Dynamic behavior of materials*: A Wiley-Interscience Publication.

NIJ Standard–0101.04 1987 - Ballistic Resistance of Personal Body Armor

NIJ Standard-0101.06 2008 - Ballistic Resistance of Body Armor

Raghavan, Srinivasa R, and Saad A Khan. 1997. "Shear-thickening response of fumed silica suspensions under steady and oscillatory shear." *Journal of colloid and interface science* no. 185 (1):57-67.

Rao, Harish, Mahesh V Hosur, J Mayo, Shifra Burton, and Shaik Jeelani. 2009. Stab Characterization of Hybrid Ballistic Fabrics. Paper read at 2009 Annual Society for Experimental Mechanics Conference, Albuquerque, NM.

Scientia Review, e-journal, "The History of Armor Protection, Mobility, and Fashion", http://scientiareview.org/pdfs/69.pdf (accessed October 23, 2013).

Shenoy, Aroon V. 1999. *Rheology of filled polymer systems*: Springer.

Shokrieh, M. M., and G. H. Javadpour. 2008. "Penetration analysis of a projectile in ceramic composite armor." *Composite Structures* no. 82 (2):269-276.

Srivastava, A, A Majumdar, and BS Butola. 2012. "Improving the Impact Resistance of Textile Structures by using Shear Thickening Fluids: A Review." *Critical Reviews in Solid State and Materials Sciences* no. 37 (2):115-129.

Srivastava, Ankita, Abhijit Majumdar, and Bhupendra Singh Butola. 2011. "Improving the impact resistance performance of Kevlar fabrics using silica based shear thickening fluid." *Materials Science and Engineering: A* no. 529:224-229.

Suhaimi, MS, R Mohamed, and MA Faiza. 2010. Effect of polymer microsphere incorporation on impact performance of STF cotton fabric composite. Paper read at IOP Conference Series: Materials Science and Engineering.

Tan, VBC, TE Tay, and WK Teo. 2005. "Strengthening fabric armour with silica colloidal suspensions." *International Journal of Solids and Structures* no. 42 (5):1561-1576.

Tanoglu, M, SH McKnight, GR Palmese, and JW Gillespie Jr. 2001. "The effects of glass-fiber sizings on the strength and energy absorption of the fiber/matrix interphase under high loading rates." *Composites science and technology* no. 61 (2):205-220.

Techniqual Guide-Kevlar® Aramid Fiber. In *Kevlar® Technical Guide-Du Pont*, 2013

Teijin Company Industrial Inc., "Technora" http://www.teijinaramid.com/aramids/technora/ (accessed October 22, 2013).

Teijin Company Industial Inc., "*What is Aramid?"* http://www.teijinaramid.com/aramids/what-is-aramid/ (accessed October 22, 2013).

Toyoba Company Indutrial ınc., "What is Zylon® ?" http://www.toyoboglobal.com/seihin/kc/pbo/ (accessed October 22, 2013).

Twaron Product Brochure, Twaron – A Versatile High-Performance Fiber. 2012.

Utracki, Leszek A. 2010. "Rigid ballistic composites (Review of literature)." *National Research Council. Canada*.

Übeyli, Mustafa, R. Orhan Yıldırım, and Bilgehan Ögel. 2007. "On the comparison of the ballistic performance of steel and laminated composite armors." *Materials & Design* no. 28 (4):1257-1262.

Visjager, Jeroen Franklin. 2001. *Ultra-high Molecular Weight Polymers: Processing and Properties of Polyethylene and Poly (tetrafluoroethylene)*, Eidgenössische Technische Hochschule Zürich.

Viswanath, Dabir S. 2007. *Viscosity of liquids: theory, estimation, experiment, and data*: Springer.

Wagner, Norman J, and John F Brady. 2009. "Shear thickening in colloidal dispersions." *Physics Today* no. 62 (10):27-32.

Wang, A., A. Essner, V. K. Polineni, C. Stark, and J. H. Dumbleton. 1998. "Lubrication and wear of ultra-high molecular weight polyethylene in total joint replacements." *Tribology International* no. 31 (1–3):17-33.

Wang, Qun, Zhaohai Chen, and Zhaofeng Chen. 2013. "Design and characteristics of hybrid composite armor subjected to projectile impact." *Materials & Design* no. 46 (0):634-639.

Wardman, Roger H, and RR Mather. 2011. *Chemistry of textile fibres*: Royal Society of Chemistry.

Wetzel, Eric D, YS Lee, RG Egres, KM Kirkwood, JE Kirkwood, and NJ Wagner. 2004. The effect of rheological parameters on the ballistic properties of shear thickening fluid (STF)-Kevlar composites. Paper read at AIP Conference Proceedings.